Università degli Studi di Trieste
Universidad de Castilla-La Mancha

New Graphene-based Composite Materials

Cristina Martín Jiménez
April 2016

Università degli Studi di Trieste

Universidad de Castilla-La Mancha

Ciclo XXVIII

Dottorato di Ricerca in Scienze e Tecnologie Chimiche e Farmaceutiche

PhD in Chemical and Pharmaceutical Sciences and Technologies (by UNITS)

Doctorado Internacional en Química

International PhD in Chemistry (by UCLM)

New Graphene-based Composite Materials

Settore scientifico-disciplinare CHIM/06

PhD student

Cristina Martín Jiménez

Thesis Supervisor at UNITs

Chiar.mo Prof. Maurizio Prato

PhD School Director

Chiar.mo Prof. Mauro Stener

Thesis Supervisor at UCLM

Chiar.ma Prof. Ester Vázquez Fernández-Pacheco

Academic year 2014/2015

Acknowledgements

I am grateful to my supervisor from University of Trieste, *Prof. Maurizio Prato* for giving me the opportunity to do a PhD in an international environment. I would also like to thank you for your knowledge and your help, especially during my stays in Trieste.

A mi directora en la Universidad de Castilla-La Mancha, *Dra. Ester Vázquez*, por confiar en mí. Gracias por tus enseñanzas, por tu ayuda constante, por tus consejos, y por darme siempre la oportunidad de aprender y trabajar en nuevas áreas de investigación.

I wish to thank *Prof. Matteo Santin* for giving me the opportunity of performing a stay in his laboratories at the University of Brighton. I would also like to acknowledge to *Dr. Mark Best*, such an affable person. Thank you for your help during my stay, but above all, thanks for your friendship.

I am also grateful to *Prof. Laura Ballerini* and her research group from International School for Advanced Studies of Trieste. Thank you for your help and collaboration in neuronal studies.

I wish also to thank *Dr. Andrea Travan* from University of Trieste for his help during the mechanical studies.

Quisiera agradecer a los profesores del departamento su buen trato y enseñanzas (*Dr. Ángel Díaz, Dra. Pilar Prieto, Dr. Andrés Moreno, Dra. Ana Sánchez-Migallón, Dr. José Ramón Carrillo, Dra. M^{a} Victoria Gómez, Dr. Enrique Díez-Barra, Dr. Juan Tejeda, Dr. Julián Rodríguez, Dra. Prado Sánchez*), y especialmente al *Prof. Antonio de la Hoz* y a la *Dra. María Antonia Herrero*, quienes siempre están dispuestos a ayudar y a resolver cualquier duda o cuestión. Por supuesto, a la *Dra. Sonia Merino*, quien empezó siendo mi profesora de Química Orgánica y desde entonces siempre ha estado ahí: gracias por tu bondad y transparencia.

A *Txiqui*, gracias por tu cercanía y dedicación diaria, y a *Rian* y a *Jesús,* por toda su ayuda en laboratorio.

Al *Prato´s Group* no sé muy bien cómo escribirles (¿quizás en español?). Thanks to all of you for your availability, your friendship and also for making nice my stays in Trieste. I would like to acknowledge to *Dr. Susanna Bosi*, especially for your help making sponges :). Gracias al aire fresco gallego (*Manu, Paula*, *Jénnifer*), a esa catalana compañera de aventuras, *Nuria*, y a los que ya os conocía de antes (*Arturo*, *Dani*), por hacerme sentir tan bien. Os deseo muchísima suerte. Querría agradecer también a los más veteranos, *Alex*, *Caroline*: gracias por vuestra ayuda incondicional. Y a todos, por los ratitos de fiesta ;).

Agradecer a mis actuales compañeros de microondas, *Almudena, José Miguel, Rosa María, Raúl, Iván, Covadonga*, y a los que lo fueron, *María, María Jesús (Chusa), Antonio, José Ramón, Alberto, Fernando, Patricia*. Tengo muy gratos recuerdos dentro y fuera del laboratorio gracias a vosotros.

¿Y a "los del IRICA"? ☺ Han sido tres años en los que habéis conseguido significar muchísimo, tanto los que estáis como los que os fuisteis. Gracias a *Mari Tere*, a *Esaú* por empujarme siempre a enredar con locos inventos :P, y por supuesto a *Verónica*, mi compi de geles. *Maribel*, simplemente especial para mí, cuánto más te conozco, más me alegra haberlo hecho. Gracias de corazón por tu compañerismo y amistad. Gracias también a *Viviana* y a *Manuel*, por vuestra ayuda en el laboratorio. A *Jose*, por tu implicación, tus constantes consejos y por compartir siempre tu experiencia. Y por supuesto, a *Ana*, sieeeeempre dispuesta a ayudar en todo con una sonrisa puesta. Estoy segura de que alcanzarás cada meta que te propongas. Ciertamente, tengo mucho que agradecerte.

A mis *compis del cafetito* a las 15:30 h. Espero que nunca perdamos costumbre. Os deseo todo lo mejor.

A todos os debo momentos inolvidables.

Naturalmente gracias a los conserjes, *Edmundi, Teresa, María*, a todos, por vuestra ayuda y sonrisa diaria.

Después están mis, desde hace tiempo, "compañeras de viaje": *María*, "una muchacha que vale un montón…"☺, eres muy importante para mí. Gran apoyo y confidente. *Ana*, mi "siame" con la que tanto he compartido, dentro y fuera del laboratorio. Gracias por tu amistad sincera. A las dos: gracias por vuestra hospitalidad durante mis estancias en Trieste.

Gracias a Satur, Kika, Albertito 2.0., y ¿cómo no? a esos "*patagallos*" y "*chanchanes*", siempre pendientes de cómo estoy y dónde ando.

Y por último, a mis otras mitades:

A mis *cuatro Ángeles*. Gracias por vuestro ejemplo.

A mi hermana *Alicia*: puedo dejar por escrito lo orgullosa que me siento de ti, claro ejemplo de persona luchadora y perseverante. Gracias por tu apoyo y preocupación, especialmente durante estos años.

A *Alberto*. Simplemente no tengo palabras que describan mi agradecimiento hacia ti. La suerte es que me conoces bien y no hace falta explicar mucho. Gracias por tu ayuda, apoyo y esfuerzo para allanar el camino durante todo este tiempo ☺.

A *mis padres*, sin los que nada de todo esto hubiera sido posible. Gracias por vuestra eterna confianza y ánimo constante, pero sobre todo: GRACIAS POR HABER CONSEGUIDO HACER DE MI LO QUE SOY.

Thanks to all. Gracias a todos.

Cristina

Index

Abbreviations

AETA	[2-(acryloyloxy)ethyl]trimethylammonium chloride
AgNW	Silver nanowire
Am	Acrylamide
Ara C	Cytosine arabinoside
CNS	Central nervous system
CTC	Circulating tumour cell
CVD	Chemical vapour deposition
DAPI	4',6-diamidino-2-phenylindole
DC	Direct current
DIPEA	*N,N* – Diisopropylethylamine
DIV	Days in vitro
DMF	Dimethylformamide
FBS	Fetal Bovin Serum
G_F	Gauge factor
GFAP	Glial-fibrillary acidic protein
GO	Graphene oxide
GOP	Graphene oxide peroxide
HBTU	(2-(1H-benzotriazol-1-yl)-1,1,3,3-tetramethyluronium hexafluorophosphate)
HPI	Hoechst and Propidium Iodide
IEI	Inter-event interval

IPN	Interpenetrating Polymer Network
IVD	Intervertebral disc
KPS	Potassium peroxydisulfate
LDH	Lactate dehydrogenase
MAAc	Methacrylic acid
MBA	*N,N´*-methylenebisacrylamide
min	Minutes
MWNT	Multi-wall carbon nanotube
^{o}C	Degree Centigrade
p(AETA)	Poly([2-(acryloyloxy)ethyl]trimethylammonium chloride)
PAm	Polyacrylamide
PBS	Phosphate-buffered saline
PDMS	Polydimethylsiloxane
PEG	Polyethylene glycol
PFA	Paraformaldehyde
p(MAAc)	Poly(methacrylic acid)
PNIPAm	Poly(*N*-isopropyl acrylamide)
PSC	Post-synaptic current
PVA	Poly(vinyl alcohol)
R	Resistance
rGO	Reduced graphene oxide
Rs	Sheet resistance

RT	Room temperature
SEM	Scanning Electron Microscopy
SiC	Silicon Carbide
SWNT	Single-wall carbon nanotube
TCP	Tissue culture plastic
TEM	Transmission Electron Microscopy
TFA	Trifluoroacetic acid
TGA	Thermogravimetric Analysis
V_{cmd}	Command voltage
V_m	Membrane potential
W_0	Weight of dried hydrogels
W_t	Weight of hydrated hydrogels at a determined time
XPS	X-ray Photoelectron Spectroscopy

η	Healing efficiency
K_{IC}	Fracture toughness
σ	Electrical conductivity
ρ	Resistivity
p_c	Percolation threshold
l	Length
s	Section area
Ω	Ohm
Ω/sq	Ohm per square

Abstract

In the field of composite materials, the number of combinations is huge and varied depending on the nature of the matrix and the additive. However, the evolution of polymers since the beginning of the 19th century has led to a boost in research, in which the latest advances have provided numerous advantages in many fields, including nanomedicine. In recent years, composites have been made from materials in which the size of at least one of the phases is in the nanometer scale, also called nanomaterials. Among all of them, graphene has unique properties owing to its sp^2 hybridised carbon atoms arranged in a 2D honeycomb lattice.

The incorporation of graphene into polymeric materials offers new options regarding the use of these composites in a wider range of fields (from sensors to biological applications). In this context, the aim of this thesis is the design of new graphene-based composites to be used in several applications depending on the specific features of the final prepared materials.

In Chapter 1, a review of composite materials is provided, mostly describing important concepts about hydrogels and interpenetrating polymer networks (IPNs). Concepts about graphene are also commented, digging down to more specific literature examples mainly based on this fascinating nanomaterial. The difficulties of dispersing pristine graphene in polymers or solvents (especially in water) are discussed, emphasising the small number of examples in which pristine graphene-based hydrogels are prepared.

Chapter 2 details the synthesis, characterisation and different applications of graphene-based composite hydrogels using acrylamide as the main monomer. Moreover the role of graphene into the network structures is studied. The final composites show excellent mechanical properties, which make them good candidates as intervertebral disc prostheses and as 3D scaffolds for cell culture, affording nucleus pulposus replacements. The de-swelling behaviour under a microwave stimulus is also

demonstrated, making these composites good candidates for on-demand drug delivery systems. Finally, a piezoresistive effect is found as a consequence of the presence of graphene into the hydrogel network. Changes in the resistivity values, depending on whether the material is being stretched or not, are measured obtaining excellent gauge factor values. These results pave the way for the use of our systems as strain sensors.

In Chapter 3 the creation of novel nanostructured systems for neural network regeneration is studied. Neurons are grown on both 2D and 3D composites. The addition of graphene to 2D substrates, previously coated with single-wall carbon nanotubes, does not show a notable enhancement in the neuron activity. In that sense, similar values for membrane capacitance are obtained for substrates with and without graphene. In a second step, neuron activity is studied in a graphene-based 3D scaffold. The most important results observed in this study are that neurons only grow and are visualised in the graphene-based hydrogel, but not in the same scaffold prepared without nanomaterial. Therefore, we could confirm that graphene is taking an important role in the neuronal growth.

Finally, in Chapter 4, new composite hydrogels with an autonomous self-healing capacity are described. Two different types of composites are studied herein. The first ones are semi-IPNs of poly (methacrylic acid) (pMAAc) and poly (vinyl alcohol) (PVA). The materials are synthesised and characterised in the presence or absence of graphene, and their self-healing abilities are subsequently analysed. They show not only an electromechanical behaviour, but also an almost complete auto-reparation. The second type of materials are prepared from the MAAc in combination with a different monomer: [2-(acryloyloxy)ethyl]trimethylammonium chloride. The repairing ability is studied and differences are found depending on the way in which the material is prepared and on the presence of graphene. In this case, the self-healing property is based on ionic interactions as the composites are based on oppositely charged polyelectrolytes. All the materials have shown good repairing ability, even the

ones prepared with graphene, highlighting one of the semi-IPNs in which a healing efficiency of almost 100% is obtained.

Riassunto

La chimica dei materiali è una scienza in continua evoluzione e i suoi campi di applicazione sono sempre più numerosi e articolati. In particolare lo studio dei polimeri, fin dai suoi inizi a partire dal XIX secolo, ha un ruolo molto importante ed è protagonista in vari settori della ricerca, tra cui, negli ultimi decenni, in nanomedicina.

Questa disciplina prevede una scala di produzione delle strutture utilizzate nel range dei nanometri motivo per cui si parla di nanomateriali. Tra i nanomateriali che sono considerati più promettenti negli ultimi anni, la scena è sicuramente dominata dal grafene. Il grafene è un materiale formato esclusivamente da atomi di carbonio disposti in modo planare che deve le sue peculiari proprietà fisiche e chimiche al fatto che atomi di carbonio ibridati sp^2 sono combinati in un reticolo 2D strutturato a nido d'ape.

L'integrazione di grafene all'interno di materiali polimerici ne permette l'utilizzo in un vasto numero di campi di applicazione (dalla sensoristica ai materiali compositi alle più svariate applicazioni biologiche). In questo contesto così vasto, l'obiettivo di questa tesi è la progettazione di nuovi derivati, basati su grafene, utilizzabili per alcune applicazioni, che tiene conto del design e delle specifiche funzionalità del composto finale.

Il primo capitolo introduce lo studio di materiali compositi descrivendo, inizialmente, i concetti più importanti per la comprensione di questa tesi come la descrizione di idrogel, reticoli polimerici interpenetranti (IPNs), e, ovviamente, del grafene, esaminando i principali riferimenti bibliografici che trattano lo studio di questo materiale così affascinante.

Il capitolo 2 fornisce dettagli sui processi di sintesi, di caratterizzazione e di applicazione di idrogel a base di grafene, ottenuti utilizzando acrilamide come principale monomero. Oltre a ciò, viene studiato il ruolo del grafene come reticolante all'interno della struttura. I composti finali mostrano eccellenti proprietà meccaniche, tali da renderli buoni candidati nella progettazione di protesi di dischi intervertebrali,

ma anche come possibili sostituti del nucleo polposo, la struttura gelatinosa sferoidale, la cui funzione è assorbire e ridistribuire in modo uniforme le sollecitazioni di carico della colonna vertebrale. Viene inoltre dimostrata la contrazione della struttura gelatinosa sotto stimoli esterni, cosa che rende i composti applicabili in sistemi di rilascio di farmaci "on demand". Infine, viene descritto in dettaglio l'effetto piezoresistivo in relazione alla presenza di grafene all'interno della rete degli idrogel. Sono stati misurati anche i fattori di trasduzione (gauge factor) dei materiali, ottenendo interessanti risultati in cui i valori di resistività cambiano se il materiale viene sottoposto a tensione o trazione. Questo comportamento induce ad ipotizzare un utilizzo dei nostri sistemi come sensori di sforzo.

Nel capitolo 3, viene presentata la creazione di nuovi sistemi nanostrutturati per la rigenerazione della rete neuronale. I neuroni vengono cresciuti sia su substrati bidimensionali (2D) sia in strutture tridimensionali (3D). Innanzitutto, l'addizione di grafene a substrati 2D, precedentemente ricoperti con nanotubi di carbonio, non ha mostrato un miglioramento dell'attività neuronale ottenendo, per esempio, valori di capacitanza di membrana simili a quelli ottenuti con il substrato ricoperto solo da nanotubi di carbonio. Successivamente, l'attività neuronale è stata studiata all'interno di una struttura 3D contenente grafene. Il risultato maggiormente rilevante di questo studio è che i neuroni crescono e vengono visualizzati all'interno dell'idrogel solo se in presenza di grafene. Alla luce di questi risultati, si può ipotizzare un importante ruolo del grafene come materiale da integrare nella rigenerazione di sistemi neuronali.

Infine, nel capitolo 4, vengono descritti nuovi idrogel con capacità di auto-riparazione. Vengono decritti due differenti tipi di composti: il primo consiste in reticoli polimerici semi-interpenetranti (semi-IPNs) di acido polimetacrilico e di alcol polivinilico. Inizialmente i materiali sono stati sintetizzati e caratterizzati sia in presenza che in assenza di grafene, e successivamente è stata analizzata la loro capacità di auto-riparazione. Tali materiali non solo mostrano un particolare comportamento elettromeccanico, ma anche una quasi completa capacità di autoripararsi. Il secondo materiale è stato preparato con acido metacrilico combinato con un monomero diverso, il cloruro di [2-(acriloilossi)etil] trimetilammonio. La

proprietà di autoriparazione è stata studiata in relazione al modo con cui si prepara il materiale e alla presenza o assenza del grafene al suo interno. In questo caso, l'auto-riparazione si basa sulle interazioni ioniche, dato che i materiali sono costituiti da polielettroliti di carica opposta. Tutti i materiali hanno dimostrato una buona tendenza alla riparazione, anche in presenza di grafene, con un'efficacia che raggiunge quasi il 100% nelle condizioni studiate.

Resumen

La ciencia de los materiales es una disciplina en continua evolución ya que las aplicaciones, que pueden beneficiarse de los nuevos compuestos sintéticos, son cada vez más amplias y variadas. La evolución de los polímeros desde principios del siglo XIX ha impulsado en gran medida la investigación en este campo y los últimos avances han proporcionado numerosas ventajas, incluso en el campo de la nanomedicina. De hecho, la preparación de materiales compuestos ha incluido en los últimos años sistemas en los que, al menos una de las fases, es de escala nanométrica, también conocidos como nanomateriales. Entre todos ellos, el grafeno, material bidimensional con una estructura consistente en una lámina de átomos de carbono unidos entre sí y con hibridación sp^2, posee propiedades únicas.

La incorporación de grafeno en materiales poliméricos crea nuevas posibilidades con respecto al uso de estos nuevos compuestos en campos de aplicación mucho más amplios (desde sensores hasta aplicaciones biológicas). En este contexto, el objetivo de esta tesis es el diseño de nuevos materiales compuestos basados en grafeno, con distintas aplicaciones que dependen de las propiedades finales del sistema.

El Capítulo 1 proporciona una revisión general de los materiales compuestos, describiendo, principalmente, algunos conceptos importantes relativos a los hidrogeles, las redes poliméricas interpenetradas (IPNs), y por supuesto al grafeno. Se discute la dificultad de preparar dispersiones de grafeno en polímeros o disolventes (especialmente agua), profundizando en los pocos ejemplos bibliográficos en los que se describen hidrogeles basados en grafeno.

El Capítulo 2 detalla la síntesis, caracterización y diferentes aplicaciones de hidrogeles compuestos basados en grafeno, utilizando la acrilamida como monómero principal. Además, se estudia el papel que juega el nanomaterial como agente entrecruzante en la red polimérica. Los compuestos finales muestran excelentes propiedades mecánicas, lo que les señala como buenos candidatos para prótesis en discos intervertebrales. También podrían aplicarse en trasplantes del núcleo pulposo, ya que han sido probados satisfactoriamente como andamios tridimensionales para el

crecimiento de células 3T3. Por otro lado, se ha demostrado que estos compuestos responden a un estímulo microondas, deshinchándose, lo que hace posible su aplicación como posibles sistemas para liberación controlada de fármacos. Finalmente, en este capítulo se describe el efecto piezoresistivo que aparece gracias a la presencia de grafeno en la red de hidrogel. En este sentido, se observan cambios en las resistividades del material con respecto a un estímulo mecánico, obteniéndose resultados excelentes de los valores de "gauge factor". Este hecho hace posible la aplicación de estos sistemas como sensores de tensión.

En el Capítulo 3 se presentan nuevos sistemas nanoestructurados para la regeneración de redes neuronales. Varios sistemas bidimensionales y tridimensionales son usados para el crecimiento de neuronas. La adición de grafeno a sustratos bidimensionales, previamente cubiertos con nanotubos de pared simple, no produce una mejora notable en la actividad neuronal, obteniéndose, por ejemplo, valores similares de capacitancia de membrana con respecto al sustrato cubierto únicamente por los nanotubos. En un segundo paso, la actividad neuronal es estudiada en estructuras tridimensionales basadas en grafeno. El resultado más importante de este estudio es que las neuronas crecen únicamente en el hidrogel formado en presencia de grafeno, y no en el hidrogel carente de nanomaterial. Por lo tanto, podríamos confirmar que el grafeno juega un papel notable en el crecimiento neuronal.

Finalmente, en el cuarto capítulo se describen nuevos hidrogeles compuestos con capacidad autónoma de auto-reparación. Se estudian dos tipos diferentes de materiales. La primera clase son semi-IPNs de poli(ácido metacrílico) (pMAAc) y poli(vinil alcohol) (PVA). En primer lugar se sintetizan y caracterizan los materiales en presencia y en ausencia de grafeno, para sucesivamente analizar su capacidad de auto-sanación. Los materiales sintetizados no solo muestran comportamiento electromecánico, sino también una auto-reparación casi completa. El segundo tipo de materiales son preparados a partir de MAAc en combinación con un monómero diferente: cloruro de [2-(acriloiloxi)etil]trimetilamonio. La capacidad de reparación es estudiada y se observan diferencias dependiendo del modo en el que se prepara el material y de la presencia o no de grafeno. En este caso, la capacidad de auto-

reparación está basada en interacciones iónicas, ya que los materiales compuestos están basados en polielectrolitos cargados opuestamente. Todos los materiales demuestran buenas propiedades de reparación, incluso las preparadas con grafeno, destacando una de las semi-IPNs formadas, en la que se consigue una eficiencia de auto-reparación de casi el 100%.

Chapter 1

Introduction

1.1. Composite materials.

A composite material is made by combining two or more materials which have sometimes very different properties. These basic elements can have any possible form: matrix, fibre, particle, sheet, etc., and the synergy between them makes it possible the composite unique properties, resolving by this way any shortcoming of a particularly useful component. In this kind of materials, the different elements do not dissolve or blend into each other.

In recent years, composites have been made from materials in which the size of at least one of the phases is in the nanometer scale (less than 100 nm). In that case, that nanometer phase has physical properties very different from that of the same element in the bulk form, and the final material is referred to as a nanocomposite. In the hybrid composite materials, instead, there is a real orbital interaction as the constituents combine at a molecular level. In that case, new materials with new properties, which are not necessarily found in the individual ones, may be obtained.

Natural composites can be found in both plants and animals. The wood or the bones in our bodies are examples of composite materials; the design of advanced materials to mimic their functions and properties is a continuous challenge for scientists. Thus, biomimetics is one of the preferred strategies to design composites materials. In fact, the main advantage of composites is their versatility in the design regarding the specific feature requirements.

Artificial composites have been created by man for a long time. One of the first examples could be mud bricks. Mud can be dried out into a brick and it is resistant to crush, but it breaks easily by bending. Fortunately, straw is resistant under tensile stress, and it is possible to make bricks that are unaffected to both squeezing and tear by mixing mud and straw together.

Nowadays, the Airbus A380 is one of the latest examples, as more than 20 % of the plane is made of composite materials, mainly plastic reinforced with carbon fibres.

Although the number of possibilities and, therefore, of examples of composite materials is huge and varied depending on the nature of the matrix (ceramic composites,[1] metal composites,[2] etc...), we will focus on polymer composites materials, as most of the work described in this thesis is related to that kind of composites.

1.1.1. Polymer composite materials

The most basic definition for polymer composite materials would be "composites in which at least one component is a polymer".[3]

The evolution of polymers in the beginning of the 19th Century led to a boost in research with new options regarding the use of novel different materials in more diversified fields. Because of that, joined to the low cost or the easy preparation techniques, polymer composites are an area of substantial scientific interest and they are the most commercially produced nowadays. On the other hand, the main disadvantages of polymer composites are that they have poor thermal resistance or thermal expansion properties.

Fortunately, the interest in nanomaterials in the form of nanotubes, nanoparticles, nanowires or 2D materials has also became popular, and the incorporation of those nanomaterials into the polymer network is being highly investigated.[4–7] The reason for that stems from the combination of those materials, which allows the modification of the final properties of the polymer composites. Some of the issues that affect the polymer composite features are the interfacial adhesion between the matrix molecules and the filler, the shape and orientation of that filler (random, longitudinally aligned, entangled, etc.) and the intrinsic properties of the matrix itself. Many times the enhancement is related to reinforcement aspects, but there are lot of examples in literature regarding other different property improvements in materials, which are applicable in a wide range of fields (Table 1).

Nanofiller	Property enhancement(s)	Application/utility
Exfoliated clay	Flame resistance, barrier, compatibilizer for polymer blends	
SWCNT; MWCNT	Electrical conductivity, charge transport,	Electrical/electronics/ optoelectronics
Nanosilver	Antimicrobial	
ZnO	UV adsorption	UV screens
Silica	Viscosity modification	Paint, adhesives
CdSe, CdTe	Charge transport	Photovoltaic cells
Graphene	Electrical conductivity, barrier, charge transport	Electrical/electronic
POSS	Improved stability, flammability resistance	Sensors, LEDs

Table 1. Examples of nanoscale filler incorporated in polymer composites for property-enhancement.[4]

Among the polymer-composite materials, the Hydrogel Composites have caught the attention of many researchers. This kind of materials will be introduced in a further section because they have been thoroughly studied in this thesis.

1.2. Hydrogel composite materials

1.2.1. Hydrogels

Hydrogels are physically or chemically crosslinked hydrophilic 3D polymer networks, which absorb and retain large amounts of water, though not soluble in it, with maintenance of shape (Figure 1).[8] The swelling ability of these materials derives mainly from the presence of hydrophilic groups in the polymer chains. Moreover, their porous structure can easily be designed by modifying the density of cross-links in the gel matrix and the affinity of the polymer networks for the aqueous media in which they are swollen.

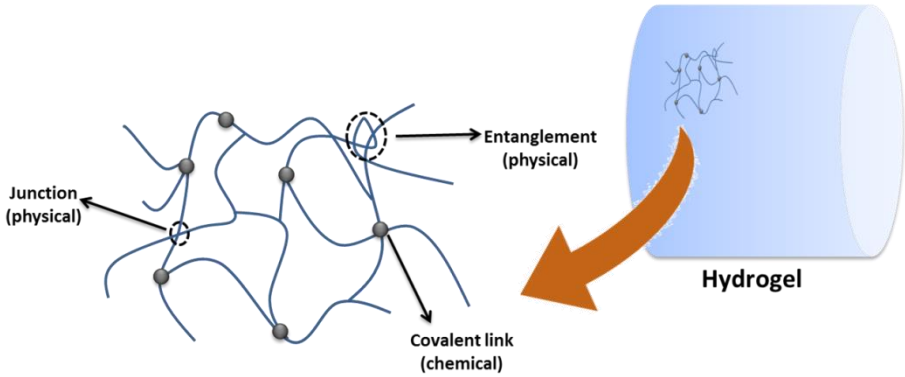

Figure 1. General scheme of hydrogel materials.

These materials are used in numerous applications, from agriculture[9] to therapeutic demands, with special emphasis on the biomedical and pharmaceutical fields. They have shown to be promising materials for cartilage or bone reparation,[10,11] as well as soft tissues replacements if they work as scaffolds for cell growth and proliferation.[12] Moreover, the application of hydrogels in biomedical devices such as films, sponges and biosensors is also known.[13] In drug delivery, hydrogels are extensively used as depot systems.[14]

1.2.1.1. Classification of hydrogels

Hydrogels can be classified in different ways depending on multiple factors. Figure 2 summarises that complex classification:

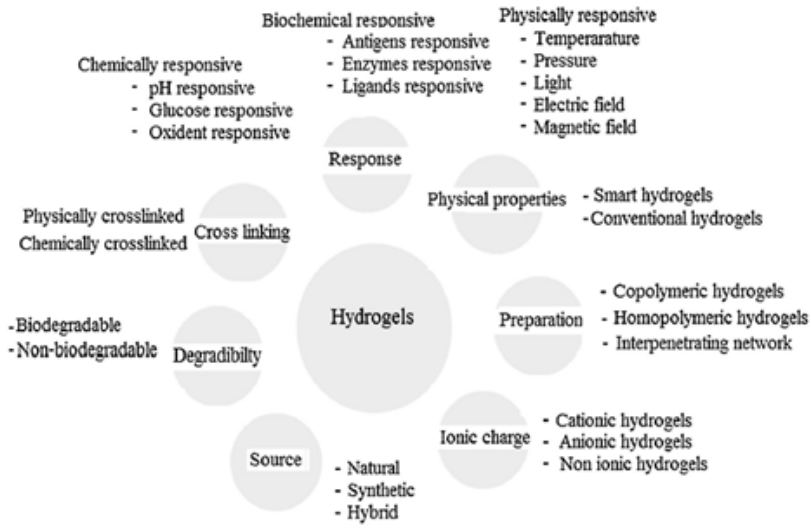

Figure 2. General classification of hydrogels.[15]

Regarding the crosslinking process, hydrogels can be physically crosslinked, if the crosslinking process is carried out by physical and reversible interactions, or chemically crosslinked, if the process is irreversible due to the formation of chemical covalent bonds. In general, the most typical crosslinking routes are radical polymerisation, chemical reaction of complementary groups, ionic interactions, or even crystallisation processes.[15]

Depending on the hydrogel preparation different materials can be obtained:

- Homopolymers, which are hydrogels formed from a single type of monomer
- Copolymers, if two different monomers are joined in the same polymer material.
- Interpenetrating Polymer Networks (IPNs). This type are hydrogels that comprise two or more networks which are at least partially interlaced at a polymer scale but not covalently bound to each other. The network cannot

be separated unless chemical bonds are broken.[16,17] If we base on arrangement pattern, we can classify the different possible types of IPN on (Figure 3):

a) Sequential IPN: if the second polymeric component network is polymerised after the polymerisation of the first component network.

b) Simultaneously IPN: if it is prepared by a process in which both component networks are polymerised concurrently.

c) Semi-IPN: if only one component of the assembly is cross linked leaving the other in a linear form.

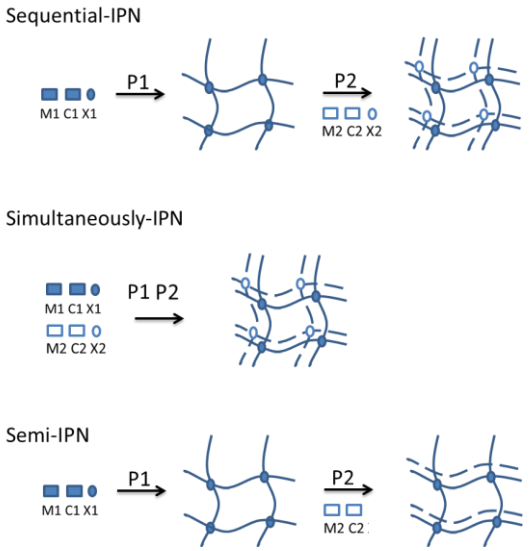

Figure 3. Schematic illustration of the different possible types of IPN based on arrangement pattern, where P=polymerisation, M=monomer, X=cross linker and C=initiator.

Responsive hydrogels are an interesting and modern type of materials that respond to an external stimulus changing some of their properties, leading in that way to intelligent hydrogels.[14,18,19] The response normally appears as a macroscopic change, for example varying the volume of the hydrogel when the water imbibed is released (Figure 4). Therefore, environmentally responsive hydrogels show radical variations in

their swelling degree because of the changes in their external conditions. This behaviour allows these materials to be applied for instance as controlled-drug delivery systems.[14]

The external stimuli can be:

- Physical, which includes mechanical stress, temperature, electric fields, magnetic fields and light.
- Chemical, which includes ionic factors, pH and chemical agents (playing with solvent/chains interactions).

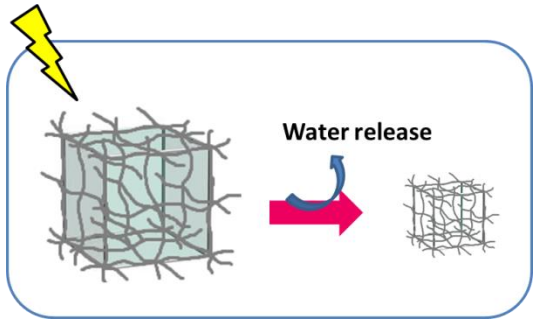

Figure 4. Scheme of the behaviour of a responsive hydrogel under the application of an external stimulus.

1.2.2. Hydrogel composites

New developments in composite hydrogels have been achieved due to the combination of novel advances, in chemical and biological fields, and the rising requirements in the biomedical sectors.[20]

Many times, the main aim of the composite formation is the enhancement of the mechanical properties. In this sense, Teramoto and co-workers developed a composite hydrogel based on fish gelatin modified with methacrylate groups, which was remarkably reinforced by adding an imogolite content of 2.0%.[21]

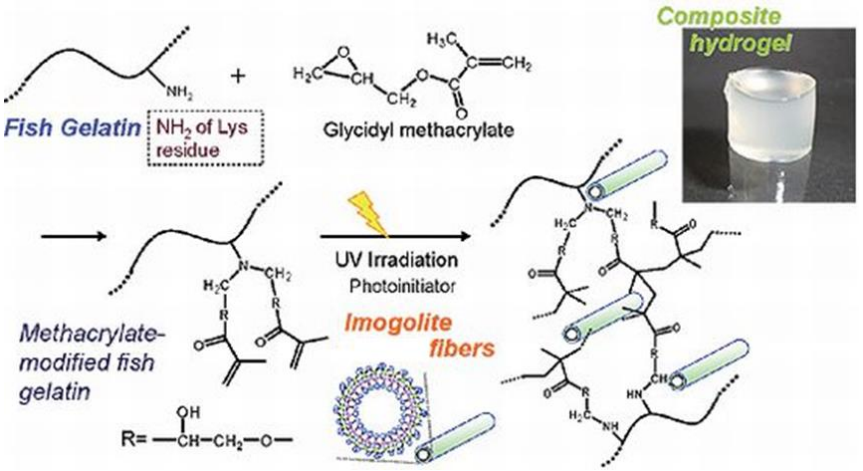

Figure 5. Preparation and photopolymerisation scheme of fish gelatin/imogolite composite hydrogel.[21]

However, other different improvements can also be achieved with the incorporation of any sort of nanofiller, obtaining nanocomposite hydrogels with diverse applications.[22,23]

Hydrogel composites based on carbon nanotubes have shown improved properties and potential applications in many fields.[24–26] This kind of materials have been even applied as energy storage devices.[27] One of the most recent examples is the construction of DNA-MWNT crosslinked hybrid hydrogels for tissue engineering.[28]

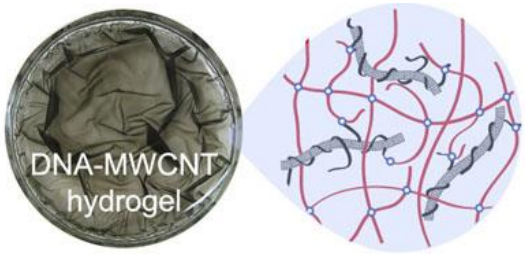

Figure 6. DNA-MWNT crosslinked hydrogel.[28]

Graphene has been considered the material of the future and research in graphene-based composites is being carried out strongly.

1.3. Graphene-based composite materials

1.3.1. Graphene

Graphene is a single layer of sp^2 hybridised carbon atoms with unique electrical, mechanical and thermal properties.[29] Since Geim and co-workers discovered the "thinnest known material" in 2004,[30] graphene is one of the most exciting materials which is being investigated nowadays.

Regarding the nanomaterial structure, graphene is a single-layer of graphite with sp^2 bonded carbon atoms arranged in a hexagonal lattice and with partially filled π-orbitals above and below the plane of the sheet (Figure 7). The lateral dimensions of graphene can vary from several nanometres to the macroscale. Few-layer graphene is a subset with between 2 and 5 well-defined and countable stacked graphene sheets of an extended lateral dimension. Multi-layer graphene consists of a number of sheets higher than 6, in which electronic structure is comparable to the graphite one.

There are two types of graphene edges: zigzag and armchair edges. Normally, all synthesised graphenes have a mixture of both types. However, the geometry of edges importantly affects the electronic structure.[31]

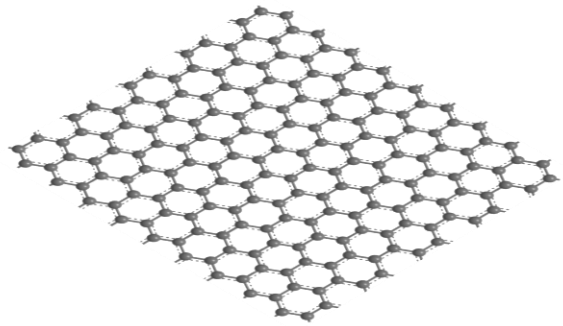

Figure 7. Single layer of graphene.

Obtaining a graphene sample of a large size with a perfect structure is very difficult. Depending mainly on the synthetic process and the conditions of preparation, the surface of graphene contains more or less defects which basically consist of structural imperfections and chemical impurities. These defects[32] influence the mechanical and transport properties of the sample.

1.3.1.1. Graphene fabrication

Since the first time that graphene samples were produced and investigated, many approaches to the synthesis of this material have been carried out, mainly guided by an end application. Graphene nanomesh has been, for instance, prepared to apply the nanomaterial in field-effect transistors operating at room temperature.[33] Nowadays, the preparation of graphene is more focused on industrially viable applications, which require large scale production and equilibrated costs. In this sense, it is important to get a balance between the cost and the quality of the final product.

The preparation methods can be divided in top-down and bottom-up approaches (Figure 8).[34] Top-down fabrication processes start from large structures and proceed to small scales. On the other hand, bottom-up approaches are done by starting with small items and building them up to larger functional creations. These two approaches cover the main graphene fabrication processes, starting from graphite in the case of the top-down techniques and from carbon precursors if we base on bottom-up processes.

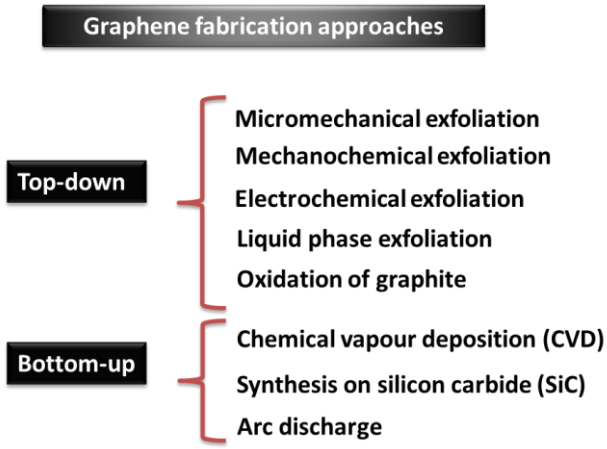

Figure 8. Scheme of the main graphene synthesis processes.

Micromechanical exfoliation of graphite: graphene sheets are separated from crystalline graphite. This approach allows separation of single-layer graphene sheets having an ordered structure.[30]

Mechanochemical exfoliation of graphite: in order to enhance the solubility of carbon nanostructures, some groups have used mechanochemical methods.[35] However, this methodology has also been successfully employed to exfoliate graphite with the use of ball-milling, a technique that is an effective way to achieve few-layer graphenes.[36,37]

Electrochemical exfoliation: this technique involves using graphite as an electrode and collecting the exfoliated material from the electrolyte solution. Sulphuric acid-potassium hydroxide solutions are mostly employed as electrolyte.[38] The resulting material has a mixture of different thicknesses of graphite flakes with few-layer graphene.

Liquid phase exfoliation: this method is based on the utilisation of surface-active organic liquids, using a layered structure of graphite and permitting the inclusion of molecules into the interlayer spaces.[39]

Oxidation of graphite: graphite is exfoliated using chemical oxidisers. Inner graphite layers are oxidised as a result of the action of strong oxidisers (oxygen, halogens,

etc.).[40] The obtained graphene oxide sheets can be reduced afterwards utilising chemicals such as hydrogen and hydrazine, but the properties of the final product are different from pristine graphene. The most used approach is the Hummers method.[41]

Chemical vapour deposition (CVD): graphene can also be obtained using high temperature pyrolysis of carbon containing gases. The optimum conditions for CVD growth depend on the metal, pressure, temperature and carbon exposure.[42] Large quantities of graphene are obtained by using this approach, but the main disadvantage is the high costs of production.

Synthesis on silicon carbide (SiC): this technique consists of the sublimation of silicon from the SiC surface followed by the graphitisation of the excess carbon atoms, obtaining the growth of a graphene film on the surface of a SiC crystal.[43]

Arc discharge: graphene can be also synthesised by direct current arc-discharge evaporation of pure graphite electrodes in a variety of gases such as CO_2, H_2, or air.[44]

1.3.1.2. Graphene properties

The above commented graphene structure is what enables the nanomaterial to break so many records in terms of strength, electron and heat conduction, among others.

Regarding the mechanical properties, the intrinsic strength of graphene is one of the highest known. This fact was demonstrated by Lee and co-workers when they measured the Young´s Modulus of a single-layer graphene using an atomic force microscope.[45]

With respect to the electronic properties, graphene is a semimetal with zero bandgap, as it has two atoms per unit cell, resulting in two conical points (K and K´) in the Brillouin zone.[46] In that points, valence and conductance bands cross, and electron energy is linearly dependent on the wave vector in that region, which is also called Dirac point (Figure 9).

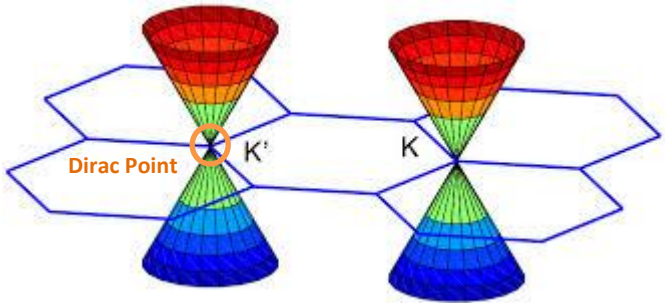

Figure 9. Schematic representation of conic energy bands in a single-layer graphene.

Graphene exhibits the highest room-temperature carrier mobility measured for any material,[47] with its charge carriers showing very high intrinsic mobility, having zero effective mass and being able to move some microns without being scattered.[48] However, electrical properties of functionalised graphene depend on some factors such as covalent bonding, adsorption or lattice incorporation, among others.[49]

Moreover, graphene has a high thermal conductivity, even 25 times that of silicon.[50] However, this property depends on the size of the sheet and it is very sensitive to the thickness of the material.

Finally, regarding the optical properties, graphene is able to absorb a rather large 2.3 % of white light,[51] even although it is only 1 atom thick. This fact is related to the mentioned electronic properties, as electrons act like massless charge carriers.

Due to the excellent properties just commented above, graphene is applied in a wide range of interesting fields[52,53,54] such as photonics and optoelectronics, energy storage, or biological ones among many others.

1.3.1.3. Graphene characterisation

The confirmation of the final structure, also after graphene functionalisation,[55] is necessary regarding the specific final applications of the nanostructure.[56] The possible modifications on graphene sheets can be characterised in a reliable way by using techniques such as thermogravimetric analysis (TGA), Raman spectroscopy, transmission electron microscopy (TEM), or X-ray photoelectron spectroscopy (XPS) among others.[29,57]

1.3.2. Graphene-based composites

Materials play an important role in technological fields such as medical preparations, sensors, computation, etc. It is always necessary to create novel materials with improved features to make our daily lives easier, satisfying human needs. Among all types of materials, composites have been studied in past few decades, and especially in the last years, the graphene-based ones.[58,59]

In that sense, lot of works based on graphene composites have been recently published,[60,61] for instance in resonance imaging and drug delivery fields.[62] An interesting example is the work carried out by Li and co-workers about antibody-modified graphene films. They achieve films with extreme sensitivity to circulating tumour cells (CTCs), due to the synergistic topographic interactions between cells and biointerfaces.[63]

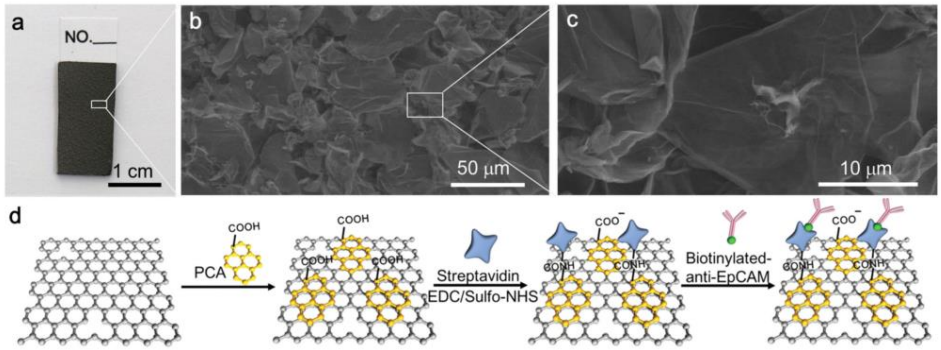

Figure 10. a) A photograph of the final film, which was used to capture CTCs directly from clinical blood samples. b) and c) SEM images of the films. d) Functionalisation of reduced graphene oxide films.[63]

However, most of the published works deal with **graphene-based polymer composites**,[64–66] because of the properties that those polymers provide to the final material. Therefore, polymer matrix nanocomposites with graphene and its derivatives as fillers have demonstrated a good potential for influential applications as electronics,

green energy, aerospace, etc. For instance, Wei and co-workers built electrodes with printed graphene inks for batteries.[67] Another interesting and very recent work is about a series of graphene-based acrylonitrile-butadiene-styrene and poly (lactic acid) polymer composites which were tested with a commercially available 3D printer.[68]

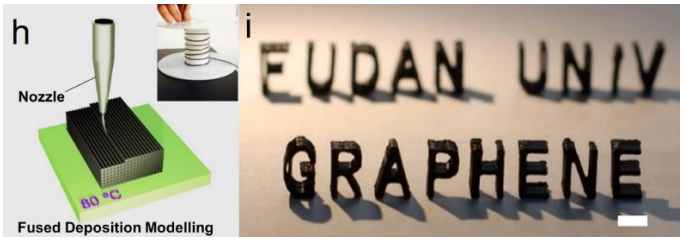

Figure 11. Schematic illustration of fused deposition modelling 3D printing process (inset is the graphene-based filament) and 3D printed model. Scale bar : 1cm.[68]

Nevertheless, one of the most interesting materials which are framed in graphene-based polymer composites are the hydrogel.

1.4. Graphene-based hydrogel composites

Due to its awesome properties, graphene has been used as filler in an ample range of new materials in order to improve its features. In particular, the development of scaffolds based on graphene-hydrogel composites is being largely investigated nowadays.[69,70]

Many efforts have been made to fabricate graphene-based hydrogel composites with enhanced properties, most of them using graphene oxide (GO),[71,72] graphene oxide peroxide (GOP),[73] or even using reduced graphene oxide (rGO),[70,74] with a polymer or a mixture of polymers regarding the final applications. However, GO sheets are electrically insulating. Because of this fact, pristine graphene is the perfect candidate as nanofiller. In addition, most of those works do not demonstrate the structural role of the nanomaterial.[75]

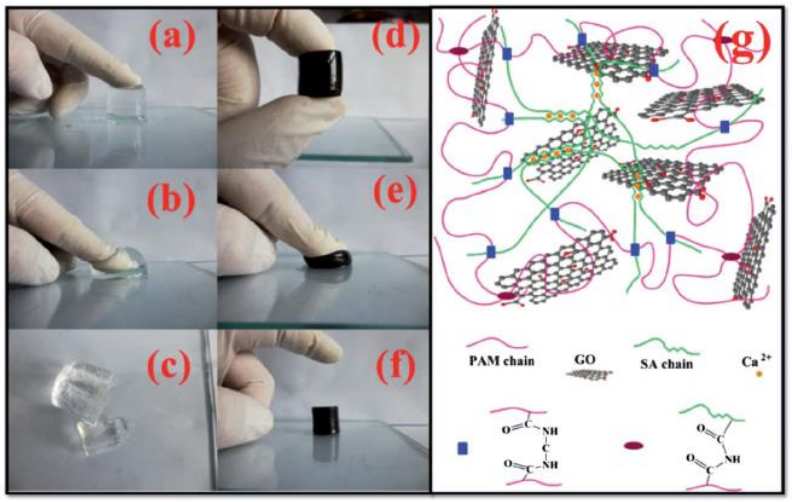

Figure 12. Photographs Scheme of GO-based composite hydrogels.[71]

There are almost no examples in literature of pristine graphene-based hydrogels,[76] mainly due to the difficulties to obtain pristine graphene aqueous solutions. Dispersing pristine graphene in polymer or solvents (especially in water) is a challenge because of

restacking of the sheets, which is caused by the strong intersheet van der Waals forces. It is even harder to achieve dispersions of pristine graphene in water in a simple, scalable and cheap way.

Das and co-workers have proposed that polyacrylamide (PAm) chains entangle with PAm-stabilised graphene sheets through physisorption and noncovalent absorption, and lead to the formation of a network.[77] Moreover, Alzari and co-authors reported a stimuli-responsive polymer hydrogel containing partially exfoliated graphite,[78] and Toumia and co-workers[79] developed a "soft" confinement of graphene in hydrogel matrixes. The final graphene/poly(vinyl alcohol) (PVA)/ poly(N-Isopropyl Acrylamide) (PNIPAm) constructions showed an active role in drug delivery, which is one of the most exploited fields regarding the use of hydrogel composites. A recent example is the work developed by Servant and co-workers,[80] who demonstrated the *in vivo* capacity of the implanted electro-responsive graphene polymer composite for pulsatile drug release. The incorporation of graphene improved the drug release and also eliminated the "resistive heating" from the hydrogel.

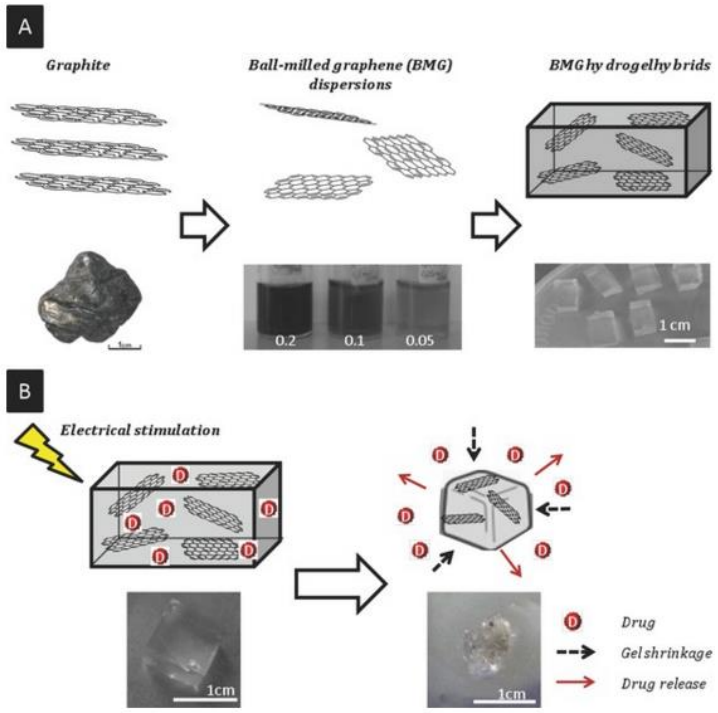

Figure 13. Electro-responsive graphene/pMAAc hydrogel composites for "on-demand" drug delivery.[80]

In this first chapter we have given a brief overview about composite materials, focusing in hydrogels and graphene in a more specific way, as they are the main materials used in this thesis. In the next chapters, we will go in depth to explain and show more specific examples from literature.

1.5. References

(1) *Handbook of Ceramic Composites*; Narottam, P. B., Ed.; 2006.

(2) Basics of Metal Matrix Composites. In *Metal Matrix Composites. Custom-made Materials for Automative and Aerospace Engineering*; 2006; p. 54.

(3) Work, W.J.; Horie, K.; Hess, M.; Stepto, R. F. T. Definition of Terms Related to Polymer Blends, Composites, and Multiphase Polymeric Materials (IUPAC Recommendations 2004). *Pure Appl. Chem.* **2004**, *76*, 1985–2007.

(4) Paul, D. R.; Robeson, L. M. Polymer Nanotechnology: Nanocomposites. *Polymer* **2008**, *49*, 3187–3204.

(5) Song, E.; Choi, J.-W. Conducting Polyaniline Nanowire and Its Applications in Chemiresistive Sensing. *Nanomaterials* **2013**, *3*, 498–523.

(6) Bae, S. H.; Lee, Y.; Sharma, B. K.; Lee, H. J.; Kim, J. H.; Ahn, J. H. Graphene-Based Transparent Strain Sensor. *Carbon N. Y.* **2013**, *51*, 236–242.

(7) Shi, Y.; Peng, L.; Ding, Y.; Zhao, Y.; Yu, G. Nanostructured Conductive Polymers for Advanced Energy Storage. *Chem. Soc. Rev.* **2015**, *44*, 6684–6696.

(8) Jagur-Grodzinski, J. Polymeric Gels and Hydrogels for Biomedical and Pharmaceutical Applications. *Polym. Adv. Technol.* **2010**, *21*, 27–47.

(9) Guilherme, M. R.; Aouada, F. a.; Fajardo, A. R.; Martins, A. F.; Paulino, A. T.; Davi, M. F. T.; Rubira, A. F.; Muniz, E. C. Superabsorbent Hydrogels Based on Polysaccharides for Application in Agriculture as Soil Conditioner and Nutrient Carrier: A Review. *Eur. Polym. J.* **2015**, *72*, 365–385.

(10) Ma, G.; Yang, D.; Li, Q.; Wang, K.; Chen, B.; Kennedy, J. F.; Nie, J. Injectable Hydrogels Based on Chitosan Derivative/polyethylene Glycol dimethacrylate/N,N-Dimethylacrylamide as Bone Tissue Engineering Matrix. *Carbohydr. Polym.* **2010**, *79*, 620–627.

(11) Santo, V. E.; Frias, A. M.; Carida, M.; Cancedda, R.; Gomes, M. E.; Mano, J. F.; Reis, R. L. Carrageenan-Based Hydrogels for the Controlled Delivery of PDGF-BB in

Bone Tissue Engineering Applications. *Biomacromolecules* **2009**, *10*, 1392–1401.

(12) Meikle, S. T.; Standen, G.; Salvage, J.; De Santis, R.; Nicolais, L.; Ambrosio, L.; Santin, M. Synthesis and Characterization of Soybean-Based Hydrogels with an Intrinsic Activity on Cell Differentiation. *Tissue Eng. Part A* **2012**, *18*, 1932–1939.

(13) Deligkaris, K.; Tadele, T. S.; Olthuis, W.; van den Berg, A. Hydrogel-Based Devices for Biomedical Applications. *Sensors Actuators B Chem.* **2010**, *147*, 765–774.

(14) Merino, S.; Martín, C.; Kostarelos, K.; Prato, M.; Vázquez, E. Nanocomposite Hydrogels: 3D Polymer–Nanoparticle Synergies for On-Demand Drug Delivery. *ACS Nano* **2015**, *9*, 4686–4697.

(15) Ullah, F.; Bisyrul, M.; Javed, F.; Akil, H. Classification, Processing and Application of Hydrogels: A Review. *Mater. Sci. Eng.* **2015**, *57*, 414–433.

(16) Shivashankar, M.; Mandal, B. K. A Review on Interpenetrating Polymer Network. *Int. J. Pharm. Sci.* **2012**, *4*, 1–7.

(17) Dragan, E. S. Design and Applications of Interpenetrating Polymer Network Hydrogels. A Review. *Chem. Eng. J.* **2014**, *243*, 572–590.

(18) Samchenko, Y.; Ulberg, Z.; Korotych, O. Multipurpose Smart Hydrogel Systems. *Adv. Colloid Interface Sci.* **2011**, *168*, 247–262.

(19) Green, R. a.; Hassarati, R. T.; Goding, J. a.; Baek, S.; Lovell, N. H.; Martens, P. J.; Poole-Warren, L. a. Conductive Hydrogels: Mechanically Robust Hybrids for Use as Biomaterials. *Macromol. Biosci.* **2012**, *12*, 494–501.

(20) Zhao, F.; Yao, D.; Guo, R.; Deng, L.; Dong, A.; Zhang, J. Composites of Polymer Hydrogels and Nanoparticulate Systems for Biomedical and Pharmaceutical Applications. *Nanomaterials* **2015**, *5*, 2054–2130.

(21) Teramoto, N.; Hayashi, A.; Yamanaka, K.; Sakiyama, A.; Nakano, A.; Shibata, M. Preparation and Mechanical Properties of Photo-Crosslinked Fish Gelatin/Imogolite Nanofiber Composite Hydrogel. *Materials* **2012**, *5*, 2573–2585.

(22) Thoniyot, P.; Tan, M. J.; Karim, A. A.; Young, D. J.; Loh, X. J. Nanoparticle-

Hydrogel Composites: Concept, Design, and Applications of These Promising, Multi-Functional Materials. *Adv. Sci.* **2015**, *2*, 1400010–1400023.

(23) Schexnailder, P.; Schmidt, G. Nanocomposite Polymer Hydrogels. *Colloid Polym. Sci.* **2009**, *287*, 1–11.

(24) Yang, Z.; Cao, Z.; Sun, H.; Li, Y. Composite Films Based on Aligned Carbon Nanotube Arrays and a poly(N-Isopropyl Acrylamide) Hydrogel. *Adv. Mater.* **2008**, *20*, 2201–2205.

(25) Gui, X.; Cao, A.; Wei, J.; Li, H.; Jia, Y.; Li, Z.; Fan, L.; Wang, K.; Zhu, H.; Wu, D. Soft, Highly Conductive Nanotube Compressibility. *ACS Nano* **2010**, *4*, 2320–2326.

(26) Cirillo, G.; Hampel, S.; Spizzirri, U. G.; Parisi, O. I.; Picci, N.; Iemma, F. Carbon Nanotubes Hybrid Hydrogels in Drug Delivery: A Perspective Review. *Biomed Res. Int.* **2014**, 825017, DOI:10.1155/2014/825017.

(27) Chen, P.Y.; Dorval Courchesne, N.M.; Hyder, M.N.; Qi, J.; Belcher, A.M.; Hammond, P. T. Carbon Nanotube-Polyaniline Core-Shell Nanostructured Hydrogel for Electrochemical Energy Storage. *RSC Adv.* **2015**, *5*, 37970–37977.

(28) Zinchenko, A.; Taki, Y.; Sergeyev, V. G.; Murata, S. DNA-Assisted Solubilization of Carbon Nanotubes and Construction of DNA-MWCNT Cross-Linked Hybrid Hydrogels. *Nanomaterials* **2015**, *5*, 270–283.

(29) Cooper, D. R.; D'Anjou, B.; Ghattamaneni, N.; Harack, B.; Hilke, M.; Horth, A.; Majlis, N.; Massicotte, M.; Vandsburger, L.; Whiteway, E.; et al. Experimental Review of Graphene. *ISRN Condens. Matter Phys.* **2012**, 501686, DOI: 10.5402/2012/501686.

(30) Novoselov, K. S.; Geim, a K.; Morozov, S. V; Jiang, D.; Zhang, Y.; Dubonos, S. V; Grigorieva, I. V; Firsov, a a. Electric Field Effect in Atomically Thin Carbon Films. *Science* **2004**, *306*, 666–669.

(31) Enoki, T.; Fujii, S.; Takai, K. Zigzag and Armchair Edges in Graphene. *Carbon N. Y.* **2012**, *50*, 3141–3145.

(32) Banhart, F.; Kotakoski, J.; Krasheninnikov, A. V. Structural Defects in Graphene.

ACS Nano **2011**, *5*, 26–41.

(33) Bai, J.; Zhong, X.; Jiang, S.; Huang, Y.; Duan, X. Graphene Nanomesh. *Nat. Nanotechnol.* **2010**, *5*, 190–194.

(34) Tour, J. M. Top-down versus Bottom-up Fabrication of Graphene-Based Electronics. *Chem. Mater.* **2014**, *26*, 163–171.

(35) Ikeda, A.; Tanaka, Y.; Nobusawa, K.; Kikuchi, J. Solubilization of Single-Walled Carbon Nanotubes by Supramolecular Complexes of Barbituric Acid and Triaminopyrimidines. *Langmuir* **2007**, *23*, 10913–10915.

(36) Zhao, W.; Fang, M.; Wu, F.; Wu, H.; Wang, L.; Chen, G. Preparation of Graphene by Exfoliation of Graphite Using Wet Ball Milling. *J. Mater. Chem.* **2010**, *20*, 5817–5819.

(37) León, V.; Quintana, M.; Herrero, M. A.; Fierro, J. L. G.; de la Hoz, A.; Prato, M.; Vázquez, E. Few-Layer Graphenes from Ball-Milling of Graphite with Melamine. *Chem. Commun.* **2011**, *47*, 10936–10938.

(38) Su, C.; Lu, A.; Xu, Y.; Chen, F.; Khlobystov, A. N.; Li, L. High-Quality Thin Graphene Films from Fast Electrochemical Exfoliation. *ACS Nano* **2011**, *5*, 2332–2339.

(39) Lotya, M.; Hernandez, Y.; King, P. J.; Smith, R. J.; Nicolosi, V.; Karlsson, L. S.; Blighe, F. M.; De, S.; Wang, Z.; McGovern, I. T.; et al. Liquid Phase Production of Graphene by Exfoliation of Graphite in Surfactant/water Solutions. *J. Am. Chem. Soc.* **2009**, *131*, 3611–3620.

(40) Stankovich, S.; Dikin, D. a.; Piner, R. D.; Kohlhaas, K. a.; Kleinhammes, A.; Jia, Y.; Wu, Y.; Nguyen, S. T.; Ruoff, R. S. Synthesis of Graphene-Based Nanosheets via Chemical Reduction of Exfoliated Graphite Oxide. *Carbon N. Y.* **2007**, *45*, 1558–1565.

(41) Hummers, W. S.; Offeman, R. E. Preparation of Graphitic Oxide. *J. Am. Chem. Soc.* **1958**, *80*, 1339–1339.

(42) Zhang, Y.; Zhang, L.; Zhou, C. Review of Chemical Vapor Deposition of Graphene and Related Applications. *Acc. Chem. Res.* **2013**, *46*, 2329–2339.

(43) Sutter, P. Epitaxial Graphene: How Silicon Leaves the Scene. *Nat. Mater.* **2009**,

8, 171–172.

(44) Wu, Z. S.; Ren, W.; Gao, L.; Zhao, J.; Chen, Z.; Liu, B.; Tang, D.; Yu, B.; Jiang, C.; Cheng, H. M. Synthesis of Graphene Sheets with High Electrical Conductivity and Good Thermal Stability by Hydrogen Arc Discharge Exfoliation. *ACS Nano* **2009**, *3*, 411–417.

(45) Lee, C.; Wei, X.; Kysar, J. W.; Hone, J. Of Monolayer Graphene. **2008**, *321*, 385–388.

(46) Novoselov, K. S.; McCann, E.; Morozov, S.V.; Fal´ko, V.I.; Katsnelson, I.; Zeitler, U.; Jiang, D.; Schedin, F.; Geim, A. K. Unconventional Quantum Hall Effect and Berry´s Phase of 2π in Bilayer Graphene. *Nat. Phys.* **2006**, *2*, 177–180.

(47) Du, X.; Skachko, I.; Barker, A.; Andrei, E. Y. Approaching Ballistic Transport in Suspended Graphene. *Nat. Nanotechnol.* **2008**, *3*, 491–495.

(48) Geim, a. K.; Novoselov, K. S. The Rise of Graphene. *Nat. Mater.* **2007**, *6*, 183–191.

(49) Sreeprasad, T. S.; Berry, V. How Do the Electrical Properties of Graphene Change with Its Functionalization? *Small* **2013**, *9*, 341–350.

(50) Balandin, A. a.; Ghosh, S.; Bao, W.; Calizo, I.; Teweldebrhan, D.; Miao, F.; Lau, C. N. Superior Thermal Conductivity of Single-Layer Graphene. *Nano Lett.* **2008**, *8*, 902–907.

(51) Nair, R. R.; Blake, P.; Grigorenko, a. N.; Novoselov, K. S.; Booth, T. J.; Stauber, T.; Peres, N. M. R.; Geim, a. K. Fine Structure Constant Defines Visual Transperency of Graphene. *Science* **2008**, *320*, 1308.

(52) Guo, S.; Dong, S. Graphene Nanosheet: Synthesis, Molecular Engineering, Thin Film, Hybrids, and Energy and Analytical Applications. *Chem. Soc. Rev.* **2011**, *40*, 2644–2672.

(53) Ferrari, A. C.; Bonaccorso, F.; Falko, V.; Novoselov, K. S.; Roche, S.; Bøggild, P.; Borini, S.; Koppens, F.; Palermo, V.; Pugno, N.; et al. Science and Technology Roadmap for Graphene, Related Two-Dimensional Crystals, and Hybrid Systems. *Nanoscale*

2014, *7*, 4598–4810.

(54) Geim, A. K. Nobel Lecture: Random Walk to Graphene. *Rev. Mod. Phys.* **2011**, *83*, 851–862.

(55) Yan, L.; Zheng, Y. B.; Zhao, F.; Li, S.; Gao, X.; Xu, B.; Weiss, P. S.; Zhao, Y. Chemistry and Physics of a Single Atomic Layer: Strategies and Challenges for Functionalization of Graphene and Graphene-Based Materials. *Chem. Soc. Rev.* **2012**, *41*, 97–114.

(56) Wick, P.; Louw-Gaume, A. E.; Kucki, M.; Krug, H. F.; Kostarelos, K.; Fadeel, B.; Dawson, K. a.; Salvati, A.; Vázquez, E.; Ballerini, L.; et al. Classification Framework for Graphene-Based Materials. *Angew. Chemie Int. Ed.* **2014**, *53*, 7714–7718.

(57) Allen, M. J.; Tung, V. C.; Kaner, R. B. Honeycomb Carbon: A Review of Graphene. *Chem. Rev.* **2010**, *110*, 132–145.

(58) Goenka, S.; Sant, V.; Sant, S. Graphene-Based Nanomaterials for Drug Delivery and Tissue Engineering. *J. Control. Release* **2014**, *173*, 75–88.

(59) Li, Z.; Liu, Z.; Sun, H.; Gao, C. Superstructured Assembly of Nanocarbons: Fullerenes, Nanotubes, and Graphene. *Chem. Rev.* **2015**, *115*, 7046–7117.

(60) Dhand, V.; Rhee, K. Y.; Ju Kim, H.; Ho Jung, D. A Comprehensive Review of Graphene Nanocomposites: Research Status and Trends. *J. Nanomater.* **2013**, 763953, DOI: 10.1155/2013/763953.

(61) Papageorgiou, D. G.; Kinloch, I. A.; Young, R. J. Graphene / Elastomer Nanocomposites. *Carbon N. Y.* **2015**, *95*, 460–484.

(62) Wang, G.; Chen, G.; Wei, Z.; Dong, X.; Qi, M. Multifunctional Fe 3 O 4 / Graphene Oxide Nanocomposites for Magnetic Resonance Imaging and Drug Delivery. *Mater. Chem. Phys.* **2013**, *141*, 997–1004.

(63) Li, Y.; Lu, Q.; Liu, H.; Wang, J.; Zhang, P.; Liang, H.; Jiang, L.; Wang, S. Antibody-Modified Reduced Graphene Oxide Films with Extreme Sensitivity to Circulating Tumor Cells. *Adv. Mater.* **2015**, *27*, 6848–6854.

(64) Kim, H.; Abdala, A. a.; Macosko, C. W. Graphene/Polymer Nanocomposites. *Macromolecules* **2010**, *43*, 6515–6530.

(65) Mittal, G.; Dhand, V.; Rhee, K. Y.; Park, S.-J.; Lee, W. R. A Review on Carbon Nanotubes and Graphene as Fillers in Reinforced Polymer Nanocomposites. *J. Ind. Eng. Chem.* **2014**, *21*, 11–25.

(66) Young, R. J.; Kinloch, I. a.; Gong, L.; Novoselov, K. S. The Mechanics of Graphene Nanocomposites: A Review. *Compos. Sci. Technol.* **2012**, *72*, 1459–1476.

(67) Wei, D.; Andrew, P.; Yang, H.; Jiang, Y.; Li, F.; Shan, C.; Ruan, W.; Han, D.; Niu, L.; Bower, C.; et al. Flexible Solid State Lithium Batteries Based on Graphene Inks. *J. Mater. Chem.* **2011**, *21*, 9762–9767.

(68) Wei, X.; Li, D.; Jiang, W.; Gu, Z.; Wang, X.; Zhang, Z.; Sun, Z. 3D Printable Graphene Composite. *Sci. Rep.* **2015**, *5*, 11181–11188.

(69) Das, T. K.; Prusty, S. Graphene-Based Polymer Composites and Their Applications. *Polym. Plast. Technol. Eng.* **2013**, *52*, 319–331.

(70) Hou, C.; Zhang, Q.; Li, Y.; Wang, H. Graphene–polymer Hydrogels with Stimulus-Sensitive Volume Changes. *Carbon N. Y.* **2012**, *50*, 1959–1965.

(71) Fan, J.; Shi, Z.; Lian, M.; Li, H.; Yin, J. Mechanically Strong Graphene Oxide/sodium Alginate/polyacrylamide Nanocomposite Hydrogel with Improved Dye Adsorption Capacity. *J. Mater. Chem. A* **2013**, *1*, 7433–7443.

(72) Cong, H.-P.; Wang, P.; Yu, S.-H. Stretchable and Self-Healing Graphene Oxide–Polymer Composite Hydrogels: A Dual-Network Design. *Chem. Mater.* **2013**, *25*, 3357–3362.

(73) Liu, J.; Chen, C.; He, C.; Zhao, J.; Yang, X.; Wang, H. Synthesis of Graphene Peroxide and Its Application in Fabricating Super Extensible and Highly Resilient Nanocomposite Hydrogels. *ACS Nano* **2012**, *6*, 8194–8202.

(74) Xu, Y.; Lin, Z.; Huang, X.; Liu, Y.; Huang, Y.; Duan, X. Flexible Solid-State Supercapacitors Based on Three-Dimensional. *ACS Nano* **2013**, *7*, 4042–4049.

(75) Xu, Y.; Sheng K.; Li, C.; Shi, G. Self-Assembled Graphene Hydrogel via a One-Step Hydrothermal Process. *ACS Nano* **2010**, *4*, 4324–4330.

(76) Fan, J.; Shi, Z.; Wang, J.; Yin, J. Glycidyl Methacrylate-Modi Fi Ed Gum Arabic Mediated Graphene Exfoliation and Its Use for Enhancing Mechanical Performance of Hydrogel. *Polymer* **2013**, *54*, 3921–3930.

(77) Das, S.; Irin, F.; Ma, L.; Bhattacharia, S. K.; Hedden, R. C.; Green, M. J. Rheology and Morphology of Pristine Graphene / Polyacrylamide Gels. *ACS Appl. Mater. Interfaces* **2013**, *5*, 8633–8640.

(78) Alzari, V.; Mariani, A.; Monticelli, O.; Valentini, L.; Nuvoli, D.; Piccinini, M.; Scognamillo, S.; Bon, silvia bittolo; Illescas, J. Stimuli-Responsive Polymer Hydrogels Containing Partially Exfoliated Graphite. *J. Polym. Sci. Part a-Polymer Chem.* **2010**, *48*, 5375–5381.

(79) Toumia, Y.; Orlanducci, S.; Basoli, F.; Licoccia, S.; Paradossi, G. "Soft" Confinement of Graphene in Hydrogel Matrixes. *J. Phys. Chem. B* **2015**, *119*, 2051–2061.

(80) Servant, A.; Leon, V.; Jasim, D.; Methven, L.; Limousin, P.; Vazquez Fernandez-Pacheco, E.; Prato, M.; Kostarelos, K. Graphene-Based Electroresponsive Scaffolds as Polymeric Implants for on-Demand Drug Delivery. *Adv. Healthc. Mater.* **2014**, *3*, 1334–1343.

Chapter 2

Graphene-based polyacrylamide hydrogels

2.1. Introduction

Conventional hydrogels have proved to be decisive in regenerative medicine and tissue engineering for decades.[1,2] However, current synthetic systems with designed stimuli-response properties are encouraging the study and the possible applications of new hydrogels in medicine. Perhaps the most addressed application of smart hydrogels in that field is related to drug delivery. Our group has recently reviewed how nanoparticles within hydrogels may exhibit synergistic interactions ending up in promising platforms for on-demand drug delivery or self-healable structures.[3]

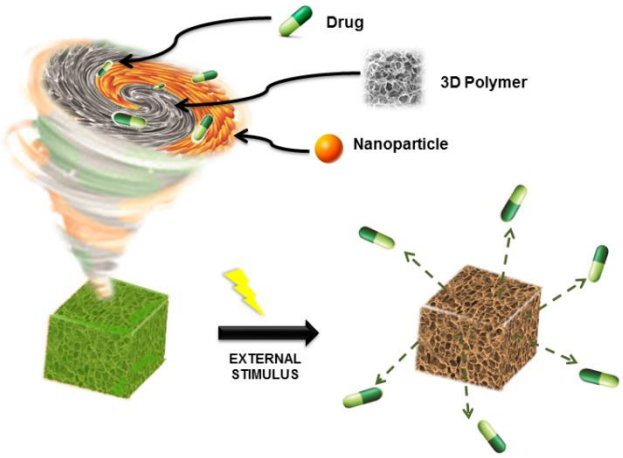

Figure 1. Scheme of the 3D polymer-nanocomposite synergy for on-demand drug delivery applications.[3]

On the other hand, procedures for culturing cells are becoming even more needed in order to study the physiology and the growth of cells, in tissue replacement studies. Natural and synthetic hydrogels have become popular as 3D scaffolds for encapsulating cells. Hydrogels are a notably attractive material to make new synthetic extracellular matrix analogues due to their ability to mimic the nature of soft tissues.[4]

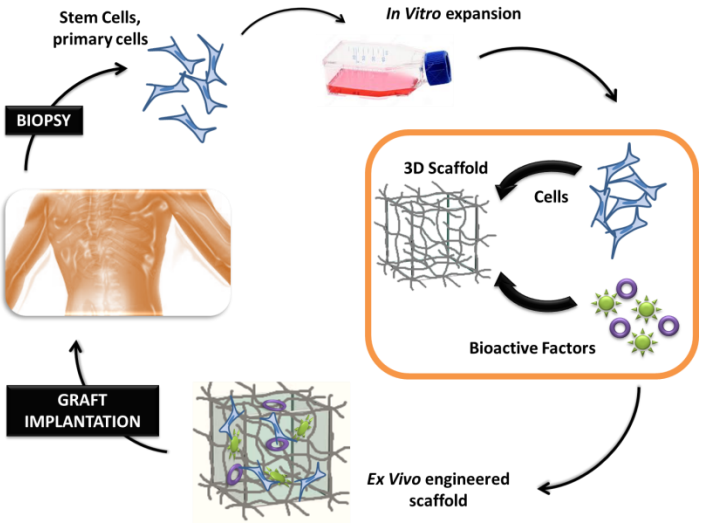

Figure 2. 3D scaffolds for tissue engineering applications.

Hydrogels can be obtained from a wide range of materials, presenting an extending spectrum of mechanical and chemical properties. However, most of these systems have some disadvantages: high cost, limitations that deal with the prototyping techniques used for hydrogel creation[5] or low mechanical strength among others.

Over the last years there has been a growing interest in reinforcing polymeric hydrogels with nanosized fillers to improve and adequate their often poor mechanical consistence. Fortunately, the nanofillers embedded in a cross-linked polymer network not only stiffen and toughen the system, but can provide novel features, depending on the filler characteristics (electrical conductivity, a specific absorption profile, etc.). Bearing this in mind, one could expect upgraded advantages of hydrogel nanocomposites in medicine, combining some of these features in a single system.

As already introduced in Chapter 1 of this thesis, one of the nanostructures that is being more thoroughly studied nowadays is graphene, the fascinating 2D sp^2-bonded monoatomic carbon sheet.

Many efforts have been made to fabricate graphene-based polymer nanocomposites with enhanced properties, mainly using graphene oxide (GO),[6,7]

graphene oxide peroxide (GOP),[8] or even reduced graphene(rGO) from GO.[9,10] However, most of them do not go into detail about the role of the nanomaterial into the network,[11] moreover GO sheets are insulating and its electronic properties differ from those of graphene. The introduction of pristine graphene as nanofiller is a challenging task.

As the hydrogel formation takes place in aqueous media, the inclusion of nanostructured fillers is in principle limited to water soluble/dispersible entities. Ideally, the creation of graphene-containing polymer hydrogels should occur via water suspensions of the filler in which the hydrogel is formed. For that reason, a stabilisation of graphene sheets in water is crucial. In fact, mainly due to those difficulties, there are almost no examples in literature of pristine graphene-based hydrogels.[12,13]

With the latest advances in graphene research, one can find a small handful of works, recently reported, which actually address this conceptual approach from top-down cleavage of graphite. Das and co-workers[14] manufactured polyacrylamide (PAm) hydrogel nanocomposites by pre-dispersion of graphite in water *ex situ* with commercial PAm and subsequent polymerisation of fresh acrylamide. In another work, Toumia and co-workers[15] dispersed graphite in an aqueous solution of a commercial amphiphilic surfactant containing aromatic moieties of polyethylene glycol 2,4,6-tris(1-phenylethyl)-phenyl ether methacrylate (PEG-PEPEMA) which was chemically grafted to a poly(vinyl alcohol) (PVA) hydrogel network (Figure 3).

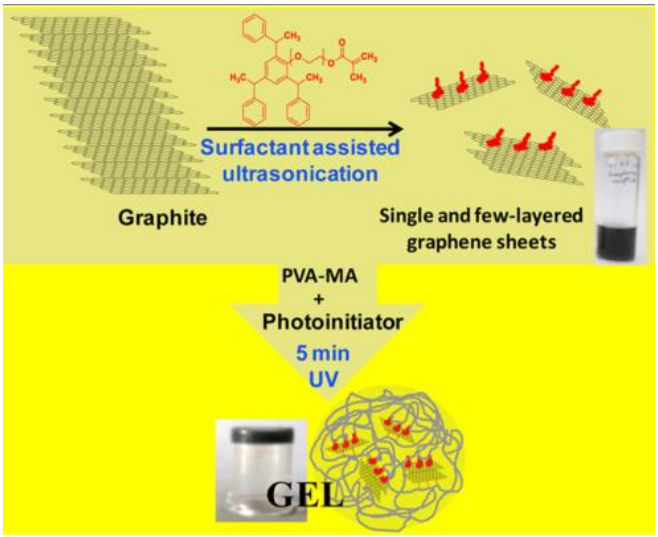

Figure 3. Synthesis scheme of the graphene-based gels developed by Toumia and co-workers.[15]

The common features in these works are the mechanical cleavage of graphite by aid of aqueous surfactants, polymers or proteins in the presence of strong and prolonged ultrasounds treatment and thorough centrifugation cycles to isolate stable few-layer graphene sheets from the remaining graphite. In contrast, we have developed in our laboratories a facile graphite exfoliation method using ball-milling with an abundant laboratory reagent: melamine.[16] Taking advantage of this aqueous graphene dispersion, our group recently reported the preparation of hydrogel nanocomposites made of poly(methacrylic acid), as electroresponsive drug delivery systems.[13]

As conclusion of this brief introduction, we could say that graphene-based hydrogels are promising materials for medicine. Although much work has been done to cover most of the current necessities, a lot of additional research has to be done from now on to improve previous results and cover future demands.

2.2. Objectives

Polymeric hydrogel materials have represented a significant invention in last decades, considering for example the development of the first examples of systems capable of responding to the application of an external stimulus. However, this kind of materials could be applied in a wide range of fields, if their excellent basic features are improved by forming, for instance, nanocomposite hydrogels.

The purpose of the present work is to provide new insights into the study of smart nanocomposite hydrogels based on graphene prepared by a mechanochemical approach, in order to achieve new features and synergies.

In order to accomplish our goal, we will use our graphene prepare by ball-milling to create and characterise new polyacrylamide-based hydrogel networks. Moreover, we will investigate in more detail some skipped aspects up to date, regarding for instance the structural role of the nanomaterial into the polymer network.

Different possible applications of the final materials will be also studied and described, such as stimuli-responsive systems, strain gauges or 3D scaffolds for cell culture.

2.3. Results and discussion

2.3.1. Synthesis of the hydrogels

Graphene-based hydrogels were formed in a "one-pot" way using an *in situ* radical polymerisation of acrylamide (Am). Figure 4 shows the scheme of the process. A chemically cross-linked pure polyacrylamide (Pam) gel (**AM**) and a series of chemically cross-linked graphene-loaded PAm gels (**AMGX**, being **X** the graphene concentration used in mg/ml) were synthesised. Pure PAm hydrogel was prepared using acrylamide (Am), *N,N´*-methylenebisacrylamide (MBA) as cross-linker and potassium peroxodisulfate (KPS) as initiator. Am was initially dissolved in doubly deionised water (200 mg/ml) with the MBA (0.2 mg/ml), and the KPS (0.4 mg/ml) was finally added.

In the case of the graphene-based hydrogels formation, the most important advance is the creation of the hydrogels using as reaction solvent a water suspension of the filler. Therefore, a similar process as the above described, was followed to synthesise the composite, adding in this case all the reactants to the aqueous graphene dispersion. The graphene content was varied from 0 mg/ml (**AM**) to 8.5 mg/ml (**AMG8.5**).

The different solutions were homogenised and let to polymerise at 75 ^{o}C for 1 hour (Figure 4).

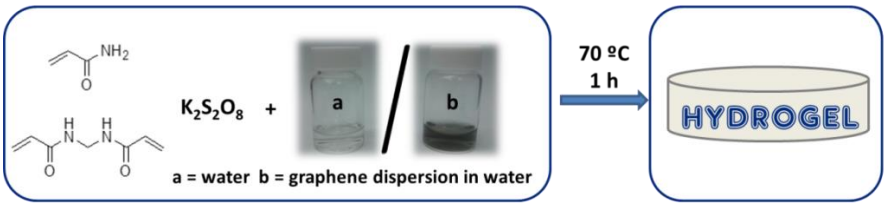

Figure 4. General synthetic scheme for the hydrogels preparation.

The graphene dispersion was obtained following a green technique that consists of the graphite exfoliation method commented in the previous introduction.[16] Thus, a milling treatment was carried out to exfoliate graphite through interactions with melamine under solid conditions and without using any oxidant substance. Moreover, melamine can be recuperated afterwards by washing with hot water (Figure 5). This method has been followed to prepare the graphene dispersions in water that have been used to form all the graphene-based composites in this thesis.

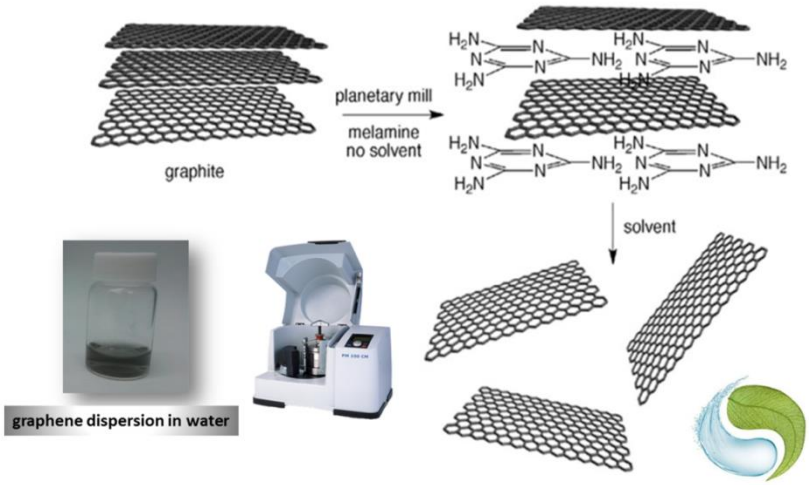

Figure 5. Scheme of the sustainable process carried out to obtain the dispersions of graphene in water.[16]

The obtained dispersions were stable at room temperature for some weeks. Figure 6 shows the transmission electron microscope (TEM) analysis of graphene obtained by ball-milling in water (0.1 mg/ml), and also the Raman spectra and the thermogravimetric analysis (TGA) profile of the nanomaterial obtained following this approach.

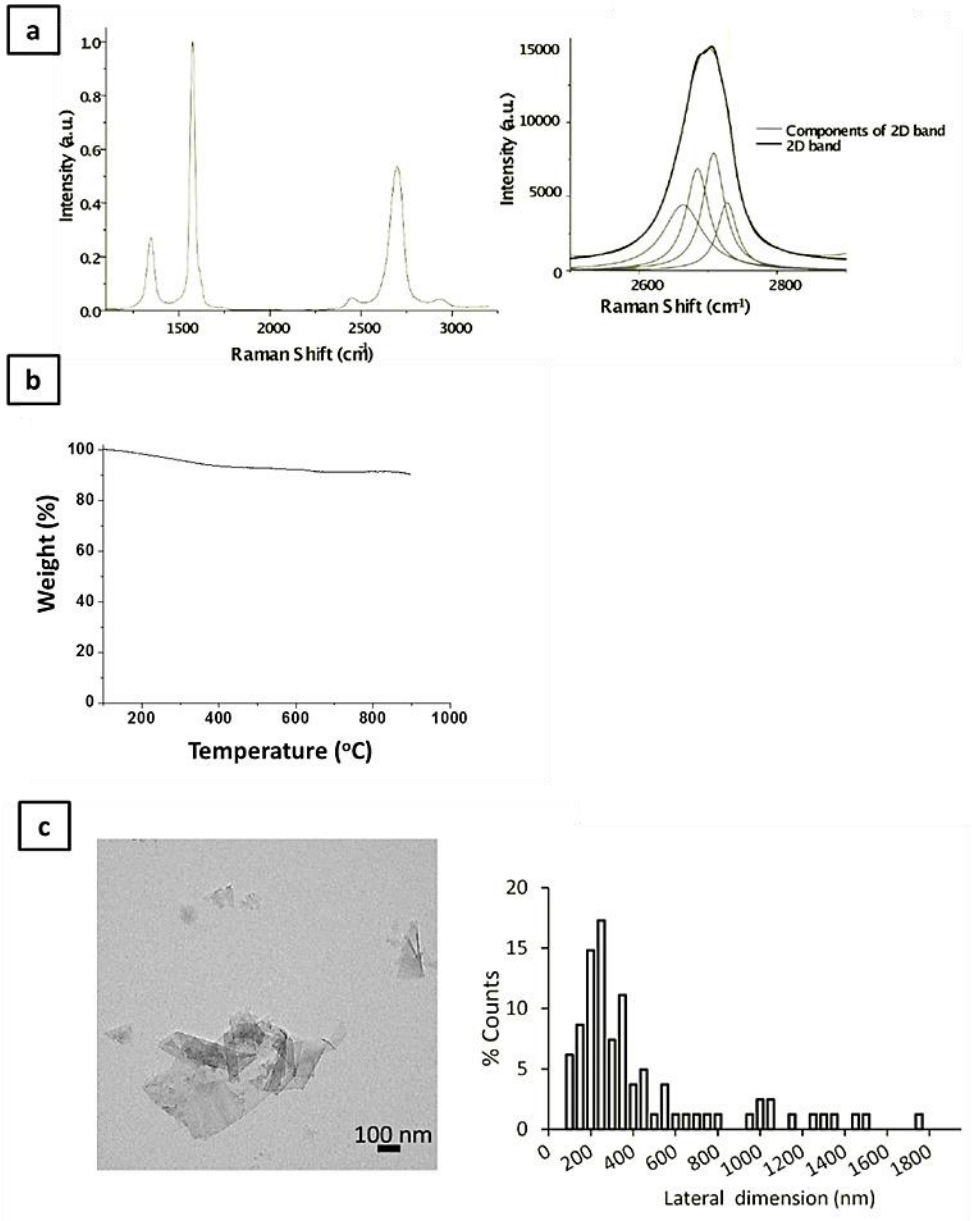

Figure 6. Characterization of few-layer graphene obtained by ball milling treatment. a) Raman spectra and 2D peak decomposed into four bands (Lorentzian-shaped peaks) (right). b) TGA profile. c) TEM picture (left) and size distribution of graphene sheets (right) in water (0.1 mg/ml).

The Raman spectrum of graphene (Figure 6a) displayed two bands at 1360 cm^{-1} and 1560 cm^{-1} characteristic of the D and G band, respectively, which are typical of carbon

structures dominated by sp^2 sites. In addition, the D band is caused by disordered structure of graphene. The evolution of the intensity ratio I_D/I_G between D and the G band has been used to provide a method to quantify the density of defects in monolayers and few-layer graphene.[17,18] In our case, the intensity ratio I_D/I_G is 0.27, which means that the graphene sheets have a small amount of defects. Moreover, the second-order Raman 2D band around 2700 cm^{-1} is sensitive to the number of layers in graphene, as has been proposed in the literature.[19] The 2D band of our graphene can be deconvoluted into four bands (Lorentzian-shaped peaks), which has been reported as a characteristic feature of few-layer graphene.

We can observe in the TGA a high thermal stability (Figure 6b), as the weight (%) keeps almost constant until at least 900 ^oC. The TGA profile only shows a slight loss of weight between 100 ^oC and 400 ^oC, which corresponds with the low quantity of defects produced in the ball milling treatment.

Finally, the size distribution was derived from TEM images after counting the lateral dimension of 100 individual graphene sheets using Image J software analysis. Most of the sizes were found between 100 and 500 μm (Figure 6c).

The general sustainability of the entire composite formation process has to be highlighted: we take advantage of non-conventional techniques, water is used as unique solvent and no waste is obtained.

2.3.2. Characterisation of the composites

2.3.2.1. Pore size studies

Figure 7a shows the appearances and the internal structures (analysed by scanning electron microscopy (SEM) experiments) of **AM** and some of the composite hydrogels based on graphene (**AMGX**s).

The just prepared samples were completely swollen and freeze-dried to yield low density aerogels. The pore size distribution in each hydrogel was analysed by SEM afterwards. Studies showed that the higher the graphene concentration, the smaller the pore size of the material (Figure 7b). This graphene-induced reduction in hydrogel pore-size correlates closely with the idea that graphene acts as a cross-linker and takes part in the hydrogel structure.

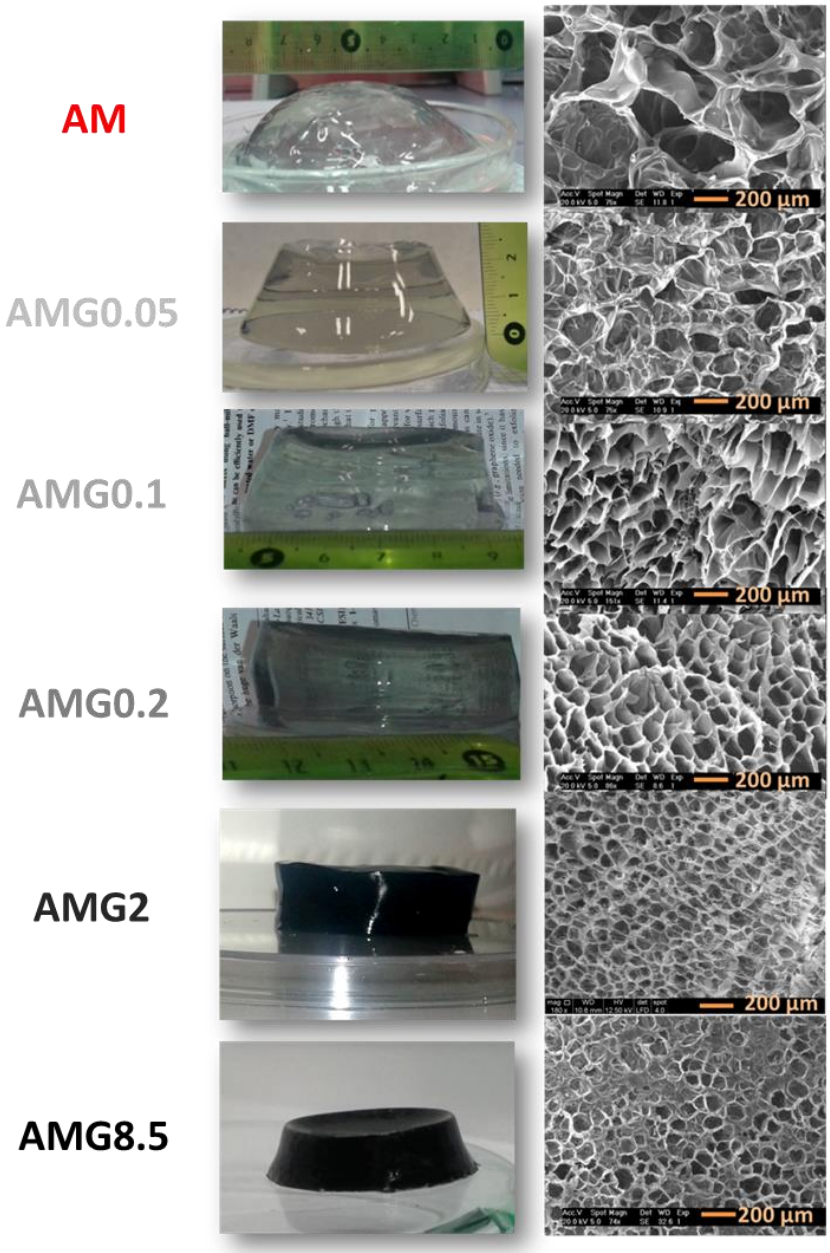
AM
AMG0.05
AMG0.1
AMG0.2
AMG2
AMG8.5
200 µm
200 µm
200 µm
200 µm
200 µm
200 µm

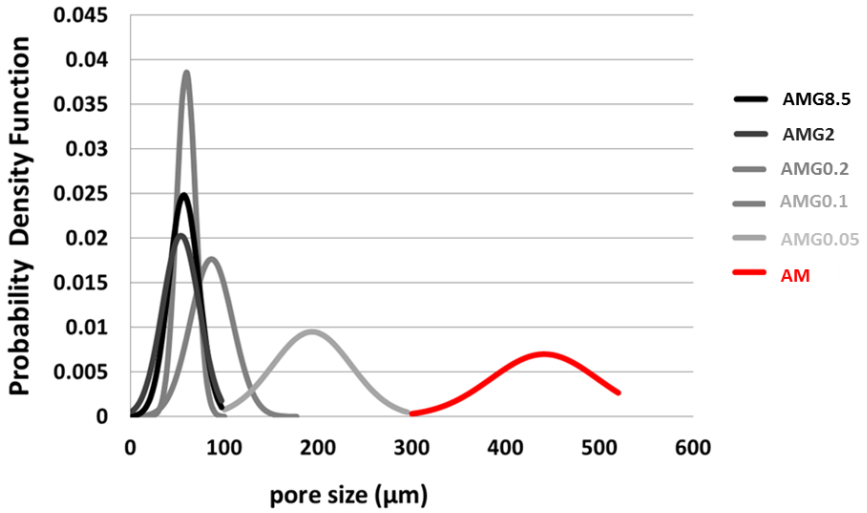

Figure 7. a) Digital, SEM pictures and b) pore size distribution of the final materials with several graphene concentrations from 0mg/ml to 8.5 mg/ml.

2.3.2.2. Swelling behaviour

The swelling ratio is an important parameter since it describes the amount of water that is contained within the hydrogel. It is a function of the network structure, hydrophilicity, and degree of ionisation of the functional groups, but it mainly depends on the effective concentration of the elastic chains of the hydrogels and, therefore, on the pore size. So, the quantity of cross-linker which is taking part in the gel network is crucial in the swelling properties of this kind of materials.

Swelling experiments were performed by immersing the freeze-dried materials in doubly deionised water (pH=7.1) at room temperature. The weights of the swollen samples were recorded at regular intervals until they reached a constant weight. Excess water on the hydrogels surfaces was removed with a filter paper before weighting. The swelling degree was then calculated according to the following equation:

$$\text{Swelling Degree} = \frac{W_t - W_0}{W_0}$$

where W_t is the weight of the gels at time "t" and W_0 is the weight of the dry gels at time "0". The swelling degree was also defined as the final swelling equilibrium after one day, when the weight of the samples was found to be constant.

The final equilibrium mass swelling ratio decreases with increasing graphene content in the composite hydrogels (Figure 8). The most notable changes occur at low graphene quantities, and the decrease in degree of swelling with the increase in graphene loading is in agreement with the results obtained from the pore size studies.

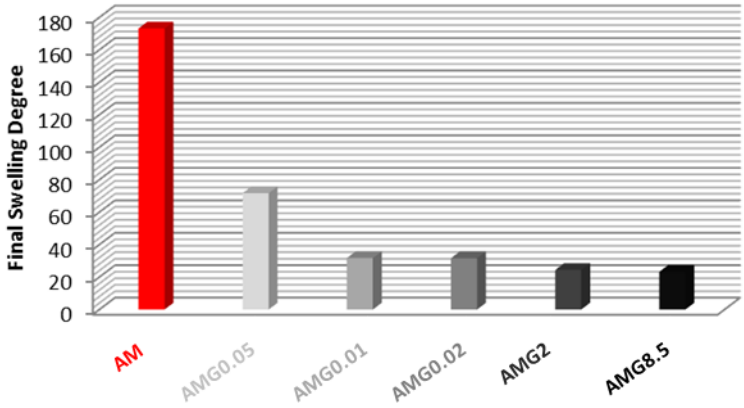

Figure 8. Swelling data of the final materials with several graphene concentrations from 0 mg/ml (**AM**) to 8.5 mg/ml (**AMG8.5**).

These results, joint to the previously discussed pore size distribution, suggest that graphene sheets may act as cross-linkers. There are some examples in literature in which GO sheets are used to form gels, which are reduced afterwards via pyrolysis at 1050 ^{o}C under nitrogen.[20] There are also some articles in which it is demonstrated that rGO interacts with polyacrylamide chains in a non-covalent way;[21] that kind of physical interaction could also be present in our composites. However, taking into account that the milligrams of nanomaterial used are in the same order than the quantity of cross-

linker, we thought that other possible cross-linking pathway could happen, throughout the existent unsaturations as result of the defects in the graphene sheets.

2.3.2.3. Structural role of graphene

To go into detail on the structural role of graphene in our composites, and in order to ascertain how far the cross-linking action of graphene takes place, we envisioned the creation of a graphene-based hydrogel without participation of any additional cross-linker. For this experiment, we mixed acrylamide and initiator in the same molar ratio than the previous materials, using our graphene aqueous dispersion as the reaction medium. We added the highest concentration of graphene prepared in this thesis (8.5 mg/mL) to maximise the expected phenomena. The mixture was heated to 75 ^{o}C for 1 hour, which means no change to the previously described conditions. At a first glance, an apparent hydrogel structure aroused, finally turning out to be a gel soluble in water. However, the same trial without nanomaterial showed a similarly consistent material that turned out to be a soluble gel in water. Nevertheless, it is clear that the graphene-polymer interactions (chemical and/or physical) were not strong enough in our case to form a permanent cross-linked polymer network.

Afterwards, we tried to analyse the possible existence of reactive unsaturations across our graphene sheets. We chose the classical Bromine Water test for this purpose, where a bromine aqueous solution can be bleached by the presence of alkenes due to the occurrence of addition reactions. In our experiments, the changes in the coloured media were determined by absorbance measurements at 393 and 262 nm (bromine bands) using graphene aqueous dispersions of different concentrations. The obtained results showed that, for an equal bromine concentration in water (1.3 mg/mL), there is an inverse relationship between the amount of graphene brought in contact with bromine and the intensity of the bands of the latter. The found variations were not excessive (Figure 9), meaning that the amount of active double bonds in our graphene sheets is not high.

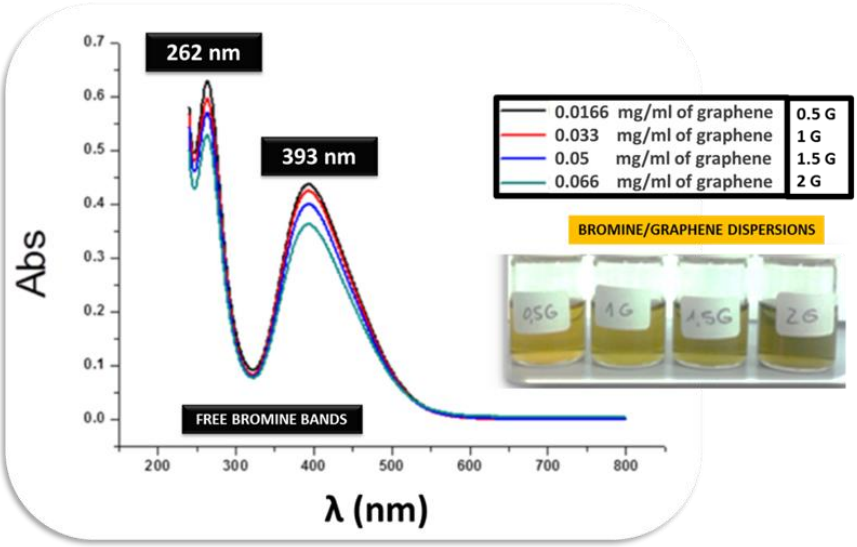

Figure 9. Bromine Water Test carried out for different graphene aqueous dispersions.

Finally, we carried out a comparative experiment in order to see the behaviour of two different hydrogels depending on how graphene had been put inside of them: *in situ* (**AMG0.2**) or absorbed by a blank (**AM**) (Figure 10).

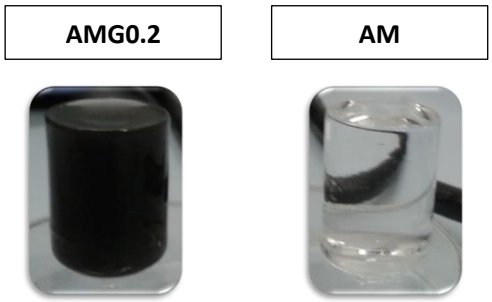

Figure 10. Just prepared samples.

The samples were completely dried in an oven and afterwards swollen in 20 ml (initial reaction volume) of water in the case of **AMG0.2**, and in a dispersion of graphene in the case of **AM**. Although the quantity of graphene used is the same in both cases (1mg), the appearance of both samples is quite different (Figure 11).

Homogeneity is appreciable only in the case of **AMG0.2**, while in **AM** the absorbed graphene was clearly located at the periphery of the blank and not much in the bulk.

Figure 11. Appearance of **AMG0.2** after having absorbed water (left) and **AM** after having absorbed the graphene dispersion (right).

Moreover, **AMG0.2** retained the nanomaterial inside after having being dried under vacuum; however, the graphene absorbed by **AM** was partially expelled and it was found to be scattered all around the flask walls, under an identical vacuum operation (Figure 12).

Figure 12. Partially released graphene from the **AM**.

After the vacuum process, both samples were submerged in water and the same vacuum/swelling cycle was repeated several times. Contrary to what was observed for the blank, **AMG0.2** retained the nanomaterial inside after several cycles. Finally, the

composite hydrogel remained intact, as originally, while **AM** was completely broken due to its poor consistency (Figure 13).

Figure 13. Final appearance of **AMG0.2** (left) and graphene dispersion absorbed by **AM** (right).

This ingenious experiment clearly shows that physical interactions between graphene and polyacrylamide chains are not sufficiently strong, by themselves, to retain graphene inside the gel.

The main conclusion we can draw from these experiments is that graphene acts as an effective cross-linker, being the responsible for a smaller pore size, as we could see from the SEM characterisation and the swelling behaviour of the composites. On the one hand, there are non-covalent interactions between the nanomaterial and the polymer chains, but they are not strong enough to form a permanent network in our case, contrary to what is reported in some literature examples.[14] On the other hand, possible active double bonds exist in our graphene sheets, but again, a permanent hydrogel network is not obtained unless a typical cross-linker is used. Therefore, we can say that both chemical and physical interactions contribute to the eventual graphene involvement, playing a role in the cross-linking process.

2.3.2.4. Mechanical properties

As already introduced in Chapter 1, mechanical reinforcement is usually one of the main interests in creating composites based on nanomaterials. Therefore, we decided to carry out some mechanical studies of our graphene-based composites.

The compressive tests were conducted on **AM** and some of the **AMGX**s composites. Figure 14a shows that the Young´s modulus (*E*) of the composite prepared in the presence of a dispersion of 2 mg/ml of graphene is considerably higher in comparison with the rest of the hydrogels. In view of these results, the fatigue behaviour was studied only for **AM** and **AMG2** (Figure 14b). In this case, the toughness of the materials was measured from the area of the stress-strain curve of non-stopped 100 compressive cycles. It is possible to observe how the incorporation of graphene makes the toughness of the material increase (Figure 14b). On the other hand, it has to be highlighted that there is a slight loss of toughness in both hydrogels only during the first five compression cycles. However, after the fifth cycle, the toughness value remains constant until at least 100 cycles, so it can be said that fatigue does not exist in these materials.

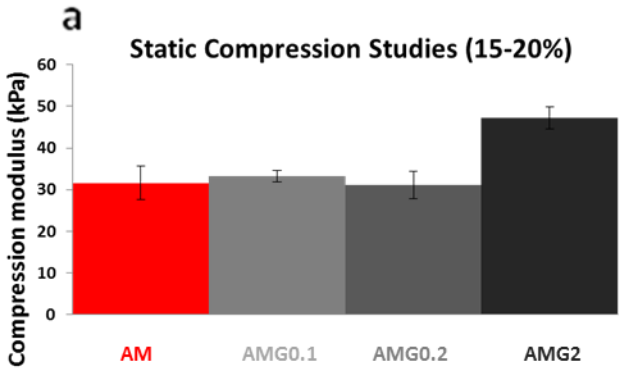

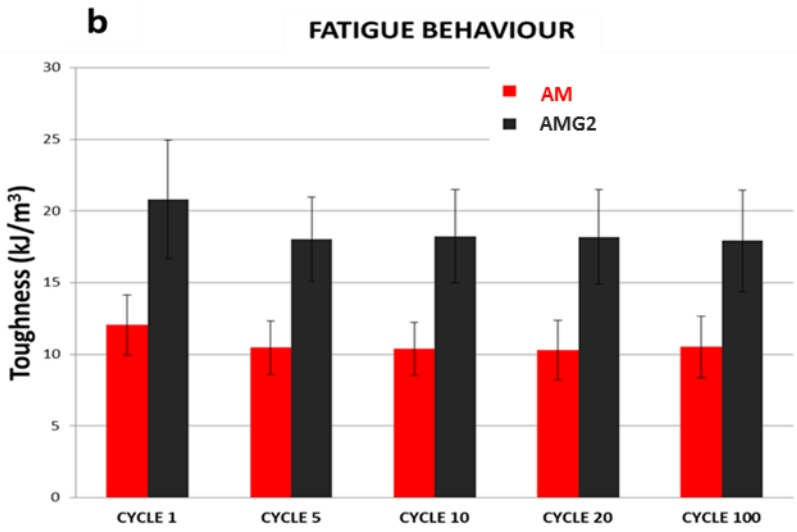

Figure 14. a) Elastic moduli of the four materials prepared with several graphene concentrations from 0 mg/ml (**AM**) to 2 mg/ml (**AMG2**). b) Fatigue behaviour of hydrogels with concentrations of graphene of 0 mg/ml (**AM**) and 2 mg/ml (**AMG2**).

Due to the above excellent results, comparable to some previously reported,[22,23] we thought about the possible application of our composite materials in intervertebral disc diseases.

2.3.3. 3D hydrogels for nucleus pulposus replacements

2.3.3.1. Introduction

Intervertebral discs (IVD) (Figure 15) are the structures located between the vertebral bodies, which are responsible for flexion, extension and rotation of the vertebral column. IVD are composed of a collagenous external layer called "annulus fibrosus" and an internal gelatinous part which is known as "nucleus pulposus". This inner part is contained also between the inferior and superior cartilage ends.

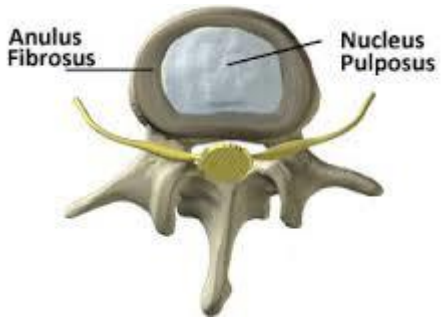

Figure 15. Intervertebral Disc scheme.

This configuration allows the discs to facilitate movements and flexibility, as the nucleus pulposus of the disc distributes hydraulic pressure in all directions under compressive loads. But with increasing age, discs lose fluidity and elasticity, developing cracks and becoming damaged.

The most usual treatment options for degenerated disc disease include symptomatic treatment or even cell transplantation therapies[24] trying to address the underlying problem. Surgical treatments are also possible options, and many examples can be found in literature, from artificial vertebral bodies[25] to annulus[26] or nucleus replacements.[27,28]

As already discussed, hydrogels are extensively applied in tissue engineering applications, and nucleus pulposus replacements are an example.[27] However, although much work is being carried out for intervertebral disc disease,[29] finding a material that fulfils all the requirements to eliminate the problem entirely, is still difficult.

Our systems are good candidates for tissue engineering as these kinds of scaffolds are based on non-toxic hydrogels with no-fatigue behaviour under continuous cyclic compressive loads. This feature makes them useful as possible intervertebral disc prostheses. However, we also studied the behaviour of cells inside the final materials, trying to apply them even as nucleus pulposus replacements for disc regeneration, as a second goal.

This part of the thesis was carried out through the granting of a scholarship from the "Cátedra Enresa" at the University of Brighton in the group of Prof. Matteo Santin, who studies and compares the behaviour of the cells regarding the presence or the absence of peptides during cell growth.

It is commonly approved that aminoacid sequences successfully mediate cellular events. There are some examples in literature, most of them based in the use of arginine-glycine-aspartic acid sequence and its subtypes to promote cell adhesion.[30] However, other adhesive peptides exist to improve the recognition of the sequence by the cell membrane, being then useful as biomimetic materials for tissue engineering.[31]

The group of Prof. Santin optimised a solid-phase synthesis method to produce poly(lysine) dendrons, the outermost branching generation which is functionalised by phosphoserine, a known catalyst for the biomineralisation process. In a recent work performed in Prof. Santin group, the dendrons were deposited onto etched titanium oxide surfaces as a near-to-monolayer film able to induce the formation of a homogeneous calcium phosphate phase in a simulated body fluid. The dendron films also stimulated MG63 and SAOS-2 osteoblast-like cells to proliferate at a rate significantly higher than etched titanium, with SAOS-2 also showing a higher degree of differentiation.[32]

2.3.3.2. Preparation of the composites

During my stay at the University of Brighton, a poly(lysine) dendrimer functionalised by carboxy betaine (**LysG3(CB)**) was introduced into our 3D scaffold based on acrylamide to compare the behaviour of the cells into different materials, regarding, for instance, the quantity of dendrimer used. We chose the **LysG3(CB)**

dendrimer because previous experiments carried out in the group demonstrated that this dendrimer is able to interact perfectly with cell membranes. Moreover, a graphene-based scaffold (**AMG8.5**) was used in the same way, in order to compare the cell growth results regarding the presence of the nanomaterial in the 3D material.

The synthesis method of the **LysG3(CB)** dendrimer basically consists of multiple aminoacids couplings and a final functionalisation with betaine, getting by this way the final dendrimer structure showed in Figure 16.

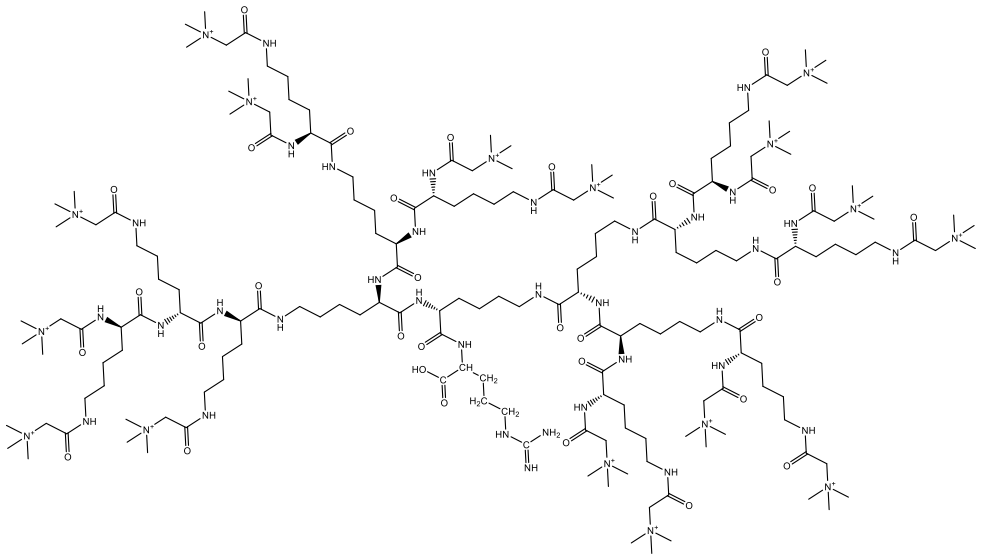

Chemical Formula: $C_{176}H_{354}N_{50}O_{33}^{16+}$
Exact Mass: 3696.75
Molecular Weight: 3699.00
m/z: 231.17 (100.0%), 231.11 (85.7%), 231.24 (50.8%), 231.05 (45.0%), 231.30 (28.8%), 231.23 (20.8%), 231.36 (14.1%), 231.30 (10.2%), 231.11 (8.3%)
Elemental Analysis: C, 57.15; H, 9.65; N, 18.93; O, 14.27

Figure 16. **LysG3(CB)** dendrimer. Structure and characterisation.

The dendrimer was added into the hydrogel in two different ways:

- *In situ* (**AM Dis X**): using the dendrimer aqueous solution as reaction solvent in the polymerisation process.
- Only absorbed (**AM Da X**): in this case the synthesis of **AM** is the first step. Then, once that hydrogel is dried, it is submerged into the dendrimer aqueous solution.

X represents the concentration of **LysG3(CB)** dendrimer used in wt%.

Figure 17 shows the SEM pictures of both hydrogels with a dendrimer concentration of 0.1 wt%.

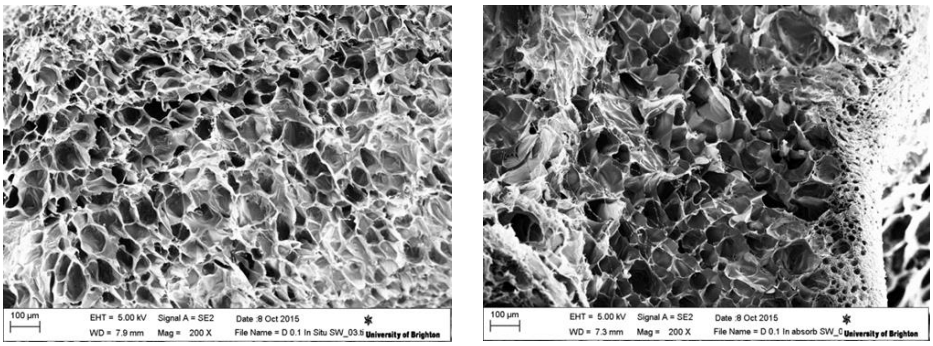

Figure 17. SEM pictures of the hydrogels with a dendrimer concentration of 0.1 wt% added *in situ* (**AM Dis 0.1** (left)) and only absorbed (**AM Da 0.1** (right)). Scale bars:100 µm.

The main information from the pictures is that a homogeneous structure is obtained only in the case of **AM Dis 0.1**, but not when the dendrimer is only absorbed.

Moreover, it is possible to observe how the pore size of **AM Dis 0.1** (73.37±17 µm) is smaller than the pore size of **AM** scaffold (Figure 7), even using such a low concentration of dendrimer. Then, we could say that the dendrimer can be acting as a physical cross-linker. The possible hydrogen bonds between the dendrimer and the polymer chains could be the cross-linking reasons.

The concentration of dendrimer was increased only in an *in situ* way (**AM Dis 10**), due to the no homogeneity of **AM Da 0.1**. Next figure (Figure 18) shows the SEM picture of the material. A smaller pore size (45.95±13.84 µm) was obtained in this case, confirming by this way the cross-linking theory commented before.

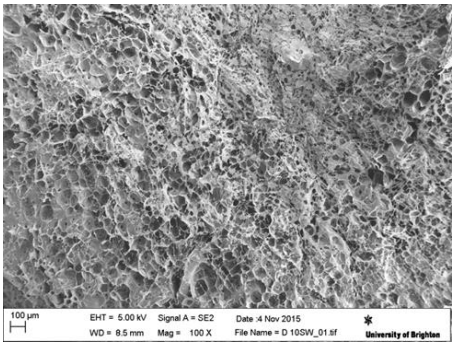

Figure 18. SEM picture and pore size value of the hydrogel with a dendrimer concentration of 10 wt%. Scale bar:100 µm.

Then, we carried out some cell culture studies using 3T3 cells (embryonic fibroblast from mouse). This type of cell was chosen in a first approach because they are cheap and easy to work with; nevertheless osteoblasts behaviour should be also tested. Samples **AM** (blank hydrogel), **AM Dis 0.1**, **AM Dis 10**, **AM Da 0.1**, (scaffolds in the presence of the dendrimer) and also **AMG8.5** (hydrogel that contains 8.5 mg/ml of graphene), were tested in order to study the toxicity of the material and the adhesion of this kind of cells to the scaffold.

2.3.3.3. Cytotoxicity studies

The cytotoxicity of the samples was firstly analysed. Two different strategies were used: LDH assay (lactate dehydrogenase) and HPI technique (Hoechst and Propidium Iodide).

LDH assay

LDH assay is the most useful tool to quantify necrosis, which is one of the major forms of cell death. Figure 19 shows the scheme of the process. Basically, the permeabilisation of plasma membrane is the key signature for necrotic cells because of the leakage of a cytoplasmic enzyme, lactate dehydrogenase, from the damaged cells. In the detection process, Formazan is quantified by standard spectroscopy.

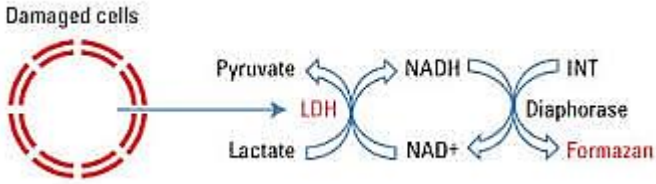

Figure 19. LDH detection process.

Next figure (Figure 20) shows the LDH results obtained for some of the samples and also for a positive control (where all the cells are sacrificed on purpose) and for a negative control: Gelatin (where all the cells are alive). Gelatin is a polymer typically used as control, where cells are easily adhered. Although its use is not mandatory, it is advisable in order to ensure a proper cell growth.

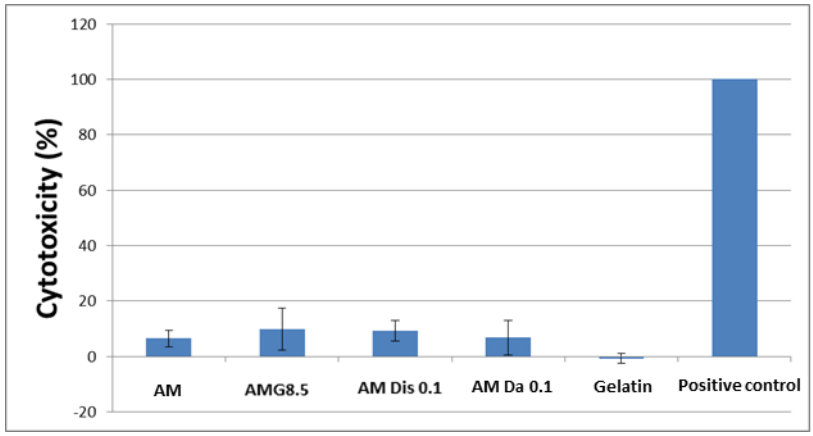

Figure 20. Cytotoxicity of some of the hydrogels, negative control (Gelatin) and positive control from LDH experiments.

Tolerated values were obtained, being even under the 20% of cytotoxicity in all the samples. It is worth noting that even a high concentration of graphene such as 8.5 mg/ml is not harmful for the cells, as **AMG8.5** shows a comparable cytotoxicity to **AM**.

HPI technique

In contrast to necrosis, which is a form of traumatic cell death that results from acute cellular injury, apoptosis is a process of programmed cell death, being highly regulated and controlled.

The blue-fluorescent Hoechst dyes are positively charged under physiological conditions and can pass through viable cell membranes. Hoechst stains the condensed chromatin of apoptotic cells more brightly than the chromatin of normal cells. On the other hand, the red-fluorescent propidium iodide dye is permeant only to dead cells. Therefore, the staining pattern resulting from the simultaneous use of the two dyes makes possible to distinguish normal, apoptotic, and dead cell populations.

3T3 cells were equally seeded and incubated for 48 hours in two different 24-well plates. Afterwards, the hydrogel samples (swollen in medium), and the supernatant mediums in which those gels had been submerged during 2 days, were put in contact with cells separately in the two different seeded plates. Therefore, we were able to study the toxicity of the gel and of the possibly contaminated medium respectively. Moreover, a "control" sample was studied. Figure 21 and figure 22 show the panels with the fluorescence results of the samples.

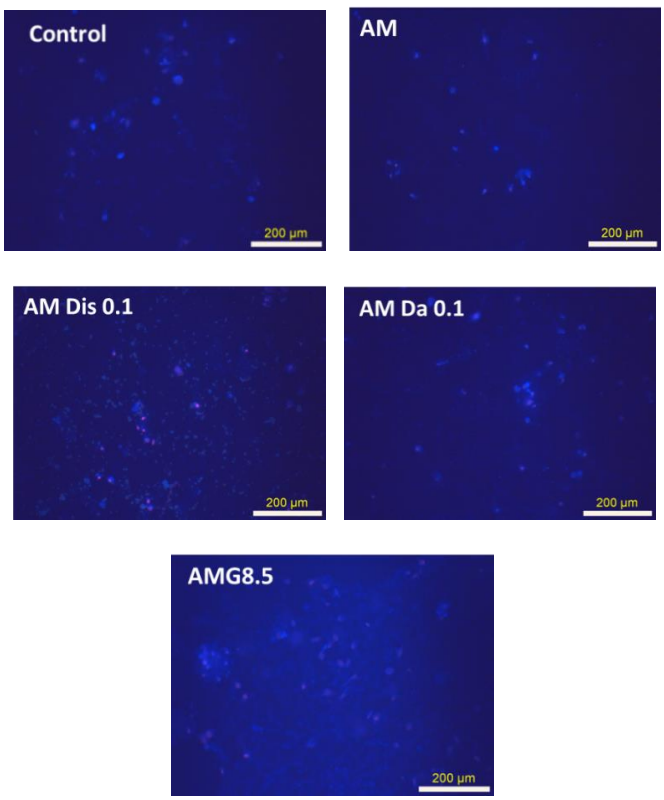

Figure 21. HPI results from the cells put in contact with the different hydrogels for 48h.

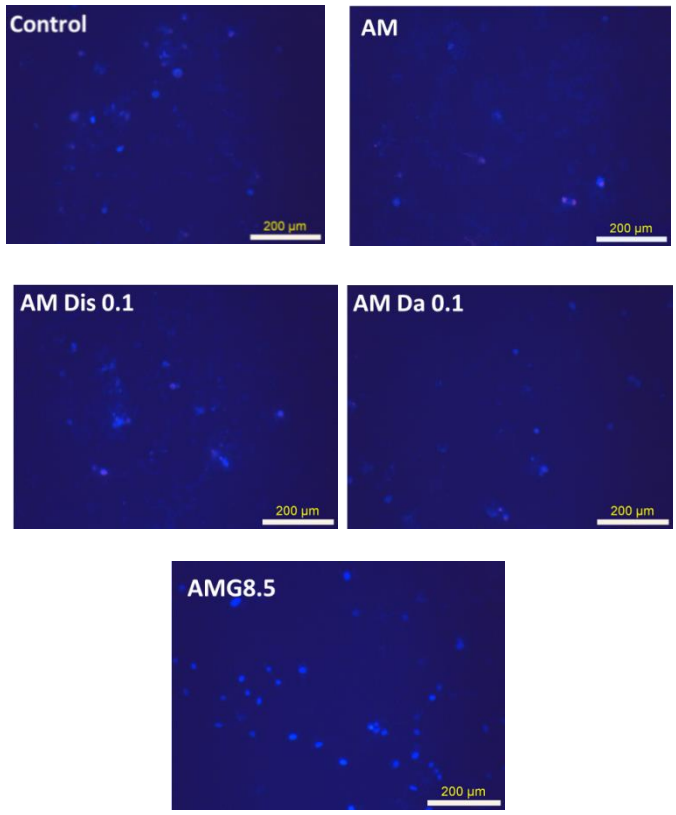

Figure 22. HPI results from the cells put in contact with the different supernatants for 48h.

The main information obtained from the panels is that neither hydrogels nor supernatants showed toxicity, as there were not differences between the studied samples and the "control" one. A very small quantity of red-fluorescent cells can be observed. In fact, the quantity of dead cells obtained in all the samples was quite similar to the control ones. These results are in accordance with the previously discussed LDH results.

2.3.3.4. 3D Cell culture studies

The first step carried out was to analyse and study the swelling capacity of the gels in the exact conditions in which cells would be seeded, in order to see how our scaffolds behave and/or swell in the seeding conditions. Thus, several and similar cylindrical shape samples (0.5 cm of diameter and 3 mm of thickness) of each freeze-

dried gel were submerged in cell culture medium and maintained in the cell seeding conditions. Then, the volume of medium absorbed by each sample was measured. The approximated absorbed values were 190 µl for **AM** and 165 µl for **AMG8.5**.

Once we knew everything was correct with our scaffolds in the seeding conditions, we carried out the cell seeding process on top of similarly prepared samples. The next picture (Figure 23) shows a 10x image of a just seeded scaffold.

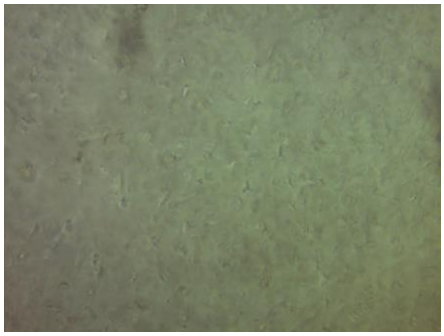

Figure 23. 10x image of one just seeded scaffold.

The seeded cells in the 3D scaffolds were incubated for 48 hours. Moreover negative and positive controls were jointly studied. Both TCP (tissue culture plastic) and Gelatin were used as 2D negative controls.

SEM studies

SEM experiments were carried out to study the presence and morphology of the cells into our 3D scaffolds. Next figure (Figure 24) shows the perfect cell morphology of the 3T3 cells after 48 hours of incubation in the control samples:

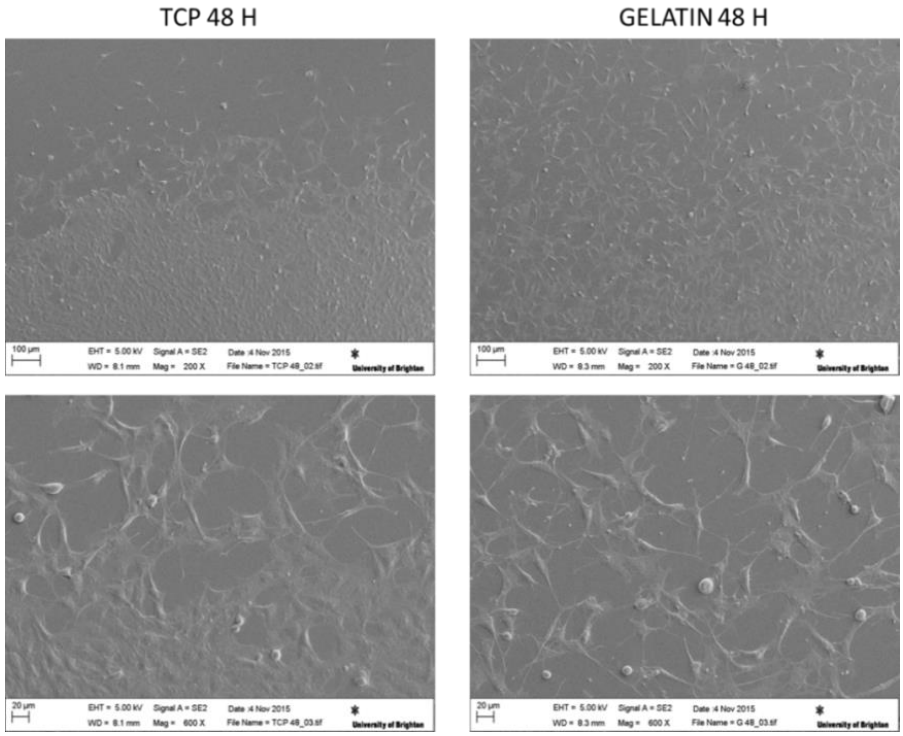

Figure 24. SEM results for the control samples.

Figure 25 shows the morphology of the cells into our 3D scaffolds. Although there are not as many cells in the 3D scaffolds as in the control samples, cells are visible in all of them. That means that 3T3 cells tolerate the final materials and attach to them without any extra treatment to improve the cell adhesion.[33] Although the cell morphology in 3D scaffolds varies in all the cases with respect to the 2D control samples (as it occurs in many other examples in literature[26]), it is possible to observe how the 3T3 cells are adhered to the pore walls of the materials, even for the one with a graphene concentration of 8.5 mg/ml.

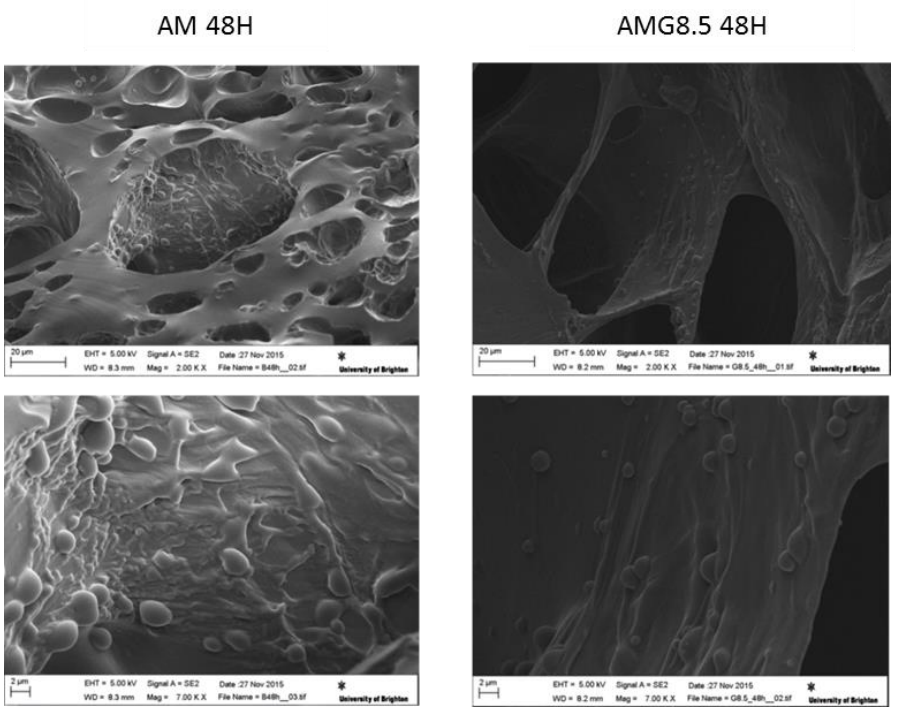

Figure 25. SEM results for **AM** and **AM G8.5** 3D scaffolds. Scale bars: 20 µm (upper) and 2 µm (below).

However, the number of cells that we could find in **AM Da 0.1** (Figure 26) was much lower than in the previous samples, probably due to the lack of homogeneity in this material, which makes that hydrogel a no cell-friendly scaffold.

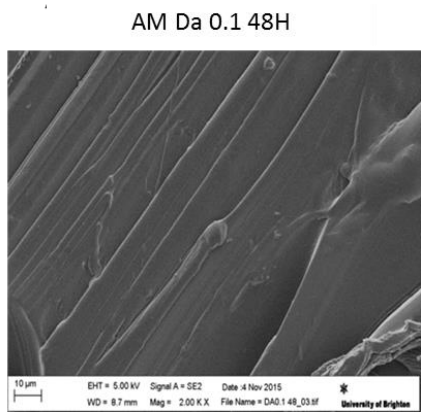

Figure 26. SEM results for the **AM Da 0.1** 3D scaffold. Scale bar: 2 µm.

Stem cells are a subject of intense and emerging interest as they are one of the fundamental supports of tissue biology. These potent agents are controlled within restricted tissue microenvironments known as "niches". How niches change with age and contribute to cancer and tissue aging is a current and modern field of research.[34] Some of the most interesting questions involve understanding the control of stem cell behaviour at the population level, for instance, in tissues undergoing regeneration in response to injury. Studies of the fruit fly *Drosophila* and of mammalian skin, intestine, bone marrow, and brain reveal that the inherent stem cell features are tightly regulated by their interaction with the cells and proteins that constitute the niche.[35] Therefore, mimicking the niche in a precise and controlled manner is very interesting regarding self-renewing tissue applications, as the signalling between cells in the niche plays a key role in sustaining stem cells and their development.[36]

In that context, the most interesting result from SEM experiments was the obtainment of tightly packed 3D spheroids in the samples that contain **LysG3(CB)**, especially in the case of **AM Dis 10** (Figure 27). It is possible to observe how the cells interact among them to form that kind of aggregates, moving even through the scaffold from the initial seeding zone. Therefore, it is important to highlight that this behaviour is very similar to the real one in niches, making our scaffolds interesting materials to mimic the real niches and advance in the knowledge of the cells mechanisms inside of them.

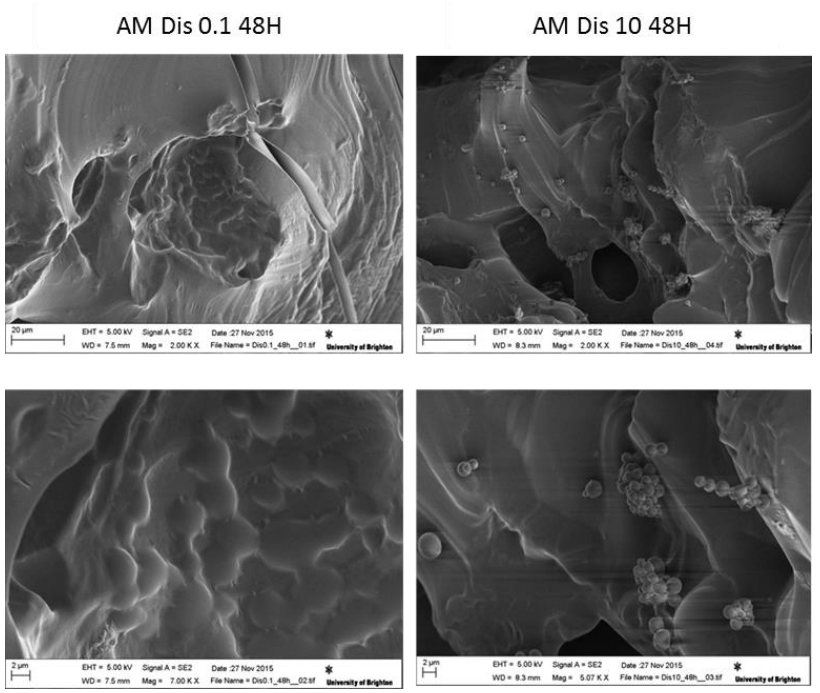

Figure 27. SEM results for **AM Dis 0.1** and **AM Dis 10** 3D scaffolds. Scale bars: 20 µm (upper) and 2 µm (below).

DAPI staining studies

Beside studying the presence and the morphology of the cells by SEM, we used DAPI (4',6-diamidino-2-phenylindole) to visualise the cells into the scaffolds, as this dye emits blue fluorescence upon binding to adenine-thymine tracts of DNA. This fact allows the view of the nuclei of the cells. We used a confocal microscope in order to have a general idea about the amount of cells in the different planes along the entire 3D material. Moreover, in some interesting cases, we were able to visualise both nuclei and the material of the scaffolds at the same time, playing with the contrast of the microscope.

The next picture shows the fluorescence results in the TCP control sample after incubation for 48 hours (Figure 28). It is possible to observe the high cell population, as all the cells are in the same plane, as well as we can observe in the Gelatin control

(Figure 29). In this case, it is possible to visualise the perfect cell cytoskeleton playing with the contrast.

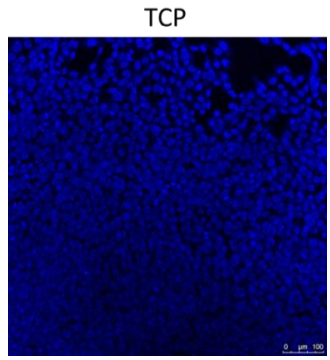

Figure 28. DAPI staining results for the TCP control after 48 hours of incubation. Scale bar:100 µm.

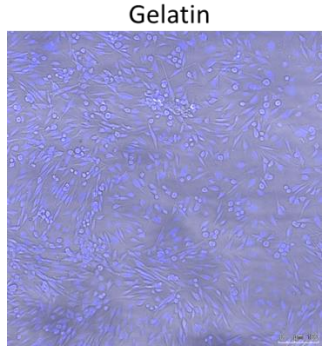

Figure 29. DAPI staining results for the Gelatin control after 48 hours of incubation. Scale bar:100 µm.

Next panel (Figure 30) shows the cell presence in a determinate plane of the hydrogel samples. It is possible to observe that **AMG8.5** contains a comparable, if not higher cell population regarding the **AM** one. This fact means that not only graphene does not limit the adhesion and proliferation of 3T3 cells, but also seems to improve those behaviours. This result corroborates what we can observe in SEM pictures. Some literature examples demonstrate that cells prefer stiffer and more hydrophobic systems for growth.[37] Although the mechanism of how graphene can improve cell adhesion is still not understood, differences in cell attachment rates could be

attributed to absorption levels of adhesion proteins:[38] proteins are more effectively adsorbed on the substrate in the presence of graphene.

On one hand, as it has been shown in previous sections, graphene makes the Young´s modulus of our acrylamide scaffolds increase: **AMG2** is stiffer than **AM**. On the other hand, **AMG8.5** could be more hydrophobic than **AM**. Therefore, the absorption levels of adhesion proteins could be higher in the case of **AMG8.5**, enhancing in this way the cell adhesion.

The cell population is comparable in **AM** and **AM Dis 0.1**, but a lower number of cells were observed in **AM Da 0.1**, probably due to the lack of homogeneity of that sample, as it has been discuss before. Finally, the tightly packed 3D spheroids were found in the samples that contain **LysG3(CB)** dendrimer. DAPI experiments showed that the aggregates were bigger in the case of the sample with the highest concentration of dendrimer (**AM Dis 10).** These results are in agreement with the conclusions from SEM experiments.

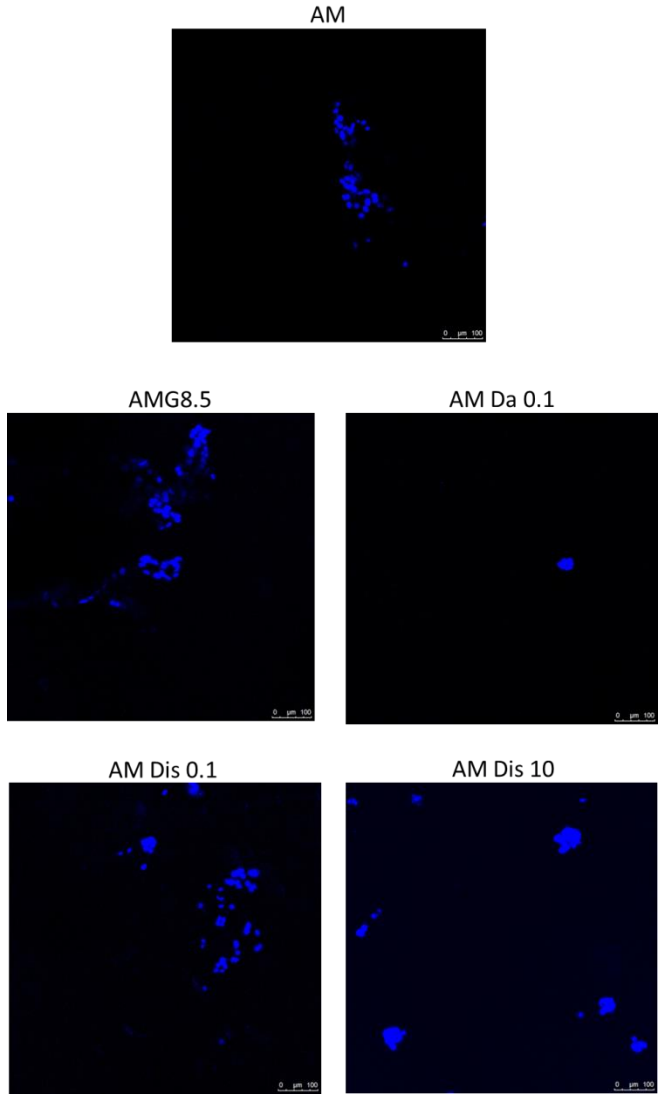

Figure 30. DAPI staining results for all the studied 3D scaffolds. Scale bars:100 µm.

We could observe, playing again with the contrast of the microscope, how cells are perfectly adhered to the material in the pore walls of the hydrogels (Figure 31). This perception is again in agreement with the SEM results of the cell-loaded 3D scaffolds.

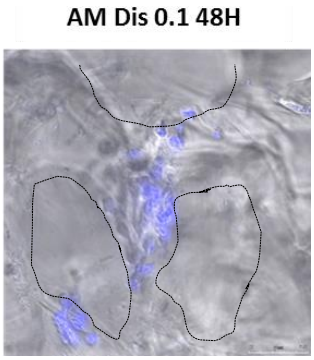

Figure 31. DAPI staining results for **AM Dis 0.1** 3D scaffold. The dotted line defines the pores of the sample. Scale bar:50 µm.

As it has been said before, the use of the confocal microscope let us to visualise the cell population through our 3D scaffolds in all the different planes. In general, DAPI experiments revealed that, although there are not as many cells in the scaffolds as in the 2D control samples, even visualising all the planes at the same time (overlap), cells are visible in every scaffold along the entire structures. Figure 32 shows the overlap of all the planes of **AM Dis 10** as an example. It is possible to observe the cell aggregates due to the cell-cell interactions previously commented in the SEM results. It is necessary to highlight that this fact demonstrates again that 3T3 cells are able to move through the material to form the spheroids.

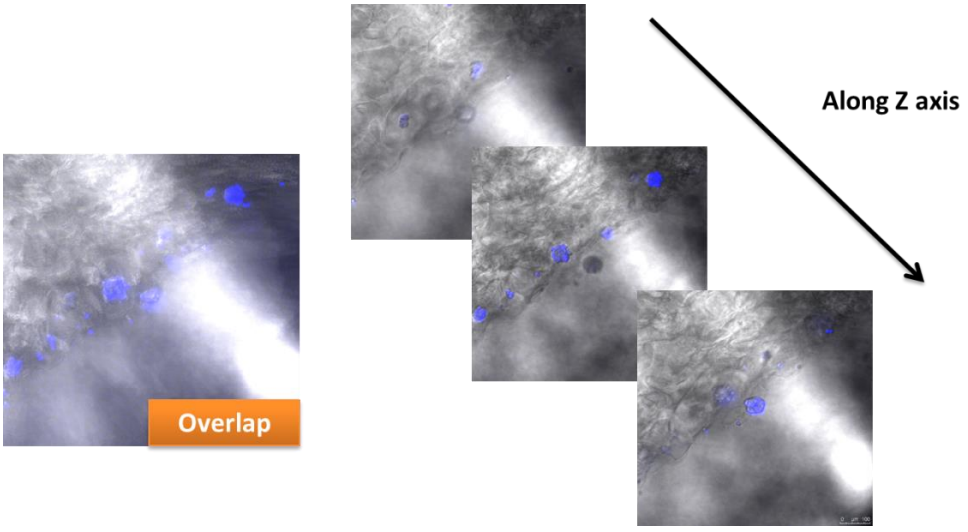

Figure 32. DAPI staining results for **AM Dis 10** 3D scaffold. Scale bars:100 µm.

We could conclude that all our composite hydrogels are biocompatible and showed good results as scaffolds for 3T3 cell adhesion, highlighting the behaviour of the cells in **AM Dis 10**, where packed 3D spheroids were observed.

It has to be noted that the sample with graphene showed good results regarding cell presence, even despite the high concentration of nanomaterial used (8.5 mg/ml). Therefore, next step should be the creation of a new composite based on both fillers, graphene and **LysG3(CB)** dendrimer, trying to combine the advantages provided by both materials.

2.3.4. De-swelling experiments: microwave responsive hydrogels

As previously described in Chapter 1, responsive hydrogels react to an external stimulus leading to intelligent materials that can vary some of their properties.[39] Drug delivery application is maybe one of the most studied fields regarding responsive hydrogels. Our group has also experience in these systems,[13] so we decided to analyse the de-swelling behaviour of the synthesised composites as a response of an external stimulus.

Electroresponsive hydrogels based on polyelectrolytes are normally applied as drug release systems. These materials respond to an electric field as it produces a force on the mobile ions and the immobile charged groups of the gel´s polymeric network.[40]

Our composite hydrogels are made from polyacrylamide, so, unless they are previously hydrolysed, they cannot respond to the external electric field. However, the main problem of hydrolysing these gels is that they lose their mechanical properties, becoming very fragile materials. Another disadvantage is related to the final application: in order to produce the de-swelling and, as a consequence, the delivery of the drug, patients must be treated by inserting the electrodes to touch the material. All these issues made us consider a different alternative: using microwaves as external stimulus.

Microwaves are electromagnetic waves with frequencies ranging between 300 MHz and 300 GHz, and although its potential use to facilitate transdermal drug transport is still in its infancy, microwave radiation has been recently reported as a potential skin permeation enhancer.[41] However, there are very few examples in literature regarding materials that respond to the microwave irradiation,[42] especially if that material is a hydrogel from which drug is released through electromagnetic stimulation. Actually, as far as we know, this kind of external stimulus has been previously used only by Rivero and co-workers,[43] who used a nanocomposite made from PANIPAm and polyaniline. The de-swelling is caused by the local heating as a

consequence of the polyaniline presence, which produces enough energy to induce the typical sol-gel transition of PANIPAm hydrogels,[44] allowing the drug release.

We carried out initial experiments using a 2.45 GHz Discover-SP CEM microwave. The completely swollen sample was weighted before irradiating. Then, it was introduced into the microwave flask to be stimulated under microwave irradiation controlling the power and the time of stimulation. The de-swelling behaviour was studied by calculating the weight loss percentage of the sample (Weight %) by using the following equation:

$$\text{Weight } \% = \frac{W_t}{W_0} \times 100$$

where W_t is the weight of the hydrogel after exposure to the microwave radiation at time "t" and W_0 is the weight of the fully swollen hydrogel at time "0".

Experiments showed that not only the hydrolysed gels responded to the microwave radiation, but also the non-hydrolysed ones. Next figure (Figure 33) shows the de-swelling behaviour of the non-hydrolysed tested samples. In our case, this behaviour is probably the consequence of the polymer chains stress, which is generated by the application of the microwaves to the composites. Therefore, contrasting with the unique previous example in literature, we are achieving a microwave response in gels that are not thermally responsive materials.

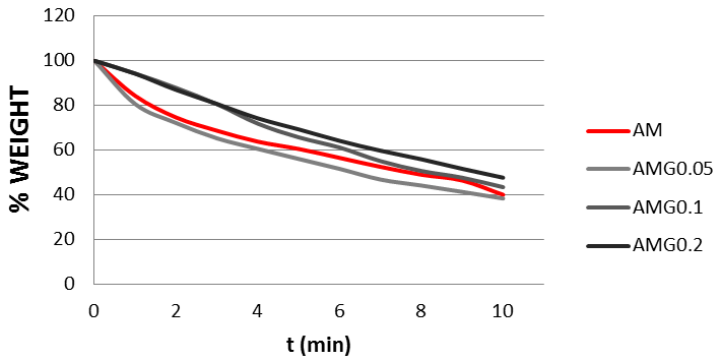

Figure 33. De-swelling behaviour of **AM**, **AMG0.05**, **AMG0.1** and **AMG0.2** under the application of microwave radiation using a 2.45 GHz frequency.

The most interesting result, observed in the graph, is the more regular slopes obtained for **AMG0.1** and **AMG0.2**, comparing with the more irregular slopes of **AM** and **AMG0.05**. It seems that gels prepared with higher concentration of graphene show a more controlled water release in comparison with gels prepared without graphene or with very small quantities of nanofiller**.** This fact could be explained by the excellent microwave absorbing properties of carbon nanostructures such as graphene:[45,46] the nanomaterial can absorb most of the radiation and water is released in a more controllable way.

A microwave instrument that operates at 915 MHz has very different features from the microwave that operates at 2.45 GHz, which is the most commonly used. Slightly polar or non-polar substances are badly heated by using a 915 MHz radiation, but the penetration depth of this wave is larger (6-8 cm) than the one that operates at 2.45 GHz (2 cm). Therefore, also encouraged by previously commented results, we decided to test the de-swelling behaviour of our hydrogels by using the microwave apparatus operating at the 915 MHz frequency, in order to achieve a de-swelling effect with a slight heating in hydrogels, which could be applied afterwards as controlled drug-delivery systems in deeper organs. Moreover, the fact of obtaining a response without increasing the temperature of the material it is important to prevent damages in tissues. Ibuprofen was used as model hydrophobic drug to carry out these experiments.

AM, **AMG0.2**, and the composite material with a more notable content of graphene (**AMG2**) were used; this last sample was chosen to prove the enhancement of the hydrogel response under the microwave radiation.

A Fiber Optic Temperature Sensor was used to analyse the real temperature of the hydrogel sample while it was being irradiated. The amount of Ibuprofen released from the samples was quantified by UV spectroscopy.

The most interesting and reproducible event was that graphene avoids the superheating of the hydrogel. Figure 34 shows the obtained temperature/time profiles:

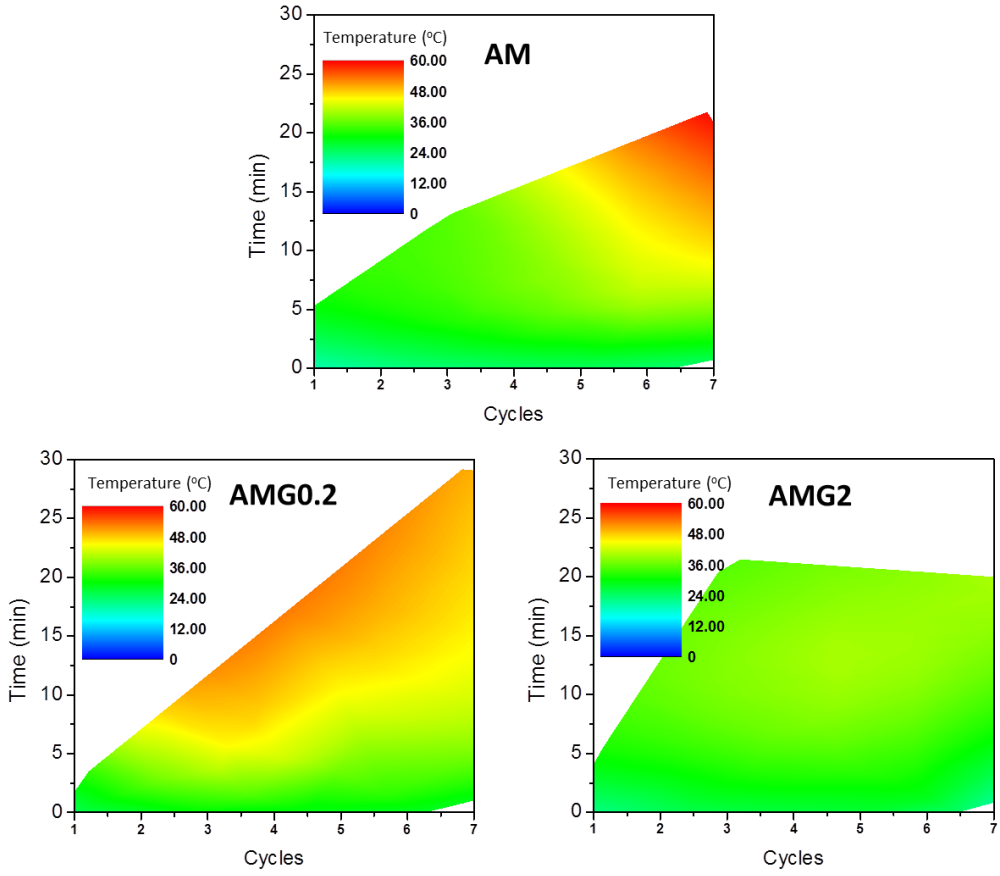

Figure 34. Temperature/time profiles of **AM**, **AMG0.2** and **AMG2** under the application of microwave radiation using a 915 MHz frequency.

It is possible to observe how **AM** reaches 60 °C, while the samples that contain graphene, **AMG0.2** and **AMG2**, reach 50 °C and 40 °C respectively in a comparable period of irradiation time. Temperature rises more regularly in the case of **AMG0.2** than in the case of **AM**, but the most interesting result is that temperature keeps constant at ≈40 °C in **AMG2**. This fact means that we would be able to release the drug for longer, in a controlled way, without causing any injury in tissue by using the latter material.

Release of Ibuprofen was observed in all cases, obtaining the following percentages of delivered drug, regarding the initial load of Ibuprofen, during the previously showed

time/temperature cycles (Figure 34): 21.8% from **AM**, 7.6% from **AMG0.02**, and 35.6% from **AMG2**.

In conclusion, those results are very promising, because the presence of graphene into the scaffold prevents the super-heating of the material, which would avoid damage in real tissues while drug is being delivered in a controlled manner.

Nevertheless this work is in progress and we are currently working on this project to apply these biocompatible composites as on-demand drug delivery systems. More experiments are being performed to go deeper into this subject.

2.3.5. Electrical properties: Strain Gauges

Strain is defined as the ratio between the initial and the final length of a material when it is stressed with an applied force. A strain sensor measures the physical deformation of a material, which results in the change of one of its properties, typically the electrical ones. This fact offers the possibility of quantifying the extent of deformation if the ratio between strain and variation of the electrical properties is known and calibrated.

In particular, Strain Gauges are electrical conductors with a geometry-dependent electrical resistance, and when stretched in a reversible manner, resistance changes due to variations in length and section.[47] This kind of materials is extensively applied in a wide range of fields. Some examples could be as embedded sensors with the capability to detect damage initiation, growth and self-healing[48] or wearable devices for recreation, virtual reality, robotics and health care.[49]

Due to the design of the graphene-based hydrogels, we thought that we could apply them as sensor gauges. Graphene is perfect as nanofiller because this nanomaterial has excellent conductive properties, and a possible piezoresistive effect could be found based on a mechanism of conductive paths.

The first step was to study the conductive behaviour of our hydrogel composites. Electrical conductivity (σ, in S/cm), or its inverse, resistivity (ρ, in Ω·cm) are intrinsic properties of materials which depend on their natural ability to allow transit of charge carriers within their structure.[50] Turning an insulating or poorly conductive material into a conducting or semiconducting one, can be reached, for instance, by adding conductive fillers. We have observed that the addition of our graphene into **AM** results in a notable increase in the electrical conductivity of the hydrogel. Figure 35 shows σ values for several low graphene loadings:

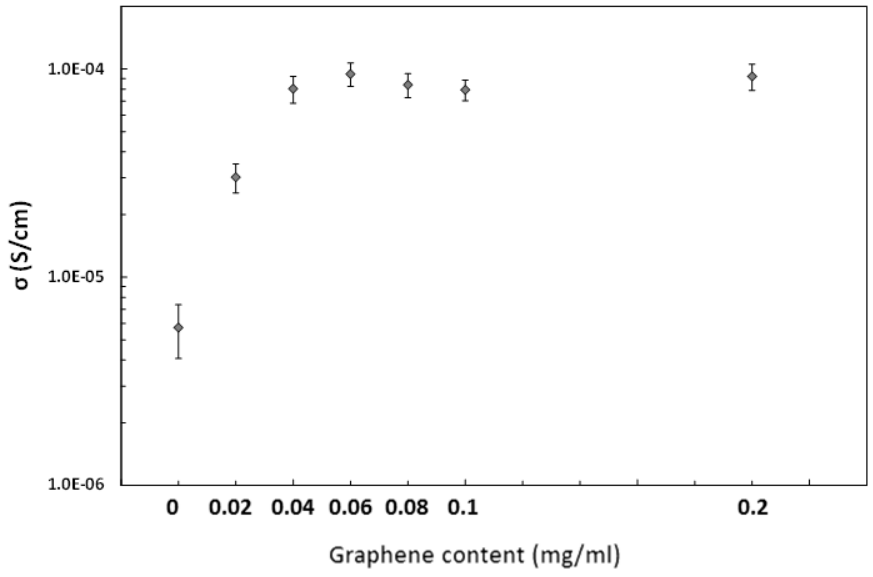

Figure 35. Electrical conductivity values for different PAm hydrogels with several graphene contents.

An increase of around 1.5 orders of magnitude can be achieved just by the introduction of small amounts of graphene. Moreover, a percolative behaviour is evidenced. The called "percolation threshold" (p_c) is the critical value where a sharp transition occurs in the conductivity because of a slight increase of the conductive filler content.

Following these basic concepts, we can estimate our p_c to be approximately at 0.02 mg/ml of graphene, which is noticeably low compared to many other polymer matrices in general, and hydrogels in particular.

Typically, high σ values are associated with low p_c values. Moreover, a good state of dispersion is generally accepted as a positive influence, as one of the main factors that affect to p_c is the quality of the dispersion: the higher the homogeneity of the dispersion, the lower the p_c value. An excellent level of graphene dispersion attained in our samples together with the synthesis approach which is based in "all-water" processing may be responsible for this low p_c. Another critical feature in electrical and percolation phenomena is the aspect ratio. In this case, it is remarkable that the p_c

value for the composite hydrogel is similar or even better than the ones obtained with other nanofillers with a more favourable aspect ratio, such as carbon nanotubes.[50]

The percolative behaviour of our nanocomposites together with the low p_c value, hinted at the possibility of a piezoresistive effect induced by stretching. Thus, electrical resistance along the cyclic stretching (at a constant rate) up to 30% strain, in different samples, was measured. We realised that there were significant changes in R in the stretched position of nanocomposites, compared to the zero position, and therefore the system itself behaves as a strain gauge.

The sensitivity of our composites was quantified through the Gauge Factor (G_F) which was calculated by using this equation:

$$G_F = \frac{(R - R_0)/R_0}{(l - l_0)/l_0}$$

where R is the electrical resistance at the stretched position, R_0 is the electrical resistance at the initial position, l is the length at the stretched position and l_0 is the length at the initial position.

The study was focused on samples with a low content on graphene, as it is widely known that the best performance of strain gauges mostly occur in the vicinity of p_c.[47,51] Figure 36 displays average G_F values for different composite hydrogels.

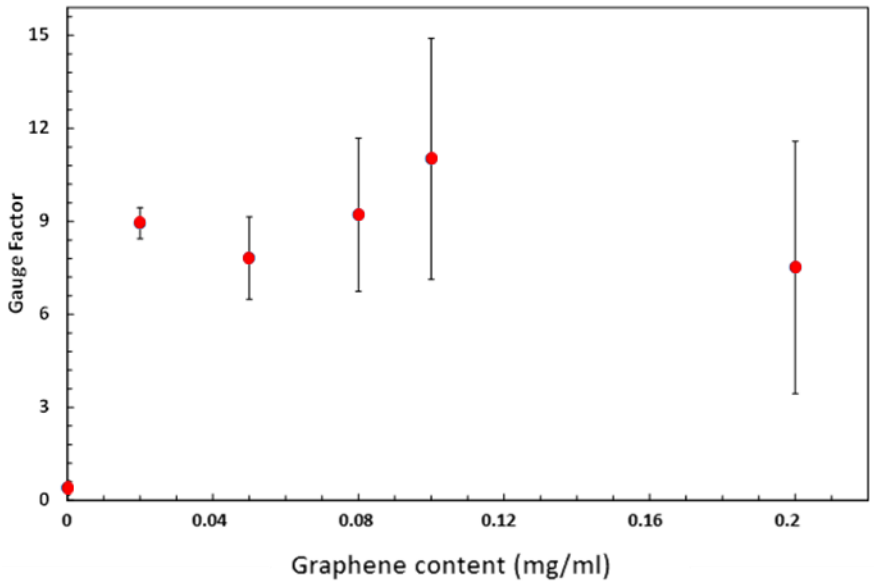

Figure 36. Relationship between gauge factor (average of 11 cycles) and graphene content for PAm composite hydrogels cyclically stretched to 30%.

These main observations can be directly drawn:

1) The strain gauge effect is exclusively caused by the filler as the neat matrix (**AM**) does not show any practical piezoresistive response, despite its appreciable electrical conductivity.

2) There is a close coincidence of the average G_F values, apparently not influenced by the graphene content in the studied range, and pointing to $G_F \sim 9$.

The higher hydrophobicity of the materials that contain graphene causes a faster drying process while stretching. Therefore, the standard deviation of each average G_F value is higher as the graphene content increases.

It is interesting to notice that the obtained average G_F values are within the pool of similar high-performance elastic strain gauges, such as that of liquid phase-exfoliated graphene infused into natural rubber,[52] or lithographically-imprinted Ag nanowires in a PDMS elastomer.[53] In our case, we achieve similar G_F values with very low amounts of graphene. Interestingly, simplicity is the key in our design, as we have "one-pot"

embedded systems without multiple sandwiching stages or delicate deposition processes.

In summary, we successfully manufactured graphene-containing hydrogel nanocomposites showing a clear strain gauge effect. The average G_F values may be ranked amongst the good-to-best in the literature.

2.4. Experimental procedures

2.4.1. Graphene-based composite hydrogels

2.4.1.1. Preparation and characterisation of graphene dispersions

The exfoliation of graphite was carried out using a ball-milling procedure developed in our group.[16] In a typical experiment, 30 mg of a graphite/melamine mixture (1:3) was ball-milled at 100 rpm for 30 minutes. The resulting solid mixture was dispersed in 20 mL of water to produce a dark suspension, and some precipitate was removed from the solution after stabilisation for 5 days. Melamine is removed afterwards washing with hot water, leading to few-layer graphenes sheets without almost defects.

TEM measurements were performed using a BioTwin instrument (Philips/FEI, USA) operating at 120 kV accelerating voltage. One drop of graphene dispersion was placed on formvar/carbon coated copper grids (Agar Scientific, Essex, UK) and the excess of sample was removed with filter paper. Size distribution was derived from TEM images after counting the lateral dimension of 81 individual graphene sheets using Image J software.

Raman spectrum of graphene was recorded after preparing the sample by drop casting of silicon oxide surface (Si-Mat silicon wafers, CZ) and after evaporation of solvent. Measurements were performed in 10 different locations in the sample, using a 100x objective at 532 nm laser excitation on an Invia Renishaw microspectrometer equipped with a He-Ne laser.

TGA was performed on a TA Instruments TGA Q50 unit with a heating rate of 10 ^{o}C/min under nitrogen atmosphere.

2.4.1.2. Synthesis of hydrogels

Pure PAm hydrogels were prepared using Am, MBA as cross-linker and KPS as initiator. Am was initially dissolved in ultrapure Milli-Q water (200 mg/ml) together

with the MBA (0.2 mg/ml). The solution was homogenised by stirring and mild sonication. Then, KPS was added (at a final concentration of 0.4 mg/ml) and the system was allowed to polymerise at 75 ^{o}C in a time period of 1 hour. In the case of the graphene-based hydrogels, an identical process was followed, except for the use of graphene aqueous dispersions instead of plain water, with the necessary concentration to end up in the desired quantity of graphene within the gel matrix. The graphene content varied between 0.02 mg/ml and 8.5 mg/ml. The resulting materials were immersed in water for at least four days, and the water was changed every day in order to remove any unreacted monomer and initiator molecules.

2.4.1.3. Characterisation

Swelling studies

Swelling studies were carried out for the hydrogels by immersing the lyophilised gels in 10 ml of ultrapure Milli-Q water at room temperature. All the samples have a similar volume of approximately 0.125 cm^3. The weights of the swollen hydrogels were recorded at regular time intervals until they reached a constant weight. Excess water on the surface of the gels was removed with a paper filter before weighting. The swelling degree was then evaluated by using the following equation:

$$\textbf{Swelling Degree} = \frac{W_t - W_0}{W_0}$$

where W_t is the weight of the gels at time "t", and W_0 is the weight of the dried gels.

SEM experiments

The hydrogel microstructure was analysed by Scanning Electron Microscopy, using PHILIPS XL30 and FEI QUANTA 250 systems. The distribution of the pore size was measured for all samples in the various SEM images by using the Fiji software. Pure and graphene-containing hydrogels were frozen and then dried overnight in a Telstar Lyoquest freeze-drier to yield dry aerogel samples. SEM samples were prepared by sputter coating with an Au layer of about 15 nm just when they were analysed using the PHILIPS instrument.

Mechanical properties

Compressive tests were performed on hydrogels at 25^{o}C with a Mecmesin Multitest 2.5-i dynamic mechanical analyser. Cylindrical disks of gels (x6) with a diameter of 1.5 cm and an initial thickness of 1.5 cm were moulded. Hydrogel disks were uniaxially compressed between two plates. The deformed hydrogels were then held under constant for an extended period of time (the samples were loaded (cell load = 100 N) at the rate of 5 mm/min). The extent of deformation was measured in terms of compression ratio which equals the ratio of the initial height of the sample to the final height of the sample. The extent of the deformation was also measured in terms of strain, which equals the ratio of the displacements of the samples. After reaching the desired deformation, the sample was de-compressed and the hydrogel was removed from the press. This behaviour was represented in the typical stress-strain curves from which it was possible to obtain the Young´s modulus. In this case that value was calculated between 15% and 20% of strain.

Moreover, fatigue behaviour was studied using the previously program in a dynamic way, reaching 100 compressive cycles with each sample.

De-swelling studies

Initial experiments were done using a 2.45 GHz Discover-SP CEM microwave. The completely swollen sample (approximate volume of 0.125 cm^3) was weighted before irradiating. Then, it was introduced into the microwave flask to be stimulated under microwave irradiation controlling the power (300 W) and the time of stimulation. The de-swelling behaviour was studied by calculating the weight loss percentage of the sample (Weight %) by using the following equation:

$$\text{Weight } \% = \frac{W_t}{W_0} \times 100$$

where W_t is the weight of the hydrogel after exposure to the microwave radiation at time "t" and W_0 is the weight of the fully swollen hydrogel at time "0".

The microwave flask was dried after each stimulation, in order to avoid the sample re-swelling.

Following experiments were done using a microwave instrument that operates at 915 MHz. The dried hydrogel samples were swollen in a determinate volume of Ibuprofen solution (0.0157 mg/ml). Afterwards, a 50 ml beaker, which contained the swollen sample, was introduced in the microwave apparatus and the Fiber Optical Temperature Sensor was as inserted as possible into the hydrogel. Microwaves were applied during several periods of time, controlling the temperature in a precise way. After each radiation cycle, the Ibuprofen solution, located in the beaker walls, was recuperated and measured by using a Cary Series UV-Vis-NIR Spectrophotometer.

Electrical properties

Direct current electrical resistance (R) measurements were performed with an Agilent multimeter, in a two-point probe configuration, to cylindrical specimens of 5 mm diameter and 10-20 mm length (moulded in plastic syringes). At least six measurements were performed for each sample, by contacting crocodile-type electrodes to the hydrogel ends, which were previously covered by a thin layer of Ag painting. Electrical conductivity (σ) was calculated as the inverse of resistivity (ρ), obtained in turn from its relationship with R:

$$R = \rho \frac{l}{s}$$

where *l* and *s* are the specimen's length and section area respectively.

The strain gauge effect was evaluated by combining the aforesaid mechanical and electrical characterisation techniques. Cylindrical specimens of 5 mm diameter (and several centimetres long) were clamped to both ends and situated in a "zero" position with the minimum possible tension. Two small Ag electrodes were painted approximately at 1/3 and 2/3 of the specimen length between clamps. Then, cyclic stretching-recovering cycles were applied at specific ratios (namely 5, 15, 30 or 50 % strain) with a 15 and -15 mm/min stretching rate, respectively, along 11 cycles.

Electrical resistance was measured in each stretched and recovered position of every cycle. Gauge factor (G_F) was calculated according to the expression:

$$G_F = \frac{(R - R_0)/R_0}{(l - l_0)/l_0}$$

where R is the electrical resistance at the stretched position, R_0 is the electrical resistance at the initial position, l is the length at the stretched position and l_0 is the length at the initial position.

Three repetitions of each case were performed, and the reported values are averages with their corresponding standard deviation.

2.4.2. Hydrogels for nucleus pulposus replacements

2.4.2.1. Synthesis of LysG3(CB)

0.5 g of TentaGel S NH2 resin were weighted into a reaction vessel. Then, 7 ml of dimethylformamide (DMF) were added to the reaction vessel and resin was left to swell for 15 minutes. DMF was finally removed and a stirring bar was added.

0.4 mmoles of Rink Amide linker, 0.4mmoles of (2-(1H-benzotriazol-1-yl)-1,1,3,3-tetramethyluronium hexafluorophosphate) (HBTU) and 140 µl (0.8 mmoles) of *N,N* – Diisopropylethylamine (DIPEA) were added into a glass vial which contained 3 ml of DMF. The mixture was sonicated for a few seconds to solubilise, and it was then added to reaction vessel. Coupling reaction was carried out in a Biotage® Initiator Classic microwave. Table 1 shows the microwave conditions.

Once the cycle was completed, the solvent was removed from the reaction vessel and the resin was washed with 3x3 ml of DMF.

3x3 ml of 20 % v/v piperidine in DMF were added to reaction vessel for deprotection steps. Deprotection conditions are showed in Table 1.

0.4 mmol of Fmoc-Arg(Pbf)-OH were then added to a glass vial, and also 0.4 mmoles HBTU and 140 µl DIPEA and 3 ml of DMF. The final mixture was finally added to the reaction vessel. Coupling and deprotection reactions were repeated using Fmoc-Lys(Fmoc)-OH and 20% v/v piperidine in DMF respectively, in the exact concentration and conditions described before, until getting the third generation dendrimer.

Same coupling conditions were carried out to finally attach betaine to achieve **LysG3(CB)**. 0.4 mmoles of betaine were used to obtain the functionalised dendrimer.

Then, 5 ml of dichloromethane were added to syringe and all the content was transfered to a pre-weighed 10 ml fritted syringe to be washed with 40 ml of dichloromethane, 8x5 ml of methanol and finally with 8x5 ml of diethylether. The content was dried at RT for a few hours.

Cleavage reaction was carried out as last step to remove the resin. Cleavage solution consisted of 95% v/v of trifluoroacetic acid (TFA), 2.5% v/v of triisopropylsilane and 2.5 % v/v of water.

Finally, the dendrimer was obtained removing the resin by filtration with glass wool. The filtrated dendrimer solution was washed with 8x5 ml of dichloromethane, 8 x5 ml of methanol and finally with 8x5 ml of diethylether. Dialysis of the product was carried out and the final pure freeze-drier dendrimer was obtained.

Program	Duration (minutes)	Power (W)	Initial Power (W)	T (^{o}C)	Pressure	Stirring Rate (rpm)	Absorption
Coupling	5	50	10	60	Off	900	High
Deprotection	2	Off	Off	Off	Off	900	High

Table 1. List of Programs for Microwave Synthesis.

2.4.2.2. Synthesis of LysG3(CB)-based hydrogels

Pure PAm hydrogels were prepared using Am, MBA as cross-linker and KPS as initiator. Am was initially dissolved in ultrapure Milli-Q water (200 mg/ml) together with the MBA (0.2 mg/ml). The solution was homogenised by stirring and mild sonication. Then, KPS was added (at a final concentration of 0.4 mg/ml) and the system

was allowed to polymerise at 75 ^{o}C in a time period of 1 hour. In the case of the dendrimer-based hydrogels, two different strategies were carried out:

AM Dis X: an identical process was followed, except for the use of dendrimer aqueous dispersions instead of plain water, with the necessary concentration to end up in the desired quantity of dendrimer within the gel matrix. The dendrimer contents used were 0.1 wt% and 10 wt%.

AM Da X: in this case the synthesis of a pure PAm hydrogel is the first step. Then, once that hydrogel is dried, it is submerged into the dendrimer aqueous solution (0.1 wt%) with a final volume equal to the native swollen state of the pure hydrogel.

2.4.2.3. SEM studies

The hydrogel microstructure was analysed by Scanning Electron Microscopy using a ZEISS SIGMA HD instrument. The distribution of the pore size was measured for all samples in the various SEM images by using Fiji software. Blank and dendrimer-containing hydrogels were frozen in their final swelling degrees and then dried overnight in a freeze-drier to yield dry aerogel samples. SEM samples were prepared by sputter coating with a platinum layer of about 4 nm.

2.4.2.4. Cytotoxicity studies

LDH assay

50 µL of supernatant was incubated with 50 µL LDH substrate (reconstituted as per kit instructions) and allowed to incubate at room temperature in the dark for 30 minutes. The reaction was ceased through the addition of 50 µL 1M hydrochloric acid, and results determined immediately by measuring absorbance at 492 nm using a spectrophotometer (Thermo Multiskan Ascent 354). Absorption was converted to a measurement of cytotoxicity based upon the percent total LDH released from the cell, using the following equation:

$$\text{Citotoxicity (\%)} = \left(\frac{((S - mean\ CF) - (mean\ NC - mean\ CF))}{((mean\ PC - mean\ CF) - (mean\ NC - mean\ CF))} \right) \text{x } 100$$

Where:

S = sample absorption

CF = average cell free blank absorbance

NC = average negative control, or non-treated healthy population absorbance value

PC = average positive control, or fully lysed cell population absorbance value.

HPI technique

3T3 cells were seeded at a density of 6.0 x 10^3 cells/cm^2 in two different 24 well plates (Thermo Scientific Nunc® 24 Microwell™, Fisher Scientific UK).

At time point of 48 hours, cell medium was aspirated and wells washed twice with PBS. After, one of the plates was filled with the different hydrogel samples and the other one was filled with the supernatants in which that hydrogels had been submerged for 48 hours. The two plates were then incubated at 37^{o}C and 5 % CO_2 for 48 hours more.

After that time, cell medium was aspirated and cell nuclei were stained with 50 µL of a fresh Hoescht-Propidium Iodide solution (10 mg/mL and 1 mg/mL final concentrations, respectively) in culture media. After 3 minutes of incubation, images were immediately taken using a fluorescent microscope.

2.4.2.5. Cell behaviour studies

Cells Seeding

Cylindrical shape samples (0.5 cm of diameter and 3 mm of thickness) were cut from bigger pieces of freeze-dried hydrogels using a borer. All the discs were sterilised under UV for 60 minutes (30 minutes each disc face).

Gelatin was also incubated for 1 hour at 37 ^{o}C 5% CO_2 (300 µL per well).

All the materials were preconditioned at 37 ^{o}C 5% CO_2 in the seeding medium (200 µL regarding some preliminary absorbing experiments). Any excess of preconditioning medium was then removed and the cells were seeded on the up surface of the

materials (seeding density = $3*10^4$ / volume around 10 µL per sample). They were then incubated for 15 minutes at 37 ^oC 5% CO_2.

After that time, 1 ml of DMEM (10% FBS) medium was added and the samples were incubated at 37 ^oC 5% CO_2 at time point of 48 hours.

DAPI experiments

The incubated discs were rinsed twice with PBS and cells were fixed in 3.7% formalin. The samples were then cut transversely and the final slides of ≈1 mm of thickness were put on a coverslip. Then, 2 drops of DAPI were added on the top of each sample and after at least 5 minutes the samples were analysed in the dark under the confocal microscope (Leica TCS SP5).

SEM studies

The incubated discs were rinsed twice with PBS and cells were fixed in 2.5% glutaraldehyde for 2 hours. Cells were dehydrated through series of graded ethanol solutions:

25% x 30'

50% x 30'

75% x 30'

100% x 30'

The samples were then air-dried under the hood and cut transversely. Finally, they were covered with a 4 nm Pt coat and analysed by SEM using a ZEISS SIGMA HD equipment.

2.5. Conclusions

Smart nanocomposite hydrogels based on graphene have been designed, synthesised and characterised. Acrylamide has been used as main monomer for the formation of the polymer network.

Noticeable features and synergies have been achieved. Hence, some new aspects not described yet for this kind of materials have been investigated. We have studied the cross-linking role of the nanomaterial into the polymer network, describing how chemical and physical interactions play a role in the cross-linking process.

Different possible applications of the final materials have been also studied and described. One of those applications is the design of drug-delivery systems, as our hydrogels respond to microwave radiation without any previous treatment. The responsive de-swelling is more consistent in the presence of graphene, and, moreover, the nanomaterial avoids any superheating of the sample.

In addition, the graphene-based composite hydrogels here presented behave as strain gauges. Indeed, gauge factor values around 9 have been obtained through the incorporation of graphene into the polymer matrix, which makes these systems good options as strain sensors.

A different improvement achieved by using graphene as filler in the hydrogels was related to the enhancement of the mechanical properties. The compressive modulus becomes notably higher for **AMG2** with respect to **AM**, and no fatigue behaviour was observed, which makes them perfect candidates as IVD prostheses. Finally, guided by those results, our composite hydrogels and other different materials based on a peptide-based dendrimer have been successfully tested as 3D scaffolds for cell culture, which makes them possible candidates in the field of nucleus pulposus replacements. Graphene does not limit the applicability of the systems in that field, and very intriguing results were obtained regarding the cell behaviour in the presence of the dendrimer. Therefore, an interesting experiment would be the creation of the

composite combining both graphene and peptide-based dendrimer to test the behaviour of osteoblasts seeded on that kind of composite hydrogel.

2.6. References

(1) Drury, J. L.; Mooney, D. J. Hydrogels for Tissue Engineering : Scaffold Design Variables and Applications. *Biomaterials* **2003**, *24*, 4337–4351.

(2) Vilela, C. A.; Correia, C.; Oliveira, J. M.; Sousa, R. A.; Reis, R. L. Cartilage Repair Using Hydrogels : A Critical Review of in Vivo Experimental Designs. *ACS Biomater. Sci. Eng.* **2015**, *1*, 726–739.

(3) Merino, S.; Martín, C.; Kostarelos, K.; Prato, M.; Vázquez, E. Nanocomposite Hydrogels: 3D Polymer–Nanoparticle Synergies for On-Demand Drug Delivery. *ACS Nano* **2015**, *9*, 4686–4697.

(4) Zhu, J. Design Properties of Hydrogel Tissue-Engineering Scaffolds. *Expert Rev. Med. Devices* **2011**, *8*, 607–626.

(5) Billiet, T.; Vandenhaute, M.; Schelfhout, J.; Vlierberghe, S. Van; Dubruel, P. Biomaterials A Review of Trends and Limitations in Hydrogel-Rapid Prototyping for Tissue Engineering. *Biomaterials* **2012**, *33*, 6020–6041.

(6) Liu, R.; Liang, S.; Tang, X.-Z.; Yan, D.; Li, X.; Yu, Z.-Z. Tough and Highly Stretchable Graphene Oxide/polyacrylamide Nanocomposite Hydrogels. *J. Mater. Chem.* **2012**, *22*, 14160–14167.

(7) Zhang, N.; Li, R.; Zhang, L.; Chen, H.; Wang, W.; Liu, Y.; Wu, T.; Wang, X.; Wang, W.; Li, Y.; et al. Actuator Materials Based on Graphene Oxide/polyacrylamide Composite Hydrogels Prepared by in Situ Polymerization. *Soft Matter* **2011**, *7*, 7231–7239.

(8) Liu, J.; Chen, C.; He, C.; Zhao, J.; Yang, X.; Wang, H. Synthesis of Graphene Peroxide and Its Application in Fabricating Super Extensible and Highly Resilient Nanocomposite Hydrogels. *ACS Nano* **2012**, *6*, 8194–8202.

(9) Hou, C.; Zhang, Q.; Li, Y.; Wang, H. Graphene–polymer Hydrogels with Stimulus-Sensitive Volume Changes. *Carbon N. Y.* **2012**, *50*, 1959–1965.

(10) Xu, Y.; Lin, Z.; Huang, X.; Liu, Y.; Huang, Y.; Duan, X. Flexible Solid-State

Supercapacitors Based on Three-Dimensional. *ACS Nano* **2013**, *7*, 4042–4049.

(11) Xu, Y.; Sheng K.; Li, C.; Shi, G. Self-Assembled Graphene Hydrogel via a One-Step Hydrothermal Process. *ACS Nano* **2010**, *4*, 4324–4330.

(12) Fan, J.; Shi, Z.; Wang, J.; Yin, J. Glycidyl Methacrylate-Modi Fi Ed Gum Arabic Mediated Graphene Exfoliation and Its Use for Enhancing Mechanical Performance of Hydrogel. *Polymer* **2013**, *54*, 3921–3930.

(13) Servant, A.; Leon, V.; Jasim, D.; Methven, L.; Limousin, P.; Vazquez Fernandez-Pacheco, E.; Prato, M.; Kostarelos, K. Graphene-Based Electroresponsive Scaffolds as Polymeric Implants for on-Demand Drug Delivery. *Adv. Healthc. Mater.* **2014**, *3*, 1334–1343.

(14) Das, S.; Irin, F.; Ma, L.; Bhattacharia, S. K.; Hedden, R. C.; Green, M. J. Rheology and Morphology of Pristine Graphene / Polyacrylamide Gels. *ACS Appl. Mater. Interfaces* **2013**, *5*, 8633–8640.

(15) Toumia, Y.; Orlanducci, S.; Basoli, F.; Licoccia, S.; Paradossi, G. "Soft" Confinement of Graphene in Hydrogel Matrixes. *J. Phys. Chem. B* **2015**, *119*, 2051–2061.

(16) León, V.; Quintana, M.; Herrero, M. A.; Fierro, J. L. G.; de la Hoz, A.; Prato, M.; Vázquez, E. Few-Layer Graphenes from Ball-Milling of Graphite with Melamine. *Chem. Commun.* **2011**, *47*, 10936–10938.

(17) Jorio, A.; Ferreira, E. H. M.; Stavale, F.; Achete, C. A.; Capaz, R. B.; Moutinho, M. V. O.; Lombardo, A.; Kulmala, T. S.; Ferrari, A. C. Quantifying Defects in Graphene via Raman Spectroscopy at Different Excitation Energies. *Nano Lett.* **2011**, *11*, 3190–3196.

(18) Jorio, A.; Lucchese, M. M.; Stavale, F.; Ferreira, E. H. M.; Moutinho, M. V. O.; Capaz, R. B.; Achete, C. A. Raman Study of Ion-Induced Defects in N -Layer Graphene. *J. Phys. Condens. Matter* **2010**, *22*, 334204.

(19) Ferrari, A.C.; Meyer, J.C.; Scardaci, V.; Casiraghi, C.; Lazzeri, M.; Mauri, F.; Piscanec, S.; Jiang, D; Novoselov, K.S.; Roth, S.; Geim, A. K. Raman Spectrum of Graphene and Graphene Layers. *Phys. Rev. Lett.* **2006**, *97*, 187401–1 – 253113–3.

(20) Worsley, M. A.; Pauzauskie, P. J.; Olson, T. Y.; Biener, J.; Satcher, J. H.; Baumann, T. F. Synthesis of Graphene Aerogel with High Electrical Conductivity. *J. Am. Chem. Soc.* **2010**, *132*, 14067–14069.

(21) Ren, L.; Liu, T.; Guo, J.; Guo, S.; Wang, X.; Wang, W. A Smart pH Responsive Graphene / Polyacrylamide Complex via Noncovalent Interaction. *Nanotechnology* **2010**, *21*, 335701–335708.

(22) Fan, J.; Shi, Z.; Lian, M.; Li, H.; Yin, J. Mechanically Strong Graphene Oxide/sodium Alginate/polyacrylamide Nanocomposite Hydrogel with Improved Dye Adsorption Capacity. *J. Mater. Chem. A* **2013**, *1*, 7433–7443.

(23) Sun, J.Y; Zhao, X.; Illeperuma, W.R.K.; Chaudhuri, O; Oh, K.H.; J.Mooney, D.; J.Vlassak J.; Suo, Z. Highly Stretchable and Tough Hydrogels. *Nature* **2012**, *489*, 133–136.

(24) Feng, G.; Zhao, X.; Liu, H.; Zhang, H.; Chen, X.; Shi, R.; Liu, X.; Zhao, X.; Zhang, W.; Wang, B. Transplantation of Mesenchymal Stem Cells and Nucleus Pulposus Cells in a Degenerative Disc Model in Rabbits: A Comparison of 2 Cell Types as Potential Candidates for Disc Regeneration. *J. Neurosurg. Spine* **2011**, *14*, 322–329.

(25) Itoh, S.; Kikuchi, M.; Koyama, Y.; Takakuda, K.; Shinomiya, K.; Tanaka, J. Development of an Artificial Vertebral Body Using a Novel Biomaterial, Hydroxyapatite/collagen Composite. *Biomaterials* **2002**, *23*, 3919–3926.

(26) Chang, G.; Kim, H. J.; Vunjak-Novakovic, G.; Kaplan, D. L.; Kandel, R. Enhancing Annulus Fibrosus Tissue Formation in Porous Silk Scaffolds. *J. Biomed. Mater. Res. - Part A* **2010**, *92*, 43–51.

(27) Reitmaier, S.; Kreja, L.; Gruchenberg, K.; Kanter, B.; Silva-Correia, J.; Oliveira, J. M.; Reis, R. L.; Perugini, V.; Santin, M.; Ignatius, A.; et al. In Vivo Biofunctional Evaluation of Hydrogels for Disc Regeneration. *Eur. Spine J.* **2014**, *23*, 19–26.

(28) Roughley, P.; Hoemann, C.; DesRosiers, E.; Mwale, F.; Antoniou, J.; Alini, M. The Potential of Chitosan-Based Gels Containing Intervertebral Disc Cells for Nucleus Pulposus Supplementation. *Biomaterials* **2006**, *27*, 388–396.

(29) Sakai, D.; Grad, S. Advancing the Cellular and Molecular Therapy for Intervertebral Disc Disease. *Adv. Drug Deliv. Rev.* **2015**, *84*, 159–171.

(30) Simmons, C. A.; Alsberg, E.; Hsiong, S.; Kim, W. J.; Mooney, D. J. Dual Growth Factor Delivery and Controlled Scaffold Degradation Enhance in Vivo Bone Formation by Transplanted Bone Marrow Stromal Cells. **2004**, *35*, 562–569.

(31) Dee, K.C.; Andersen, T.T.; Bizios, R. Design and Function of Novel Osteoblast-Adhesive Peptides for Chemical Modification of Biomaterials. *J. Biomed. Mater. Res.* **1998**, *40*, 371–377.

(32) Meikle, S. T.; Bianchi, G.; Olivier, G.; Santin, M. Osteoconductive Phosphoserine-Modified Titanium Oxide Surface Functionalization and Response of Osteoblast-like Cell Lines. *J. R. Soc. Interface* **2013**, DOI: 10.1098/rsif.2012.0765.

(33) Tan, J.; Gemeinhart, R. a.; Ma, M.; Mark Saltzman, W. Improved Cell Adhesion and Proliferation on Synthetic Phosphonic Acid-Containing Hydrogels. *Biomaterials* **2005**, *26*, 3663–3671.

(34) Morrison, S. J.; Spradling, A. C. Review Stem Cells and Niches : Mechanisms That Promote Stem Cell Maintenance throughout Life. *Cell* **2008**, *132*, 598–611.

(35) Fuchs, E.; Tumbar, T.; Guasch, G. Socializing with the Neighbors : Stem Cells and Their Niche. *Cell* **2004**, *116*, 769–778.

(36) Wurmser, A. E.; Palmer, T. D.; Gage, F. H.; Holland, P. In the Stem Cell Niche. *Science* **2004**, *304*, 1253–1255.

(37) Aryaei, A.; Jayatissa, A.H.; Jayasuriya, A. C. The Effect of Graphene Substrate on Osteoblast Cell Adhesion and Proliferation. *J. Biomed. Mater. Res. - Part A* **2015**, *102*, 3282–3290.

(38) Shi, X.; Chang, H.; Chen, S.; Lai, C.; Khademhosseini, A. Regulating Cellular Behavior on Few-Layer Reduced Graphene Oxide Films with Well-Controlled Reduction States. *Adv. Funct. Mater.* **2012**, *22*, 751–759.

(39) Green, R. a.; Hassarati, R. T.; Goding, J. a.; Baek, S.; Lovell, N. H.; Martens, P. J.;

Poole-Warren, L. a. Conductive Hydrogels: Mechanically Robust Hybrids for Use as Biomaterials. *Macromol. Biosci.* **2012**, *12*, 494–501.

(40) Tanaka, T.; Nishio, I.; Sun, S.T.; Ueno-Nishio, S. Collapse of Gels in a Electric Field. *Science.* **1982**, *218*, 467–769.

(41) Wong, T. W. Electrical , Magnetic , Photomechanical and Cavitational Waves to Overcome Skin Barrier for Transdermal Drug Delivery. *J. Control. Release* **2014**, *193*, 257–269.

(42) Budhlall, B. M.; Marquez, M.; Velev, O. D. Microwave , Photo- and Thermally Responsive PNIPAm - Gold Nanoparticle Microgels. *Langmuir* **2008**, *24*, 11959–11966.

(43) Rivero, R. E.; Molina, M. A.; Rivarola, C. R.; Barbero, C. A. Sensors and Actuators B : Chemical Pressure and Microwave Sensors / Actuators Based on Smart Hydrogel / Conductive Polymer Nanocomposite. *Sensors Actuators B. Chem.* **2014**, *190*, 270–278.

(44) Jeong, B.; Wan, S.; Han, Y. Thermosensitive Sol – Gel Reversible Hydrogels. *Adv. Drug Deliv. Rev.* **2012**, *64*, 154–162.

(45) Vázquez, E.; Prato, M. . Carbon Nanotubes and Microwaves : Interactions, Responses, and Applications. *ACS Nano* **2009**, *3*, 3819–3824.

(46) Wang, C.; Han, X.; Xu, P.; Zhang, X.; Du, Y.; Hu, S.; Wang, J.; Wang, C.; Han, X.; Xu, P.; et al. The Electromagnetic Property of Chemically Reduced Graphene Oxide and Its Application as Microwave Absorbing Material The Electromagnetic Property of Chemically Reduced Graphene Oxide and. *Appl. Phys. Lett.* **2011**, *98*, 072906, DOI: 10.1063/1.3555436.

(47) Stassi, S.; Cauda, V.; Canavese, G.; Pirri, C. Flexible Tactile Sensing Based on Piezoresistive Composites: A Review. *Sensors* **2014**, *14*, 5296–5332.

(48) Thostenson, B. E. T.; Chou, T. Carbon Nanotube Networks : Sensing of Distributed Strain and Damage for Life Prediction and Self Healing. *Adv. Mater.* **2006**, *18*, 2837–2841.

(49) Yamada, T.; Hayamizu, Y.; Yamamoto, Y.; Yomogida, Y.; Izadi-najafabadi, A.;

Futaba, D. N.; Hata, K. Human-Motion Detection. *Nat. Nanotechnol.* **2011**, *6*, 296–301.

(50) González-Domínguez, J.M.; Díez-Pascual, A.M.; Ansón-Casaos, A.; Gómez-Fatou, M.A.; Martínez, M. Functionalization Strategies for Single-Walled Carbon Nanotubes Integration into Epoxy Matrices. In *Polymer Nanotube Nanocomposites*; 2014; pp. 45–116.

(51) Gonzalez-dominguez, J. M.; Anso, A.; Martinez, M. T.; Ferreira, A.; Vaz, F. Piezoresistive Response of Pluronic- Wrapped Single-Wall Carbon Nanotube – Epoxy Composites. *J. Intell. Mater. Syst. Struct.* **2016**, *23*, 909–917.

(52) Boland, C. S.; Khan, U.; Backes, C.; Neill, A. O.; Mccauley, J.; Duane, S.; Shanker, R.; Liu, Y.; Jurewicz, I.; Dalton, A. B.; et al. Terms of Use Bodily Motion Sensors Based on Graphene À Rubber Composites. *ACS Nano* **2014**, *8*, 8819–8830.

(53) Martinez, V.; Stau, F.; Adagunodo, M. O.; Forro, C.; Vo, J.; Larmagnac, A. Stretchable Silver Nanowire − Elastomer Composite Microelectrodes with Tailored Electrical Properties. *ACS Appl. Mater. Interfaces* **2015**, *7*, 13467–13475.

Chapter 3

Nanostructured composites for neuronal network regeneration

3.1. Introduction

3.1.1. Neuronal networks

A neuronal network refers to a population of physically interconnected neurons or a group of diverse neurons whose inputs or signalling targets delimit an appreciable circuit. Neuronal networks are able to perform specific physiological functions, and thanks to that activity, our central nervous system (CNS) has the ability to perform complex functions such as memory or pattern discrimination.

Neuronal networks consist of two main kinds of cells. The first one is glial cells, which have a supportive, protective and regulatory role, and represent the majority of the cells. The four different types of glial cells found in the CNS are Ependymal cells, Astrocytes, Microglial cells and oligodendrocytes. The second type of cells in neuronal networks is neurons: the primary computing element that provides communication within the nervous system.

A neuron is an electrically excitable cell that processes and transmits information through electrical and chemical signals. Although neurons can have different shapes and sizes (pyramidal cell, granule cell, small reticular formation, etc.), all of them consist of three basic common parts (Figure 1):

- Cell body, where all the important and needed organs for cell survival are located.
- Dendrites, which are projecting outwards from the cell body. The role of dendrites is to receive signals from other neurons by increasing the available surface area. Some neurons may have up to 400.000 dendrites.
- Axon, also known as nerve fibre. This structure extends from the cell body and finishes in other cells (its length can vary from less than a millimetre to

longer than a metre). Axon conducts electrical signals, called action potentials, away from the neuron.

Neurons are secretory cells as they secrete a particular chemical messenger called "neurotransmitter" when an electrical stimulus is transmitted to the end of the neuron. Neurotransmitter molecules are released from the end of the axon and move to specific receptors on the receiving neurons. The neurotransmitter diffusion region is called "synapse" (Figure 1).

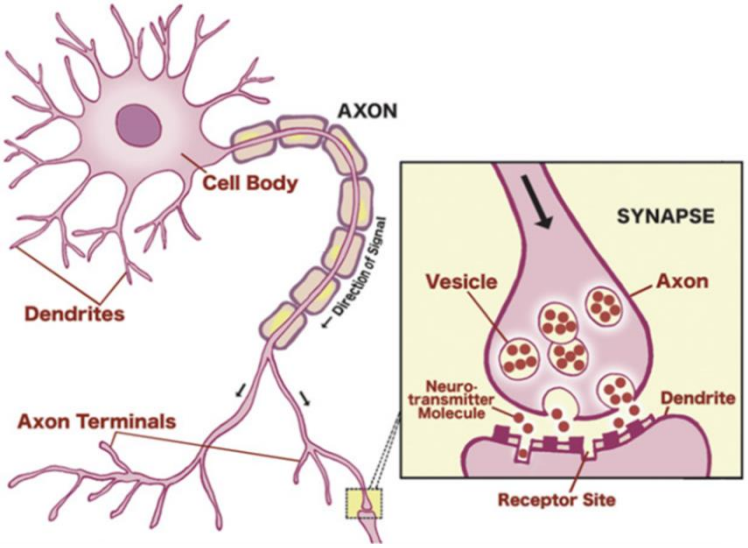

Figure 1. General structure of neurons.

Neurons can be functionally classified as:

- Sensory neurons, which carry somatic nervous system signals from joints, skeletal muscles, or sensory organs to the CNS, the brain and spinal cord.
- Interneurons, which are found exclusively within the spinal cord and brain and are stimulated by signals from sensory neurons, other interneurons or both of them.

- Motor neurons, which conduct action potentials out of the CNS. In this case, the cell body and the dendrites are located in the CNS, but axons run inside the nerves to the muscles and glands that carry out the response. These cells are normally stimulated by interneurons, but the can be also stimulated by sensory neurons directly.

Our comprehension of individual neurons has enhanced enormously in the last couple of decades due to new microscopy imaging technologies. However, intensive research is being carried out in order to ascertain how the CNS performs its complex functions, owing to the activity of neuronal networks. The two main ways to investigate this event are: (i) the identification of the most basic mechanism of neural codes generation,[1] and (ii) the understanding of underlying laws in CNS processes for the creation of artificial neural networks.[2]

3.1.2. Electrical properties of neurons

Neurons are the most common excitable cells, but they are limited by the cell membrane, which is made of a phospholipidic bilayer. There is an unequal distribution of ions on the two sides of a nerve cell membrane, with the cell interior negative with respect to the exterior. Actually, the membrane potential (V_m) is the difference between the voltages of the outside and the inside solutions. The V_m for a neuron of the CNS at the steady state is set at -70 mV (resting membrane potential), because the external solution is conventionally set as the zero voltage.

The cell membrane acts as barrier preventing the mixing of intracellular fluid with the extracellular one. It also contains voltage-gated ion channels and ion pumps. Ion channels transport ions according to the concentration gradient and they are responsible for the membrane voltage changes, as they respond when the cell is stimulated. On the other hand, ion pumps work against the concentration gradient consuming cell energy.

An action potential is a very rapid change in V_m that occurs when an external stimulus is applied to the neuron, and it specifically goes from the resting potential to positive values in just milliseconds. The reason of this rapid variation is the change in the permeability of the membrane, as the gates that are selective for sodium ions open when the neuron is stimulated. Therefore, all the positive ions go inside the nerve cell, which interior is positive now, regarding its exterior part. In this moment the cell is depolarised and sodium gates are now blocked. Moreover, potassium-selective channels open to recover the initial state. Finally, the neuron is repolarised and the resting potential is reached again due to the action of the Na^+/K^+ pumps because they re-establish the ion concentration inside and outside of the cell.

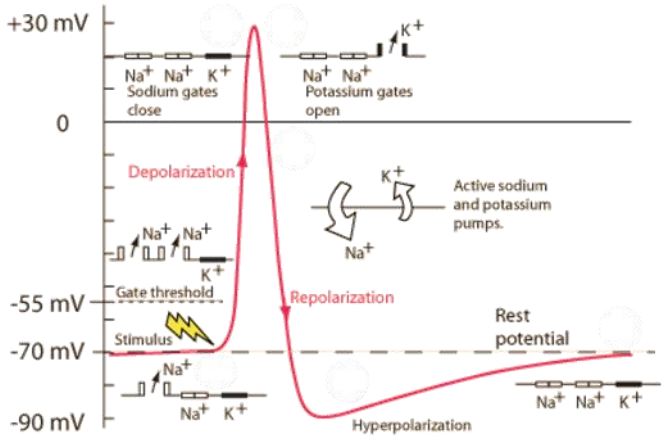

Figure 2. Scheme of the Action Potential

The polarity varies across the membrane as the action potential travels by the axon, and it stimulates other cells (neurons, muscles or glands) when the signal reaches the axon terminal. Actually, the arrival of an action potential opens voltage-sensitive calcium gates at the presynaptic level. The key thing about calcium coming into the cell is it serves as an intracellular messenger that initiates many types of physiological events. Indeed, electrical signalling would be useless without calcium channels because every physiological event that is initiated by an electrical signal is initiated by calcium coming into calcium channels.[3] The influx of Ca^{2+} causes vesicles filled with neurotransmitters to migrate to the surface and deliver their contents. The neurotransmitters then bind to specific receptors on the postsynaptic cell.

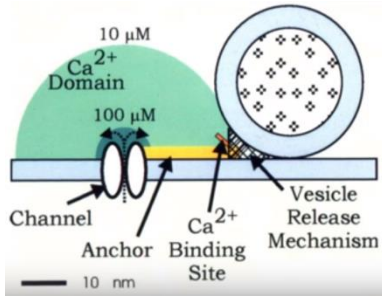

Figure 3. Scheme of the calcium channel action.

3.1.3. Neurophysiology methods

Neurophysiology is "a branch of physiology and neuroscience that is concerned with the study of functioning of the nervous system". In last decades, the study of action potentials has induced the creation of experimental neurophysiology techniques. Voltage clamps, current clamps, electrophysiology in couple of neurons, calcium imaging or optogenetics are possible examples. Here, only some of those tools will be described, just to understand in a proper way the obtained results from the performed neuronal culture experiments.

3.1.3.1. Voltage clamp technique

One difficulty in studying the behaviour of the conductance in the neuron membrane is that it varies over time, rising and falling as the action potential advances, and also because it changes with voltage. The voltage clamp technique makes it possible to study changes in sodium and potassium conductance because the voltage across the membrane can be controlled, to whatever value, using this method.

First, the neuron to be studied is placed in a saline solution. V_m is measured by an amplifier using an internal recording electrode inserted into the cell, and a reference one in the bath. The command voltage (V_{cmd}) is the desired membrane voltage, and it is set by the researcher. The difference between V_m and V_{cmd} is determined and converted into a current by the amplifier. That current is injected into the neuron to make equal both voltages. Then, the amount of current which is necessary to keep V_m equal to V_{cmd} is measured and recorded.

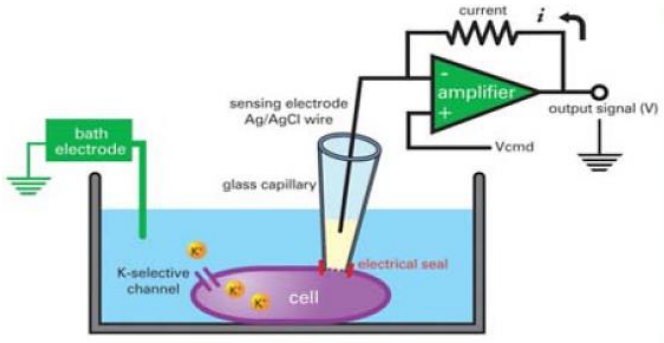

Figure 4. Scheme of voltage clamp technique.

3.1.3.2. Imaging of calcium activity

As it has being explained before, calcium ions generate versatile intracellular signals that control key functions in neurons. Calcium imaging is especially important as calcium signals exert their specific functions in well-defined cellular subcompartments.

Therefore, this second method is based on calcium indicators, which are fluorescent molecules that respond to the joining of Ca^{2+} ions by varying their fluorescence properties regarding the synaptic transmission. There are two main types of calcium indicators: chemical and genetically encoded ones. This tool allows study Ca^{2+} signalling in a wide range of cell types and neuronal activity. Actually, there are multiple mechanisms of neuronal calcium signalling.[4] In a few words, calcium signals report the activation of specific receptors at the level of individual dendrites. Then, it is possible to observe a coupling between presynaptic action potentials and postsynaptic flashes of calcium when an axon is stimulated.

3.1.4. Nanostructured materials for neuronal studies

The behaviour of the cells *in vivo* is usually defined by the biological signals that they receive from the extracellular matrix, which has nanometer features.[5] Hence, nanomedicine develops new materials and devices which are able to work intracellularly,[6] so it is evident that nanotechnology plays an important role in the treatment and diagnosis of disease. Nanomaterials interact with cells and change their properties,[7,8] so designing tissue-engineering scaffolds based on nanostructures could improve cell growth and performance.[9,10]

Moreover, neuroscience is highly promising regarding the knowledge of the pathological pathways. Parkinson´s or Alzheimer´s diseases, for instance, could be treated in an easier way by developing new nanostructured materials, taking into account all those concepts. In particular, these materials have to be designed focusing the attention on three main necessary and important features for neuronal prostheses: biocompatibility, stability and conductivity.

Although there are several examples in literature based on multifunctional nanoparticles to enhance the electrical activity of neuronal networks,[7,11] carbon nanotubes (CNTs) have been the most exiting used nanomaterials for neuronal regeneration.[12,13] This nanomaterial represent biocompatible substrates, and they can be functionalised with polymers to modulate neuronal survival and growth.[14]

The group of Prof. Maurizio Prato has large experience in this field. They showed that nanotubes could affect neuronal information processing:[15] planar sections of neurons grown on single-wall or multi-wall carbon nanotubes (SWNTs or MWNTs) showed a healthy organisation of neuronal networks with the presence of synaptic contacts. Their considerations represented the first attempt at linking electrical phenomena in nanomaterials to neuronal excitability.

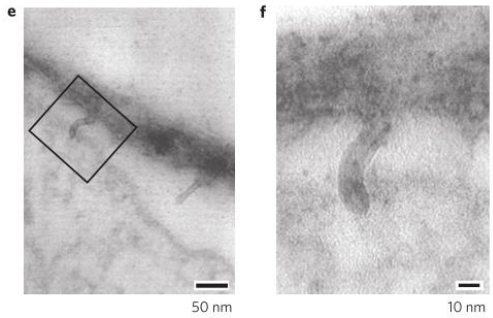

Figure 5. TEM pictures of the ultrastructural interaction between nanotubes and neurons. Rectangular box represents the presence of synaptic contact.[15]

Moreover, 3D scaffolds are being highly investigated as they are showing better results not only in relation to neuronal differentiation,[16] but also regarding neurons growth[17] and improvement of functional organisation and synchronisation in small neuronal assemblies, comparing with 2D substrates.[18]

As already discuss in this memory, graphene is attracting the attention of many researchers as it possesses unique electrical, physical and chemical properties that point it out as a potential bioscaffold for neuronal regeneration. Actually, graphene has demonstrated to be biocompatible with neurons.[19] Moreover, Park and co-workers demonstrated in 2011 that graphene is better than glass for human neuronal stem cells growth, exhibiting a greater ratio of neurons to glial cells, and the substrate could even deliver currents to the neurons, which is very useful for neuronal stimulation.[20]

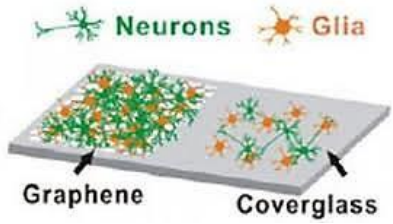

Figure 6. Scheme of the nerve/glial cells growths in graphene and coverglass.[20]

A work performed in collaboration with the group of Prof. Prato and Prof. Ballerini has recently reported that graphene-based interfaces do not alter target nerve cells.[21] In this study, it is shown that graphene-based substrates produced by liquid phase exfoliation or ball-milling exfoliation of graphite are inert to neuron-interfacing, being able to preserve the basal physiological level of neuronal activity.

A very interesting example is related to 3D porous graphene foam, which is a new scaffold for neural stem cells *in vitro*. Li and co-workers developed this material, and they found that the graphene-foam can not only support cells growth, but also keep them at an active proliferation state better than 2D graphene films.[22]

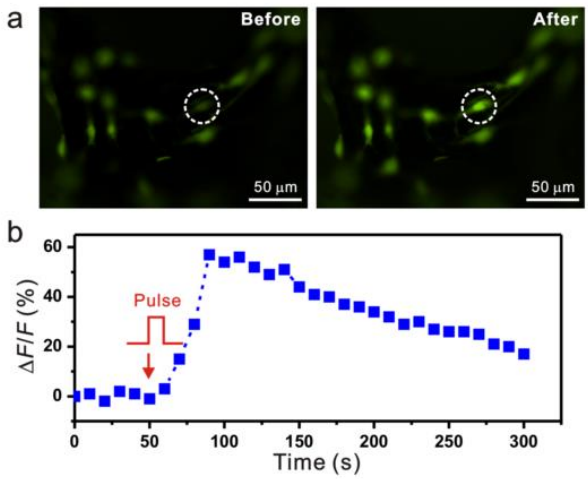

Figure 7. Electrical stimulation of neurons on the 3D graphene foam. a) Fluorescence imaging of cells pre-incubated with Fluo-4 AM dye before and after stimulation. b) Fluorescence intensity change of the circled cell in a) versus stimulation time period.

There are not many examples yet, based on graphene, about differentiation into nerve cells[23] or improvements of electrical signalling in neuronal networks,[24] but this fascinating nanomaterial greatly expands the range of possibilities.

3.2. Objectives

The unavoidable loss of nerve tissue, caused by degenerative diseases, is devastating mainly because of the poor regenerative abilities of the CNS. Because of that, establishing controlled and reliable ways to guide neuronal regeneration has been a challenge in this field.

As it has been explained before, synthetic materials at the nanoscale can instruct neuron-specific behaviours. Therefore, the main objective is to exploit the design of artificial man-designed devices that collaborate with neuronal network activity, developing nanostructured materials capable of crossing the barriers between artificial devices and nerve cells.

To reach our purpose, we thought about creating new nanostructured systems using different nanomaterials with excellent electrical properties, such as carbon nanotubes, silver nanowires and graphene, arranged in an ingenious 2D mode.

Moreover, we consider studying the activity of neurons on 3D polymeric scaffolds based on graphene, due to the excellent results obtained not only by using this interesting nanomaterial, but also regarding the improvements reached in this field by using 3D structures.

3.3. Results and Discussion

3.3.1. 2D substrates

One of the most influential works of neuron patterning are those by Letourneau, who studied in 1975 the preferential adhesion and growth of dorsal root ganglion neurons on patterned substrates.[25,26] Since then, thousands of studies have been done in relation to this field. CNTs-based substrates have been one of the most developed materials in the last years regarding neural network regeneration. In order to improve the results obtained from all those studies, we thought about the creation of new 2D substrates based on different nanostructured designs: SWNTs+Graphene-based substrates and AgNWs-based substrates.

3.3.1.1. SWNTs+Graphene-based substrates

This first kind of devices is related to substrates made from the combination of two different nanomaterials with incredible electrical properties: SWNTs and graphene.

The main idea about the preparation of this kind of composite devices was to cover a preliminary film of sprayed SWNTs with graphene. By this way, the neurons would be seeded on a uniform and homogeneous carpet of nanomaterial, being in contact with an awesome electrical composite along all the substrate. This fact could improve the general activity of the cultured neurons. Therefore, our main aim here was to verify whether SWNTs, when masked by a graphene film, still retain the ability to interact at the interface with neurons and neuronal networks leading to increased neuronal synaptic connectivity.

Preparation and characterisation

We used a spray coating technique to cover glass substrates with both nanomaterials. Spray coating is one of the most common techniques in industrial

production and it is used when it is necessary to obtain homogeneous substrates in a simple and scalable way.[27]

In particular, SWNTs were dissolved in ethyl acetate and the proper amount of solution was sprayed on a glass coverslip placed on a hot plate at 100 ^{o}C until achieving a density around $7 \cdot 10^{-5}$ mg/mm^2. Then, layered coverslips were placed in an oven at 350 ^{o}C under nitrogen atmosphere for 20 minutes to de-functionalise the carbon nanotubes preserving their electronic structure, obtaining the SWNTs substrates.

After that, ethanol dispersions of graphene were prepared: starting from aqueous dispersions of graphene prepared by ball-milling treatment,[28] water was exchanged by ethanol by filtration. The resultant dispersions were sprayed at the same time on the SWNTs sprayed coverslips, on new pure coverslips and also on the control ones (Figure 8). The control coverslips consisted of glass substrates painted with a silver paste in a detailed way to fabricate several electrodes and be able to measure the conductivity of the film in an accurate way.

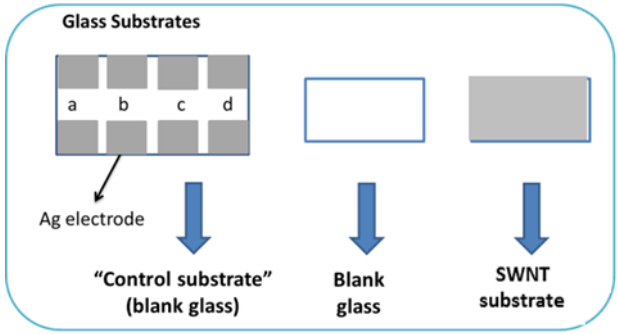

Figure 8. Scheme of the locations of the coverslips while they were being sprayed with the dispersion of graphene. The letters show the four points (a, b, c and d) where both the resistance and the transmittance were measured.

In this case, the concentration of the graphene dispersion in ethanol was 0.05 mg/ml and the plate temperature was 100 ^{o}C. The coverslips were coated until a graphene film with an average sheet resistance (Rs) of 154.3 kΩ/sq was achieved. All the substrates were then put in an oven at 350 ^{o}C for 20 minutes, obtaining graphene films with an average Rs of 30.4 kΩ/sq and an average transmittance of 37%. Each control coverslip showed similar values of resistivity and transmittance due to the good homogeneity achieved in each substrate.

Figure 9. Appearance of graphene (left) and SWNTs+graphene (right) substrates.

The sprayed substrates were also characterised by scanning electron microscopy (SEM). It was possible to observe the homogeneous surfaces of the films (Figure 10). As expected, no morphological variations were observed between both kinds of substrates.

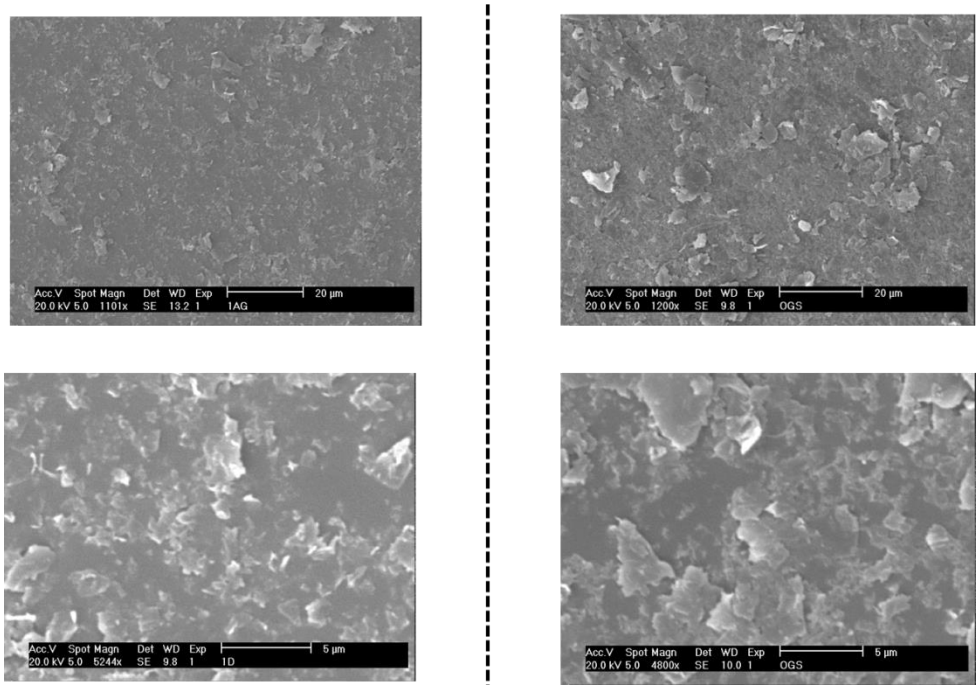

Figure 10. SEM pictures of graphene (left) and SWNTs+graphene (right) substrates at different scales.

Neuronal studies

The neuronal studies carried out in this thesis have been performed in collaboration with the group of Prof. Laura Ballerini at the International School for Advanced Studies in Trieste.

Dissociated hippocampal cultures were seeded on graphene, SWNTs and SWNTs+graphene substrates, in order to evaluate the effects of the different substrates on the synaptic activity of neuronal cells. We recorded the network activity of dissociated hippocampal cells through the patch clamp technique in voltage clamp modality.

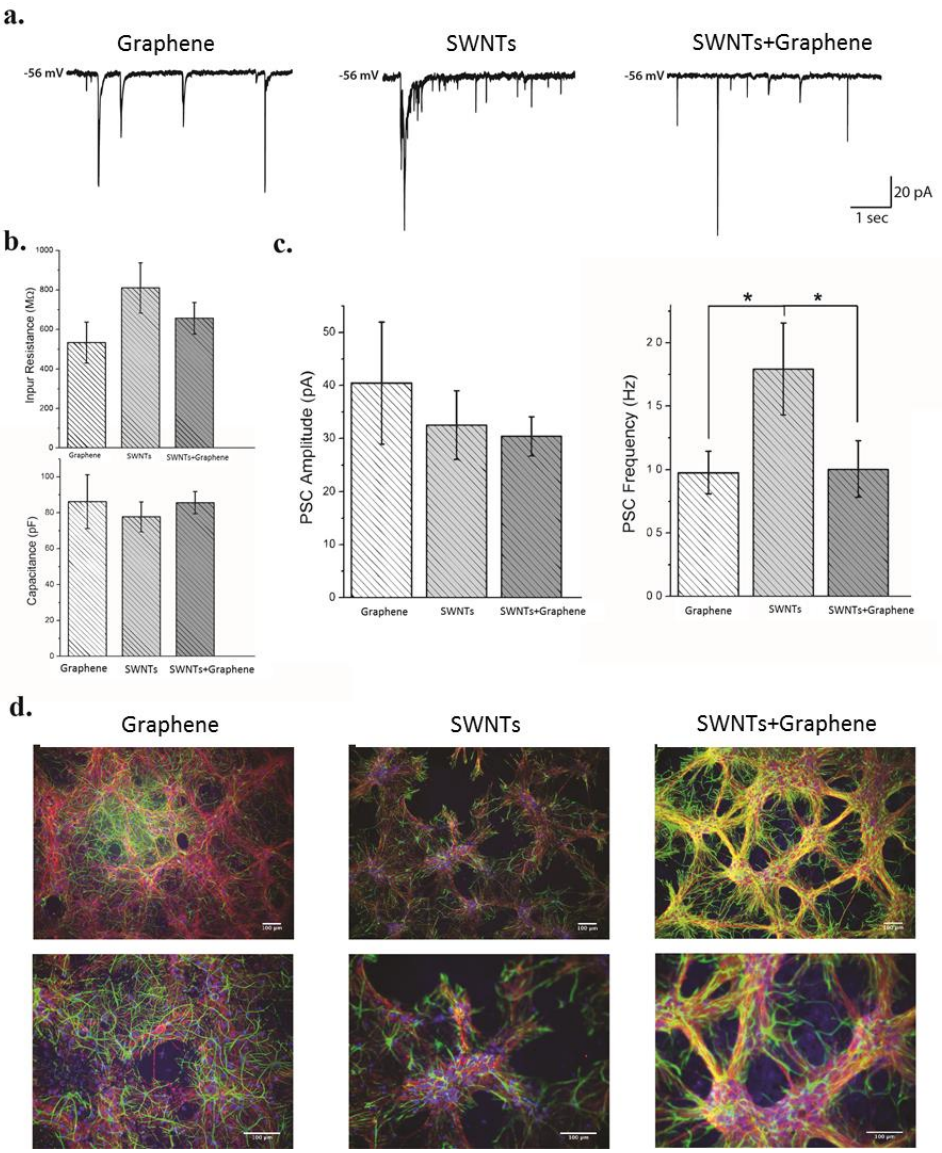

Figure 11. Hippocampal primary cultures grown on Graphene, SWNTs and SWNTs+graphene substrates; a. Representative current tracings showing heterogeneous post-synaptic currents (PSCs; inward deflections); b. histograms summarising the values of cell membrane passive properties; c. the amplitude (left) and frequency (right) of spontaneous PSCs detected in Voltage Clamp modality; d. fluorescent micrographs of immunostained cultures (top panels:10x, bottom panels:20x).

Experiments were performed after 8-10 days *in vitro* (DIV). All the substrates used were biocompatible, as shown in Figure 11d, they supported *in vitro* growth and development of both neurons and glial cells. In addition to the healthy cell condition, the neurons passive membrane properties displayed, for all the tested substrates, values in agreement with previous control assessments.[29]

In order to study the ability of graphene and SWNTs, when masked by a graphene film, to interact at the interface with neuronal networks, we tested the main electrophysiological parameter known to be affected by SWNTs: the frequency of the spontaneous post-synaptic currents (PSC) generated by the neuronal network activity. Figures 11a shows representative recordings of spontaneous synaptic activity (mixed PSCs are appearing as inward current deflections) from voltage clamped neurons in all conditions. We quantified synaptic activity as average frequency and amplitude of the detected PSCs.

In Figure 11c plots summarise the PSC amplitude values (left), which were similar among the three conditions indicating that no major changes occurred in the neuronal post-synaptic membranes (40±11 pA in graphene, 32±6 pA in SWNTs and 30±4 pA in SWNTs+graphene). Also, no significant differences were found regarding the PSC frequency (right) of neurons grown on the graphene alone (1±0.5 Hz, $P>0.05$) and SWNTs+graphene (1±0.7 Hz, $P<0.05$), while the PSC frequency was significantly increased in cultures grown on SWNTs alone (1.8±1.2 Hz).

Figure 11b shows the membrane passive properties. Membrane capacitance (top) measured in graphene (white; n=9), SWNTs (light gray; n=11), and SWNTs+graphene (dark gray; n=10), displayed similar values in all tested conditions, 86±15 pF in graphene, 77±8 pF in SWNTs and 86± 6 pF in SWNTs+graphene. Regarding the input resistance (bottom), the values were also found to be similar among the different culturing conditions being 533±102 MΩ in graphene, 810±126 MΩ in SWNTs and 656±80 MΩ in SWNTs+graphene, indicating similar properties, health conditions, growth and cell phenotypes among the different groups.

We also immune-labeled one culture series to visualise neurons and astrocytes (Figure 11d). Left panels represent graphene samples, middle ones SWNTs samples and right panels depict cultures grown on SWNTs+graphene cultures. In red β-tubulin III (to visualise neurons), in green glial-fibrillary acidic protein (GFAP, to visualise astrocytes) and in blue DAPI (to visualise all cell nuclei). A similar morphology was observed among graphene alone and SWNTs alone, while the graphene mixed with SWNTs seemed to induce a more pronounced aggregation of cells when cultured for 8-10 days cultures. Given that these are preliminary observations, with images taken only from one culture series, we could not perform any quantification on the morphology of neurons.

In a few words, this essay confirms the ability of SWNTs to boost neuronal network activity and reports the relatively neutral impact of multi-layered graphene either alone or when covering SWNTs substrates, ultimately impairing direct SWNTs interactions with neuronal networks.

In order to study whether the unique response of SWNTs was due, not only to the electrical properties of the material but also, to their tubular shape, we thought about using a different nanomaterial for the substrates preparation: silver nanowires (AgNWs), which are, as well as SWNTs or graphene, very good conductors.

3.3.1.2. AgNWs-based substrates

This second design is based on silver nanowires. Although this kind of metallic nanostructure is extensively used to construct transparent films for electronic applications such as touch screens,[30] it has not been used as nanomaterial to improve neuronal activity. Therefore, the fabrication of 2D substrates based on AgNWs could be a great idea regarding the electrical properties of this filament-shaped nanomaterial.

Preparation and characterisation

Spray coating technique was used to cover glass substrates placed in a hot plate (100 ^{o}C) with AgNWs. In this case, a nanowires dispersion from Grupo Antolin[31] with a concentration of 0.1 mg/ml in ethanol was sprayed at the same time in the "control" substrate (which has the corresponding silver electrodes), and in the pure glass (the useful sample for neuron culture).

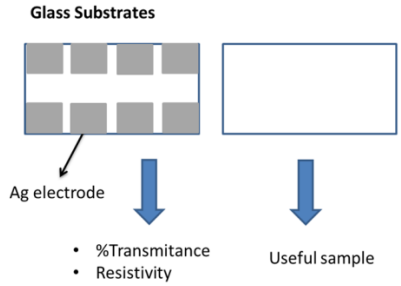

Figure 12. Scheme of the locations of the coverslips while they were being sprayed with the dispersion of AgNWs.

Three different types of substrates were prepared depending on the quantity of sprayed AgNWs. Therefore, coverslips were coated with nanowire films until sheet resistances of approximately 1000 Ω/sq , 100 Ω/sq and 50 Ω/sq, in order to study how this parameter affects to the neuronal activity.

All the substrates were then put in an oven at 200 ^{o}C for 20 minutes, obtaining AgNWs films with average sheet resistances of 82.12 Ω/sq, 11.34 Ω/sq and 3.88 Ω/sq and average transmittances of 74.71 %, 73.96 % and 62.71 % respectively. Although Rs values are different among them, transmittance values are quite similar because few "extra" wires are needed to create new conductive paths, improving the conductivity of the film and avoiding a worse transmittance value. Each control coverslip showed again similar values of resistivity or transmittance due to the good homogeneity achieved in each substrate. These values are very close to that displayed by

commercially available indium tin oxide, so these films could be also applied in the electronic field.

Figure 13. Appearance of a AgNWs substrate.

The sprayed substrates were also characterised by SEM. It was possible to observe the homogeneous surfaces of the films (Figure 14). As expected, all of them had quite similar surfaces but a slightly higher quantity of wires was observed in the substrates with the lowest Rs values.

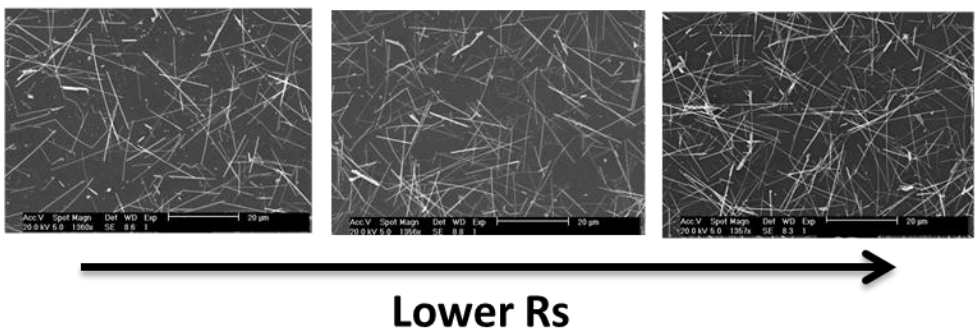

Figure 14. SEM pictures of three different AgNWs substrates depending on the Rs values. Scale bars:20 µm.

Neuronal studies

In order to evaluate the effects of the different substrates on the synaptic activity of neuronal cells, dissociated hippocampal cultures were seeded on AgNWs substrates. We tried to record the network activity of dissociated hippocampal cells through the

patch clamp technique in voltage clamp modality, so experiments were performed after 8-10 DIV. However all the seeded cells died: the substrates were cytotoxic.

The reason could be the silver itself, as some studies show that silver nanoparticles are toxic, depending on the size, to different types of cells, including lung, nerve and skin cells.[32] A different reason for the cytotoxicity may be the presence of polyvinylpyrrolidone on the substrates. Polyvinylpyrrolidone is necessary for the AgNWs to be stable in the ethanol dispersion, and, although this polymer has been used in culture medium, it can be cytotoxic at high polymer concentrations.[33] We are currently working on this subject, in order to obtain useful non-cytotoxic substrates based on metal NWs for neuronal network regeneration.

3.3.2. 3D scaffolds

From the numerous challenges associated with nanotechnology applications in neuroscience, understanding how the nervous system works or how we can interfere at a molecular level has a significant impact. Thankfully, engineered nanomaterials provide new opportunities to improve materials with potential benefits. Our idea was to use the 3D porous scaffold based on graphene and acrylamide, described in Chapter 2, to support neuronal growth and neuronal signalling.

Hydrogels have been used to obtain more realistic tissue constructs as they are the synthetic materials which most resemble living tissues.[34–36] It is highly known that hydrogels are the best candidates as extracellular matrix mimics for 3D cell culture.[37] Moreover, one of the main advantages of this kind of polymers is its versatility, as they can be designed to have the desired properties (mechanical, electrical, etc.) depending, for instance, on the used monomers. Likewise, this kind of materials can be functionalised in a controlled way. This fact makes it possible to improve cell culture by anchoring, for example, growth factors to the polymer network, which makes these systems even more similar to the reals *in vivo*. Additionally, the pore size of the hydrogels is easily adjustable, as it depends mainly on the quantity of cross-linker used to form the hydrogel. In this case, it has been demonstrated that graphene can also modify the porous structure (Chapter 2, Figure 7). This event is very important from the point of view of neuronal growth, as the porous of the scaffolds must have optimal sizes.

Preparation and characterisation

As previously reported (Chapter 2), this kind of scaffolds is based on polyacrylamide hydrogels which are synthesised in a sustainable way using water as unique solvent. The good mechanical and electrical properties of these materials, joined to their non-cytotoxicity and their internal porous structures, make them suitable for neural network regeneration.

In general, hydrogels used in this chapter were synthesised by *in situ* radical polymerisation of acrylamide in the presence of a cross-linker (MBA) and a radical initiator (KPS) in the presence (**AMG0.2**) or not (**AM**) of graphene dispersions in water (0.2 mg/ml) (graphene dispersions in water were prepared following the ball-milling process described in the previous chapter (Chapter 2, Figure 5)). The hydrogel samples were then washed with ultrapure water for at least 4 days, changing water every day. Finally, hydrogels were freeze-dried in their final swelling degree, obtaining useful scaffolds with open pores (Figure 15).

Figure 15. Final appearance of the **AMG0.2** samples once they have been freeze-dried.

Neuronal studies

Cells were seeded and grown in three different materials: in 2D polyornithine substrate (control sample), and also in the hydrogels in the presence (**AMG0.2**) or not (**AM**) of graphene (0.2 mg/ml), with pore size dimensions about 60 μm and 440 μm respectively.

Immunofluorescence techniques and confocal microscopy were performed to compare neuronal growth in the 2D control substrate and also in the 3D hydrogels with and without graphene. The cells were fixed with paraformaldehyde (PFA) for 20 minutes and labelled for: β-tubulin III (red colour to visualise neuronal cells), GFAP (green colour to visualise glial cells) and DAPI (blue colour to visualise both type of nuclei). Epi-fluorescence and confocal acquisition were then carried out (Figure 16):

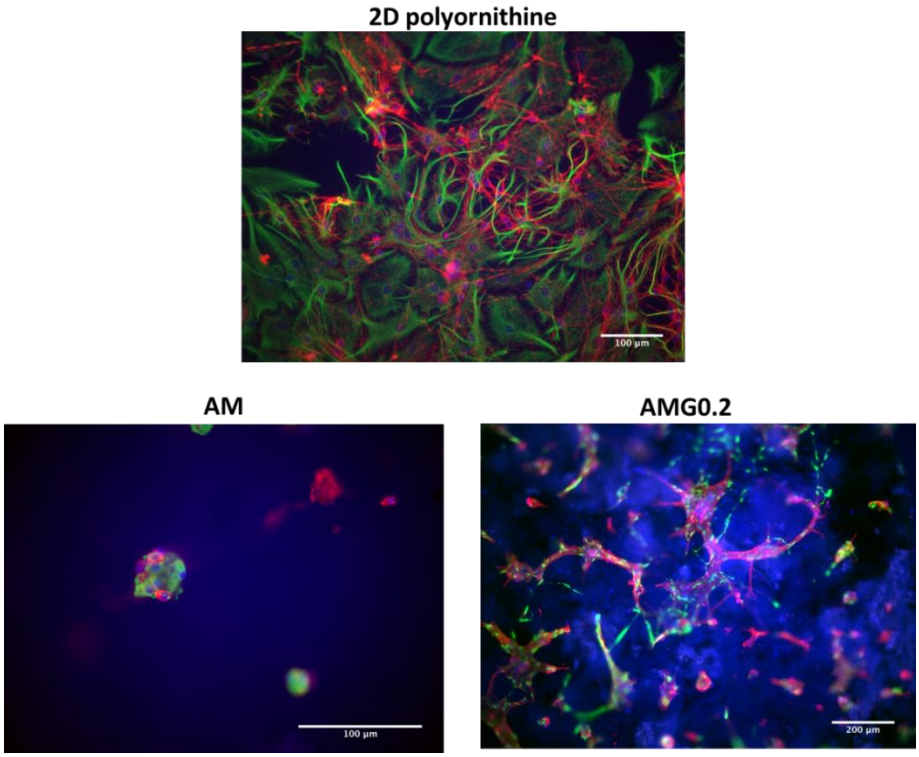

Figure 16. Confocal acquisitions of 2D polyornithine (control sample), **AM** and **AMG0.2** hydrogels.

Appropriate neuron morphology can be visualised in both 2D polyornithine control and **AMG0.2** scaffold. However, neurons hardly grew on **AM**, where the majority of red spots that were found in the images are salts-crystals derived from the PBS washes.

In the case of **AMG0.2**, we found neurons only on the superficial layer of the hydrogel. There was a nice layer of neurons on top of the sample of around 20 µm thick, but they did not penetrate below that distance.

The neuronal activity was investigated via Ca^{2+} imaging experiments in the three different samples. In the case of hydrogel scaffolds, slices of a maximum thickness of 500 µm were cut and glued with polydimethylsiloxane (PDMS) to a glass coverslip

(Figure 17). Prior to plating, all the samples were sterilised with an UV lamp for 30 minutes. Cells were then plated on polyornithine-coated substrate and also on the 3D scaffolds and incubated.

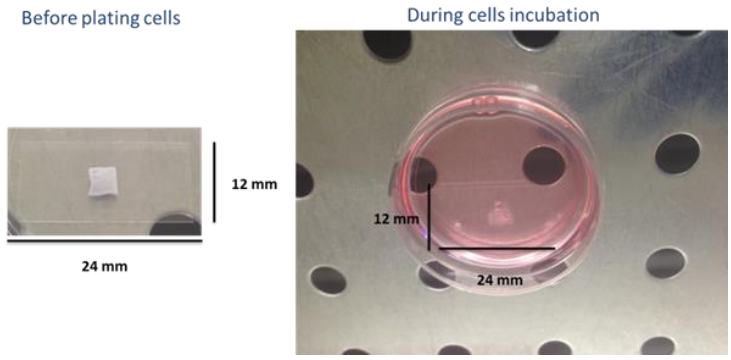

Figure 17. **AM** slice before plating cells (left) and during cells incubation (right).

After 9 days of incubation *in vitro*, hippocampal dissociated cells were loaded with Oregon-green AM BAPTA Ca^{2+} membrane permeable dye and calcium activity was monitored. In each field there were 6±2 cells, and three sessions of cultures were performed in total (n=9 2D polyornithine control substrates, n=9 **AM** samples, n=9 **AMG0.2** samples).

Ca^{2+} transients were found only in the 2D control sample and in **AMG0.2** hydrogel, but not in the **AM** scaffold, where cell activity was not found. This fact is in agreement with the result obtained in the immunofluorescence experiments: cells are only found in the scaffold with graphene, but not in the hydrogel without nanomaterial.

Figure 18 shows the obtained transients that were expressed as fractional amplitude increase ($\Delta F/F_0$, where F_0 is the baseline fluorescence level and ΔF is the rise over baseline).

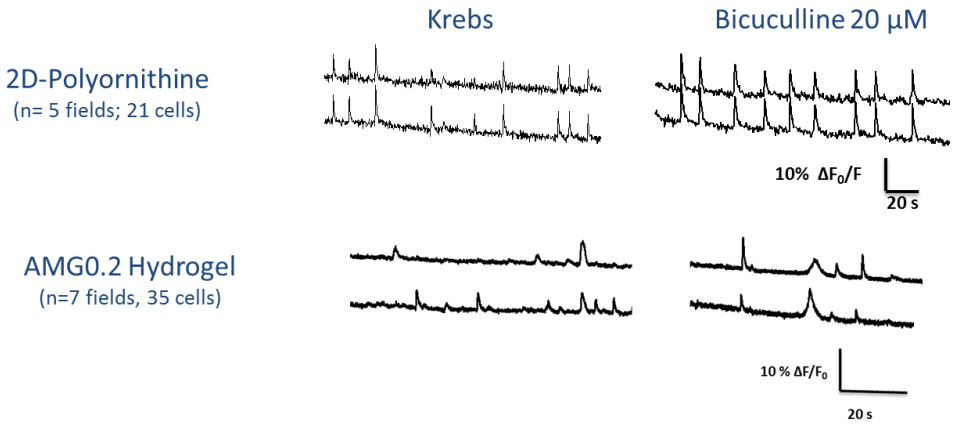

Figure 18. Repetitive Ca^{2+}-events in control sample and **AMG0.2** scaffold, spontaneously (Krebs) or bicuculline induced, recorded in hippocampal cultures of 9 days *in vitro*.

Next figure (Figure 19) shows the histograms of the percentage of spontaneous active cells in 2D polyornithine and in **AMG0.2** sample. Moreover, we measured the occurrence of spontaneous Ca^{2+} episodes by quantifying the inter-event intervals (IEI) in active cells (both spontaneous active cells (Krebs) and disinhibited ones (bicuculline)). Bicuculline is used to pharmacologically block the inhibitory action of $GABA_A$ ionotropic receptors in neurons. This antagonist of inhibitory connections is known to alter network activity patterns:[38] the addition of bicuculline significantly decrease the average IEI of episodes detected in the samples.

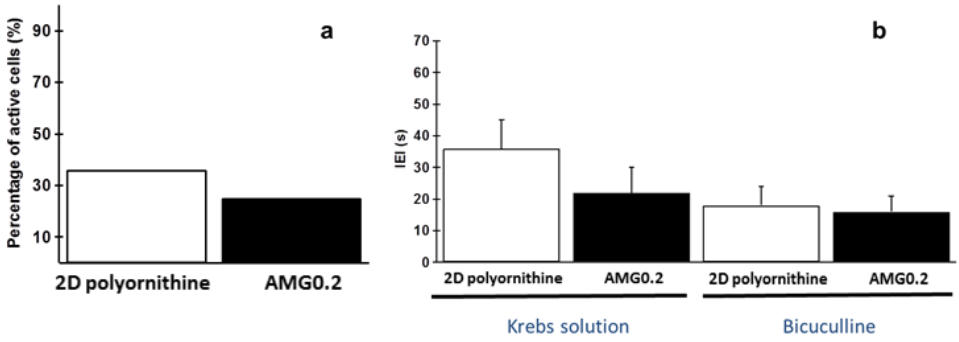

Figure 19. a) Percentages of spontaneous active cells and b) inter-event intervals (IEI) of control cells (krebs) and disinhibited ones (bicuculline).

Although the percentage of active cells is slightly lower for **AMG0.2** than for the control sample (Figure 19a), the IEI value obtained from spontaneous active cells and also the IEI value obtained from the disinhibited ones, are shorter in the 3D scaffold when compared to the 2D control substrate (Figure 19b), thus suggesting a different functional activity of neurons due to the presence of graphene, even though neurons are only present on top of the 3D scaffold (≈ 20 μm thick).

The main conclusion of this work is that graphene is necessary for the growth of neurons in this kind of scaffolds: we only visualised neurons in the 3D scaffold in the presence of graphene, but not in the hydrogel without nanomaterial, in which neurons hardly grew. Therefore, graphene is taking an important and notable role regarding the neuronal growth in this kind of hydrogels. This behaviour could be due to different reasons:

- **AMG0.2** is more hydrophobic than **AM**: some literature examples demonstrate that cells prefer stiffer and more hydrophobic systems for growth.[39] Although the mechanism of how graphene can improve cell adhesion is still not well understood, differences in cell attachment rates could be attributed to the absorption levels of adhesion proteins:[40] proteins are more effectively adsorbed on the substrate in the presence of graphene.

- Pore size dimensions: as it is already discussed (Chapter 2, Figure 7), the pore size of these kind of scaffolds decreases in the presence of graphene, which has a cross-linking role in the hydrogel structure. Therefore, the pore size acquired in **AMG0.2** (≈ 60 μm) is more suitable for neurons than the pore size of **AM** (≈ 440 μm).
- A third possible reason could be the mechanical properties of the final materials, which as it is well-known, regulate adherent cell behaviour.[39] The introduction of graphene increases the stiffness of our acrylamide scaffolds (Chapter 2, Figure 14). Moreover, the viscoelastic properties of the materials, the rate of stress relaxation, has been recently reported as an important feature regarding cell spreading, proliferation, and differentiation of stem cells.[41] Therefore, graphene could improve the viscoelastic behaviour of the scaffolds, enhancing in this way the neuronal growth. We are currently working on studying this behaviour.

However, an amplified response as that expected of a 3D scaffold was not obtained from neurons in **AMG0.2**, maybe due to the fact that we only visualised neurons on top of this scaffold. Therefore, we could not detect changes in the neuronal connectivity between **AMG0.2** and 2D polyornithine control.

Future experiments will be developed to further adjust the characteristics of the material, for neurons to grow throughout the entire scaffold. This task is challenging but, as discussed above, the great advantage of the hydrogels is its versatile design, starting from different monomers which can be previously functionalised, especially in our case where the pore size and the mechanical properties are easily adjustable depending on the amount of graphene in the material. In addition, new scaffolds from different components, also based on graphene, are being tested in our group, as useful sponges for regeneration of neural networks.

3.4. Experimental procedures

3.4.1. SWNTs+Graphene-based substrates

3.4.1.1. Substrates preparation

Commercial glass coverslips (12x24 mm) are dipped in a "piranha" solution (H_2SO_4:H_2O_2 3:1; 100 ml for 50 coverslips) at 90 °C for 16 hours, then rinsed many times with water and dried at 80 °C in an oven.

SWNTs (Hipco, Unydim) are functionalised by 1,3-dipolar cycloaddition with sarcosine and heptaldehyde. The resulting TGA show a 3 % weight loss.

Functionalised SWNTs are dispersed at a concentration of 0.1 mg/ml in ethyl acetate and sonicated in a sonic bath for 20 minutes. 3 ml of dispersion is then sprayed onto glass coverslips placed on a hot plate at 200°C using an Aldrich® chromatography sprayer (size 10 ml). The density achieved is around $7 \cdot 10^{-5}$ mg/mm^2. For the defunctionalisation of SWNTs, deposited coverslips are burned at 350 °C under nitrogen flow in an oven for 20 minutes.

Control coverslips were prepared by painting silver electrodes in a detailed way with a silver conductive paint. Squares of 0.5 cm^2 were painted on a glass substrate as Figure 20 shows:

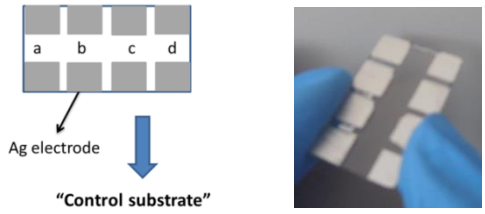

Figure 20. Scheme and real appearance of the prepared control coverslip after painting silver electrodes.

Water of an aqueous dispersion of graphene prepared by ball-milling treatments[28] was exchanged by ethanol. The graphene dispersion (0.05 mg/ml) is then sprayed onto 3 different glass coverslips placed all together on a hot plate at 100°C using an Air Brush Junior 140 (DEFYNIK by SAGOLA) until reaching a sheet resistance of around 150 kΩ/sq. The distance between the Air Brush and the plate was around 20 cm, and the nitrogen pressure used was 2 bars. The three coverslips were (Figure 8): SWNTs previously sprayed coverslips, new pure coverslips and the control ones.

The substrates were then put in an oven at 350 ^{o}C for 20 minutes to remove solvent traces. Finally, sheet resistance and transmittance (550 nm) were measured in the points "a", "b" , "c" and "d" by using a digital Agilent multimeter and a Cary Series UV-Vis-NIR Spectrophotometer respectively.

Scanning Electron Microscopy (SEM) of the substrates was performed using a PHILIPS XL30 system. The samples were placed under vacuum and coated with a 10 nm layer of gold, and the surface of each substrate was analysed by SEM.

3.4.1.2. Neurophysiology methods

Cell cultures

Standard dissociated hippocampal cultures were prepared according to Malgaroli et al (1992) with slight modifications.[29] Hippocampi were dissected from 2-3-days-old Wistar rats. Briefly, after isolation and slicing tissue was digested with trypsin in the presence of DNase, then digestion was blocked by Trypsin Inhibitor on ice, and tissue was dissociated in culture medium containing DNase. Cell suspension was then centrifuged at 1000 rpm for 5 minutes, cells were recovered and plated on polyornithine-coated substrate and also on peptide-free glass coverslips coated with Graphene, SWNTs or Graphene layered on SWNTs. Coverslips were then placed in Petri dishes and cultured in the presence of 5% serum-containing culture medium in a 5% CO_2 humidified incubator for 8-10 days. Culture medium was renewed every two

days, and was supplemented with the proliferation inhibitor cytosine arabinoside (Ara C).

Electrophysiology

Recordings were obtained with glass micropipettes of 4-8 MΩ resistance containing (mM): 120 K gluconate, 20 KCl, 10 HEPES, 10 EGTA, 2 $MgCl_2$, 2 Na_2ATP, pH 7.3. The external solution containing (mM): 150 NaCl, 4 KCl, 1 $MgCl_2$, 2 $CaCl_2$, 10 HEPES, 10 glucose, pH 7.4. All experiments were performed at 18-22 °C. Cells were voltage clamped with a V_{cmd}=-56 mV (not corrected for the liquid junction potential, calculated to be 14 mV). Data were collected using a Multiclamp 700A Amplifier (Molecular Devices, US), and analysed using Clampfit 10.3 (Molecular Devices). Recordings were performed on two culture series.

Immunostaining

Cultures were fixed in paraformaldehyde (PFA) 4% in PBS for 20 min, permeabilised with 0.3% Triton-X-100 and subsequently incubated with primary antibodies for 30 min at room temperature (RT) and after PBS washes incubated with secondary antibodies for 30 min. Cultures were then mounted in Vectashield (Vector Laboratories) on 1 mm thick slides. To visualise neurons we used rabbit anti beta tubulin III (β tubulin III), 1:250 (SIGMA) primary antibody and Alexa 594 goat anti rabbit secondary antibody, 1:500 (Invitrogen); to visualise Astrocytes we used mouse anti Glial fibrillary acidic protein (GFAP) 1:200 primary antibody (Molecular Probes) and Alexa 488 goat anti mouse secondary antibody (Invitrogen); to visualise cell nuclei we used DAPI, 1:1000 (Invitrogen). Images were acquired using an epifluorescence microscope (DM 6000, Leica; 10x and 20x objectives). Immunostainings were performed on one culture series.

3.4.2. AgNWs-based substrates

3.4.2.1. Substrates preparation

Control coverslips were prepared by painting silver electrodes in a detailed way with silver conductive paint. Squares of 0.5 cm^2 were painted on a glass substrate as Figure 21 shows.

Two different cleaned glass coverslips (new pure coverslips and the control ones) were placed together on a hot plate at 100°C. Then, a AgNWs dispersion from Grupo Antolin (0.1 mg/ml) was sprayed on both of them using an Air Brush Junior 140 (DEFYNIK by SAGOLA) until reaching sheet resistances of approximately 1000 Ω/sq, 100 Ω/sq and 50 Ω/sq. The distance between the Air Brush and the plate was around 20 cm, and the nitrogen pressure used was 2 bars.

The substrates were after put in an oven at 200 ^{o}C for 20 minutes to remove solvent traces. Finally, sheet resistance and transmittance (550 nm) were measured in the points “a”, “b” , “c” and “d” by using a digital Agilent multimeter and a Cary Series UV-Vis-NIR Spectrophotometer respectively.

Scanning Electron Microscopy (SEM) of the substrates was performed using a PHILIPS XL30 system. The samples were placed under vacuum and coated with a 10 nm layer of gold, and the surface of each substrate was analysed by SEM.

3.4.2.2. Neurophysiology methods

Cell cultures

Standard dissociated hippocampal cultures were prepared according to Malgaroli et al (1992) with slight modifications.[29] Hippocampi were dissected from 2-3-days-old Wistar rats. Briefly, after isolation and slicing tissue was digested with trypsin in the

presence of DNase, then digestion was blocked by Trypsin Inhibitor on ice, and tissue was dissociated in culture medium containing DNase. Cell suspension was then centrifuged at 1000 rpm for 5 minutes, cells were recovered and plated on polyornithine-coated substrate and also on peptide-free glass coverslips coated with AgNWs. Coverslips were then placed in Petri dishes and cultured in the presence of 5% serum-containing culture medium in a 5% CO_2 humidified incubator for 8-10 days. Culture medium was renewed every two days, and was supplemented with the proliferation inhibitor cytosine arabinoside (Ara C).

3.4.3. 3D scaffolds

3.4.3.1. Preparation of the 3D scaffolds

Preparation of graphene-based hydrogels

Chemically cross-linked pure PAm gels and graphene-loaded chemically cross-linked PAm gels were synthesised. Pure PAm hydrogels were prepared using acrylamide (Am), *N,N´*-methylenebisacrylamide (MBA) as cross-linker and potassium peroxydisulfate (KPS) as initiator. Am was initially dissolved in doubly deionised water (200 mg/ml) with the MBA (0.2 mg/ml) and the KPS (0.4 mg/ml). The solution was homogenised and let to polymerise at 75 ^{o}C for 1 hour (**AM**). In the case of the graphene-PAm composite hydrogels, a similar process was followed, adding all the reactants to the aqueous graphene dispersion[28] in this case. The graphene content used was 0.2 mg/ml (**AMG0.2**).

The samples were then washed with ultrapure water for at least 4 days, changing the water occasionally. Hydrogels were lyophilised Telstar Lyoquest freeze-drier in their final swelling degree and Scanning Electron Microscopy (SEM) of the samples was performed using a FEI QUANTA 250 system.

Slices of maximum 500 µm were cut from the freeze-dried hydrogels, and they were finally glued with a layer of PDMS cured at 120 ^{o}C to a cleaned glass coverslip (12x24 mm).

3.4.3.2. Neurophysiology methods

Cell cultures

Hippocampi were dissected from 2-3-days-old rats. Briefly, hippocampal cells were isolated from the rest of the brain and upon enzymatic treatment neurons were dissociated by pipetting.

One hour before plating, 3D scaffolds were sterilised with an UV lamp. Cells were then plated on polyornithine-coated substrate and also on the 3D scaffolds (3D growth conditions). Coverslips were after placed in Petri dishes and cultures were incubated and grown in a culture medium composed by MEM (Gibco), supplemented with Fetal Bovin Serum (FBS) and cytosine arabinoside (Ara C) in a 5% CO_2 humidified incubator at 37 ^{o}C for 8-10 days. Culture medium was renewed every two days.

Calcium imaging

Hippocampal Dissociated Cells, after 9 days of incubation *in vitro*, were loaded with Oregon-green AM BAPTA Ca^{2+} membrane permeable dye and samples were then placed in a recording chamber mounted on an inverted microscope where they were continuously superfused by a recording solution (mixture of salts and glucose). Ca^{2+}-imaging measurements were carried out at room temperature. The obtained transients that were expressed as fractional amplitude increase ($\Delta F/F_0$, where F_0 is the baseline fluorescence level and ΔF is the rise over baseline).

In order to induce rhythmic burst, 20 µM bicuculline methiodide was bath-applied after 10 minutes recording; at the end of each experiment 1 µM TTX (a voltage-gated,

fast Na^+ channel blocker) was added to the recording solution to confirm the neuronal nature of the recorded signals.

Immunofluorescence

Cells were fixed in paraformaldehyde (PFA) 4% in PBS for 20 min, permeabilised with Triton-X-100 and subsequently incubated for labelled (β-tubulin III to visualise neuronal cells, GFAP to visualise glial cells and DAPI to visualise both type of nuclei) with primary antibodies for 30 min at room temperature and after PBS washes incubated with secondary antibodies for 30 min. Samples were mounted in Vectashield on coverslips of 1 mm thickness and upon immunofluorescence staining, hippocampal cultures were imaged using a confocal microscope. At least a total of 18 µm in Z-profile was analysed.

3.5. Conclusions

In this work we designed new composite materials to study neuron activity for future application in neuronal network regeneration. The prepared systems can be classified as 2D substrates or 3D scaffolds. Regarding the first kind, two different types of substrates were prepared: SWNTs/Graphene-based, and AgNWs-based. With respect to the 3D scaffolds, graphene-based hydrogels were synthesised and used for the study.

Although electrophysiology study on the AgNWs-based 2D substrates was impossible as they were not biocompatible, some conclusions can be deduced when hippocampal cells were cultured on SWNTs/Graphene-based 2D substrates. Briefly, membrane passive properties were studied and results indicated similar properties, health conditions, growth and cell phenotypes among different substrates: graphene coated, SWNTs coated, or SWNTs+graphene coated.

However, important improvements were achieved when graphene was added to 3D scaffolds. The most important fact observed in this study is that neurons are only visualised in the graphene-based hydrogel, but not in the scaffold without nanomaterial. Therefore, we could confirm that graphene is taking an important and notable role regarding the neuronal growth in this kind of hydrogels. The advantages of these nanocomposites lie in their versatile design, especially in our case where the pore size and the mechanical properties are easily adjustable depending on the amount of graphene, which make these materials promising scaffolds for 3D neuronal growth.

3.6. References

(1) Eidelberg, D. Metabolic Brain Networks in Neurodegenerative Disorders: A Functional Imaging Approach. *Trends Neurosci.* **2009**, *32*, 548–557.

(2) Laughlin, S. B.; Sejnowski, T. J. Communication in Neuronal Networks. *Science* **2003**, *301*, 1870–1874.

(3) Haydon, P. G.; Henderson, E.; Stanley, E. F. Localization of Individual Calcium Channels at the Release Face of a Presynaptic Nerve Terminal. *Neuron* **1994**, *13*, 1275–1280.

(4) Grienberger, C.; Konnerth, A. Imaging Calcium in Neurons. *Neuron* **2012**, *73*, 862–885.

(5) Daley, W. P.; Peters, S. B.; Larsen, M. Extracellular Matrix Dynamics in Development and Regenerative Medicine. *J. Cell Sci.* **2008**, *121*, 255–264.

(6) Riehemann, K.; Schneider, S. W.; Luger, T. a; Godin, B.; Ferrari, M.; Fuchs, H. Nanomedicine--Challenge and Perspectives. *Angew. Chem. Int. Ed. Engl.* **2009**, *48*, 872–897.

(7) Gramowski, A.; Flossdorf, J.; Bhattacharya, K.; Jonas, L.; Lantow, M.; Rahman, Q.; Schiffmann, D.; Weiss, D. G.; Dopp, E. Nanoparticles Induce Changes of the Electrical Activity of Neuronal Networks on Microelectrode Array Neurochips. *Environ. Health Perspect.* **2010**, *118*, 1363–1369.

(8) Sucapane, A.; Cellot, G.; Prato, M.; Giugliano, M.; Parpura, V.; Ballerini, L. Interactions Between Cultured Neurons and Carbon Nanotubes: A Nanoneuroscience Vignette. *J. Nanoneurosci.* **2009**, *1*, 10–16.

(9) Shah, S.; Solanki, A.; Lee, K.-B. Nanotechnology-Based Approaches for Guiding

Neural Regeneration. *Acc. Chem. Res.* **2016**, *49*, 17–28.

(10) Aldinucci, A.; Turco, A.; Biagioli, T.; Toma, F. M.; Bani, D.; Guasti, D.; Manuelli, C.; Rizzetto, L.; Cavalieri, D.; Massacesi, L.; et al. Carbon Nanotube Scaffolds Instruct Human Dendritic Cells: Modulating Immune Responses by Contacts at the Nanoscale. *Nano Lett.* **2013**, *13*, 6098–6105.

(11) Carvalho-de-souza, J. L.; Treger, J. S.; Dang, B.; Kent, S. B. H.; David, R. Photosensitivity of Neurons Enabled by Cell - Targeted Gold Nanoparticles. *Neuron* **2015**, *86*, 207–217.

(12) Mazzatenta, a.; Giugliano, M.; Campidelli, S.; Gambazzi, L.; Businaro, L.; Markram, H.; Prato, M.; Ballerini, L. Interfacing Neurons with Carbon Nanotubes: Electrical Signal Transfer and Synaptic Stimulation in Cultured Brain Circuits. *J. Neurosci.* **2007**, *27*, 6931–6936.

(13) Bosi, S.; Fabbro, A.; Cantarutti, C.; Mihajlovic, M.; Ballerini, L.; Prato, M. Carbon Based Substrates for Interfacing Neurons: Comparing Pristine with Functionalized Carbon Nanotubes Effects on Cultured Neuronal Networks. *Carbon N. Y.* **2016**, *97*, 87–91.

(14) Lu, Y.; Li, T.; Zhao, X.; Li, M.; Cao, Y.; Yang, H.; Duan, Y. Y. Electrodeposited Polypyrrole/carbon Nanotubes Composite Films Electrodes for Neural Interfaces. *Biomaterials* **2010**, *31*, 5169–5181.

(15) Cellot, G.; Cilia, E.; Cipollone, S.; Rancic, V.; Sucapane, A.; Giordani, S.; Gambazzi, L.; Markram, H.; Grandolfo, M.; Scaini, D.; et al. Carbon Nanotubes Might Improve Neuronal Performance by Favouring Electrical Shortcuts. *Nat. Nanotechnol.* **2009**, *4*, 126–133.

(16) Lee, Y.; Lee, J. M.; Bae, P.-K.; Chung, I. Y.; Chung, B. H.; Chung, B. G. Photo-Crosslinkable Hydrogel-Based 3D Microfluidic Culture Device. *Electrophoresis* **2015**, *36*,

994–1001.

(17) Puschmann, T. B.; Pablo, Y. De; Zande, C.; de Pablo, Y.; Zanden, C.; Liu, J.; Pekny, M. A Novel Method for Three-Dimensional Culture of Central Nervous System Neurons. *Tissue Eng. Part C Methods* **2014**, *20*, 485–493.

(18) Bosi, S.; Rauti, R.; Laishram, J.; Turco, A.; Lonardoni, D.; Nieus, T.; Prato, M.; Scaini, D.; Ballerini, L. From 2D to 3D: Novel Nanostructured Scaffolds to Investigate Signalling in Reconstructed Neuronal Networks. *Sci. Rep.* **2015**, *5*, 9562–9573.

(19) Sahni, D.; Jea, A.; Mata, J. a; Marcano, D. C.; Sivaganesan, A.; Berlin, J. M.; Tatsui, C. E.; Sun, Z.; Luerssen, T. G.; Meng, S.; et al. Biocompatibility of Pristine Graphene for Neuronal Interface. *J. Neurosurg. Pediatr.* **2013**, *11*, 575–583.

(20) Park, S. Y.; Park, J.; Sim, S. H.; Sung, M. G.; Kim, K. S.; Hong, B. H.; Hong, S. Enhanced Differentiation of Human Neural Stem Cells into Neurons on Graphene. *Adv. Mater.* **2011**, *23*, 263–267.

(21) Fabbro, A.; Scaini, D.; Leon, V.; Vázquez, E.; Cellot, G.; Privitera, G.; Lombardi, L.; Torrisi, F.; Tomarchio, F.; Bonaccorso, F.; et al. Graphene-Based Interfaces Do Not Alter Target Nerve Cells. *ACS Nano* **2016**, *10*, 615–623.

(22) Li, N.; Zhang, Q.; Gao, S.; Song, Q.; Huang, R.; Wang, L.; Liu, L.; Dai, J.; Tang, M.; Cheng, G. Three-Dimensional Graphene Foam as a Biocompatible and Conductive Scaffold for Neural Stem Cells. *Sci. Rep.* **2013**, *3*, 1604–1610.

(23) Akhavan, O.; Ghaderi, E.; Abouei, E.; Hatamie, S.; Ghasemi, E. Accelerated Differentiation of Neural Stem Cells into Neurons on Ginseng-Reduced Graphene Oxide Sheets. *Carbon N. Y.* **2014**, *66*, 395–406.

(24) Tang, M.; Song, Q.; Li, N.; Jiang, Z.; Huang, R.; Cheng, G. Enhancement of Electrical Signaling in Neural Networks on Graphene Films. *Biomaterials* **2013**, *34*,

6402–6411.

(25) Letourneau, P. C. Possible Roles for Cell-to-Substratum Morphogenesis Adhesion in Neuronal. *Dev. Biol.* **1975**, *91*, 77–91.

(26) Letourneau, P. C. Cell-to-Substratum Adhesion and Guidance of Axonal Elongation. *Dev. Biol.* **1975**, *44*, 92–101.

(27) Pawlowski, L. *The Science and Engineering of Thermal Spray Coatings*; 2008.

(28) León, V.; Quintana, M.; Herrero, M. A.; Fierro, J. L. G.; de la Hoz, A.; Prato, M.; Vázquez, E. Few-Layer Graphenes from Ball-Milling of Graphite with Melamine. *Chem. Commun.* **2011**, *47*, 10936–10938.

(29) Cellot, G.; Toma, F. M.; Kasap Varley, Z.; Laishram, J.; Villari, a.; Quintana, M.; Cipollone, S.; Prato, M.; Ballerini, L. Carbon Nanotube Scaffolds Tune Synaptic Strength in Cultured Neural Circuits: Novel Frontiers in Nanomaterial-Tissue Interactions. *J. Neurosci.* **2011**, *31*, 12945–12953.

(30) Madaria, A. R.; Kumar, A.; Zhou, C. Large Scale, Highly Conductive and Patterned Transparent Films of Silver Nanowires on Arbitrary Substrates and Their Application in Touch Screens. *Nanotechnology* **2011**, *22*, 245201–245208.

(31) Lopez-Diaz, D.; Merino, C.; Velázquez, M. M. Modulating the Optoelectronic Properties of Silver Nanowires Films : Effect of Capping Agent and Deposition Technique. *Materials* **2015**, *8*, 7622–7633.

(32) Söderstjerna, E.; Johansson, F.; Klefbohm, B.; Englund Johansson, U. Gold- and Silver Nanoparticles Affect the Growth Characteristics of Human Embryonic Neural Precursor Cells. *PLoS One* **2013**, *8*, 1–13.

(33) Hirao, Y. In Vitro Growth and Development of Bovine Oocyte-Granulosa Cell

Complexes on the Flat Substratum: Effects of High Polyvinylpyrrolidone Concentration in Culture Medium. *Biol. Reprod.* **2003**, *70*, 83–91.

(34) Drury, J. L.; Mooney, D. J. Hydrogels for Tissue Engineering : Scaffold Design Variables and Applications. *Biomaterials* **2003**, *24*, 4337–4351.

(35) Hoffman, a S. Hydrogels for Biomedical Applications. *Ann. N. Y. Acad. Sci.* **2001**, *944*, 62–73.

(36) Lee, K. Y.; Mooney, D. J. Hydrogels for Tissue Engineering. **2001**, *101*, 1869–1878.

(37) Tibbitt, M. W.; Anseth, K. S. . NIH Public Access. *Biotechnol. Bioeng.* **2009**, *103*, 655–663.

(38) Tibau, E.; Valencia, M.; Soriano, J. Identification of Neuronal Network Properties from the Spectral Analysis of Calcium Imaging Signals in Neuronal Cultures. *Front. Neural Circuits* **2013**, *7*, 199.

(39) Aryaei, A.; Jayatissa, A.H.; Jayasuriya, A. C. The Effect of Graphene Substrate on Osteoblast Cell Adhesion and Proliferation. *J. Biomed. Mater. Res. - Part A* **2015**, *102*, 3282–3290.

(40) Shi, X.; Chang, H.; Chen, S.; Lai, C.; Khademhosseini, A. Regulating Cellular Behavior on Few-Layer Reduced Graphene Oxide Films with Well-Controlled Reduction States. *Adv. Funct. Mater.* **2012**, *22*, 751–759.

(41) Chaudhuri, O.; Gu, L.; Klumpers, D.; Darnell, M.; Bencherif, S. A.; Weaver, J. C.; Huebsch, N.; Lee, H.; Lippens, E.; Duda, G. N.; et al. Hydrogels with Tunable Stress Relaxation Regulate Stem Cell Fate and Activity. *Nat. Mater.* **2016**, *15*, 326–336.

Chapter 4

Smart Self-healing hydrogels

4.1. Introduction

Inspired by nature, self-healing materials[1,2] represent one of the vanguards of recent developments in the synthesis of new smart materials.

All natural or synthetic materials accumulate damage at macro or microscale, losing even the function of the device due to the deterioration or disappearance of their desirable properties. However, self-healing materials can reverse or repair the damage zone once or several times because they are able to recover their capabilities. This fact enhances the lifetime of these kinds of materials.

Self-healing materials can be divided into different classes:

- Non-autonomic self-healing materials, which require an external stimulus: heat, light, etc.
- Autonomic self-healing materials, which do not need any additional external stimulus because the damage itself is the motivating force for the healing.

Regarding the self-healing process, these materials can be:

- Extrinsic self-healing materials; if the healing process is based on external healing components normally embedded into the matrix material.
- Intrinsic self-healing materials; if the process requires no separate healing agents. In this case, the healing is due to the formation of chemical bonds or physical interactions between the interfaces of the crack.

While extrinsic self-healing materials are healed in an autonomous way, most of the examples of intrinsic self-healing materials have to do with an external trigger. The most challenging systems are the ones with autonomic intrinsic self-healing properties (Figure 1) and, weaker interactions which include supramolecular chemistry,[3,4,5]

hydrogen bonding,[6,7] ionic interactions,[8,9] or π-π stacking,[10] seem to be promising chances to obtain these materials.[11,12]

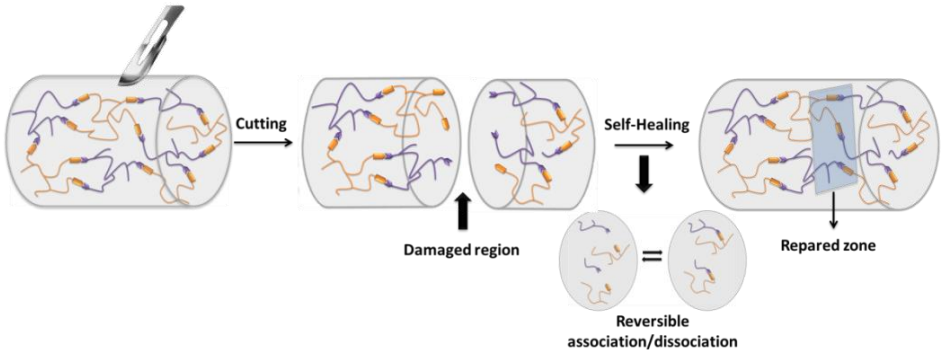

Figure 1. Schematic representation of an autonomous intrinsic self-healing gel.

4.1.1. Self-healing gels

Over the past 60 years, the use of polymers has transformed our lives completely. Their awesome properties, easy accessibility and low price in most of the cases, let us use them in ever more advanced applications.

Nowadays, polymers, or composite polymers, are the most investigated materials in the field of self-healing.[13] Novel smart gels have been developed with self-repairing properties that can restore their functionalities after harm.[14,4] However, the investigation of self-healing gels is still in its infancy.

4.1.1.1. Self-healing strategies

There is a multitude of strategies used to synthesise self-healing gels. One of the most accepted theories for intrinsic self-healing polymers was developed by Wool and O´Connor.[15] They determined five stages of crack healing to disclose the complexity of the self-healing process at polymer interfaces. Thus, the reparation of cracks and

microscopic damage is described in terms of the following stages: (i) surface rearrangements, which affect initial diffusion function and topological feature; (ii) surface approach, related to healing patterns; (iii) wetting; (iv) diffusion, the main factor that controls recovery of mechanical properties; (v) randomisation, ensuring disappearance of cracking interface.

Overall, the chain diffusion at the interface of the damaged region was considered to be the primary driving force for repairs. By the end of wetting stage, potential barriers associated with the inhomogeneities at the interface disappear and chains are free to move across the interface in the following stages. By this way, the repairing process can be viewed as chain conformational changes: different equilibrium states during which, each chain, escapes and changes its position in a given time. The lower the molecular weight of the polymer, the more favourable the repairing conditions.[16]

In addition, multicomponent thermosetting systems harness the ability of embedded chemical agents to repair cracks. Perhaps, the most feasible examples include blending of shape memory thermosetting polymers with small amounts of thermoplastics repairing the damage by diffusion, entanglements and/or polymerisation.[17,18] In that context, it is worth noting that the most commonly occurring reactive species resulting from bond cleavage are free radicals. Their affinity for reacting with surroundings is high in gaseous and liquid phases, but significantly lower in solid polymer networks. In spite of relatively long lifetimes of free radicals, if two separated reactive chain ends have to be coupled between them, both ends must diffuse towards each other and polymerise before being intercepted by prevailing oxidative processes.[19] In order to maintain free radical stability, suitable reaction conditions must be maintained.

Considering all that strategies, **intrinsic healing** has been pursued by chemical principles in numerous studies, giving multiple chemical approaches being used for macroscale healing. Some of them have to do with shape memory polymers[20] and

polymer blends.[21] Others are based, for instance, on constitutional dynamic chemistry,[14] which are summarised in Figure 2.

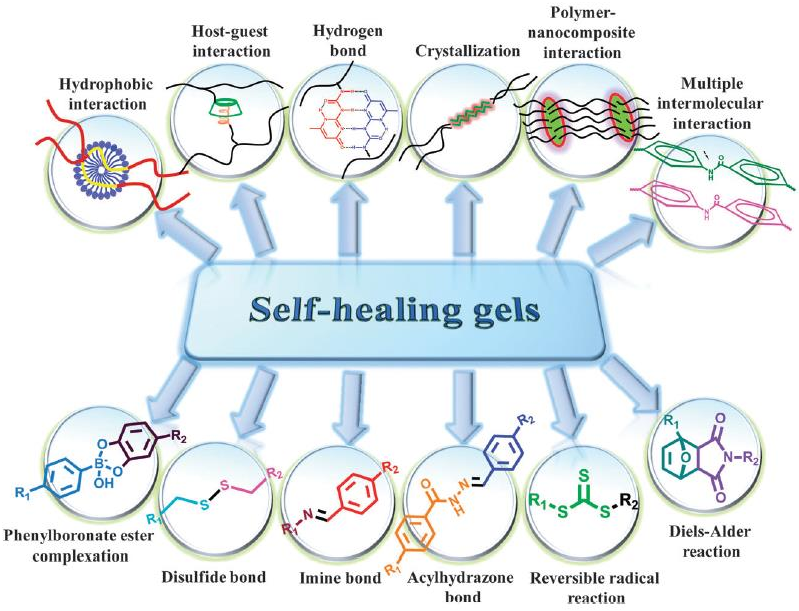

Figure 2. Various strategies used to form self-healing gels based on constitutional dynamic chemistry.[14]

In the case of **extrinsic self-healing** approaches, the repair procedure has to do with a healing agent (generally liquid) which is incorporated into the matrix as capsules.[22,23]

Sometimes, the combination of more than one chemical principle can cover the necessity of achieving new self-healing materials with superior properties, improving for instance the mechanical properties of the final material.

4.1.1.2. Self-healing quantification

The healing efficiency can be quantified in several ways, even by manual elongation tests, using a normal rule.[24] However, the most accurate way to measure this capacity

is with tensile mechanical measurements by using an appropriate test machine.[25] Therefore, maybe one of the most useful approaches to quantify the healing efficiency is to use the following equation:[1]

$$\eta = \frac{K_{IC}^{Healed}}{K_{IC}^{Virgin}} \times 100$$

where K_{IC}^{Healed} is the fracture toughness of the healed specimen and K_{IC}^{Virgin} is the fracture toughness of the virgin hydrogel. In this way, it is possible to obtain an accurate value of the healing efficiency of a determined material.

4.2. Objectives

Synthetic materials which are able to heal in an autonomous way upon damage are being studied at a fast pace due to their potential applications. The development of self-repairing substances is highly desirable because they highly increase the lifetime of a functional material. However, self-healing properties are occasionally found in inanimate systems and achieving self-healing in permanently cross-linked gels has remained tricky.

The aim of the work is to synthesise new composite hydrogels based on graphene with an autonomous self-healing capacity. The formation of multicomponent systems increases the number of possible applications, in some cases due to the combination of the properties of each material separately.[26] In this context the nanomaterial can improve the properties of the final self-healing material, for instance the mechanical behaviour or the electric properties of the final composite. Mechanical properties are normally also improved with the formation of an interpenetrating polymer network.[27]

There are some examples of graphene-based hydrogels with self-healing ability. However, most of them use graphene peroxide,[28] graphene oxide,[7,29] or even reduced graphene oxide,[30] and pristine graphene is used in few cases.[31,32]

The objective in this chapter is the preparation of more complex systems than the hydrogels described in the previous chapters, which were based on a unique main monomer. In this section, different types of interpenetrating polymer networks will we developed by using several monomers, achieving in this way autonomic self-healing hydrogels. Moreover, graphene prepared by ball-milling treatment[33] will be used in low quantity as filler, trying to obtain self-healing materials with improved electrical properties.

4.3. Poly(methacrylic acid) / poly(vinyl alcohol) hydrogels

As explained in the first chapter, an interpenetrating polymer network (IPN) is a polymer comprising two or more networks which are at least partially interlaced on a molecular scale, but not covalently bonded to each other. The networks cannot be separated unless chemical bonds are broken.[34,27]

In this case, different semi-IPNs of poly (methacrylic acid) (p(MAAc)) and poly(vinyl alcohol) (PVA) based on graphene were prepared.

Poly(methacrylic acid) is a usual employed polymer for hydrogel formation, mainly for biological applications due to its excellent swelling properties, which make them promising carriers for drug delivery as they are also biocompatible materials.[35] Most of the time, this polymer is combined with other different ones[36] or even with carbon-based nanomaterials. This fact makes the improvement of the final composite possible, regarding, for instance, the bulk resistance.[37] On the other hand, the poly(vinyl alcohol) is a well-studied biodegradable and non-toxic polymer, which has been commonly used in the preparation of hydrogels.[38] This polymer is also suitable for preparing a self-healable hydrogel based on hydrogen bond interactions.[39]

Although these semi-IPNs present a self-healing ability as main feature, they also have other interesting properties which will be described in subsequent sections.

4.3.1. Synthesis of the semi-IPNs

The preparation of these materials was carried out by radical polymerisation of the methacrylic acid (MAAc) (2) and the cross-linker *N,N´*-methylenebisacrylamide (MBA) (3), in the presence of PVA (1), using potassium peroxydisulfate (KPS) (4) as initiator. Graphene was also added in different concentrations. The graphene dispersions in water were prepared following the ball-milling process described in the second chapter of this thesis (Chapter 2, Figure 5). Figure 3 shows the synthetic scheme and the appearance of the four final materials depending on the graphene quantity used:

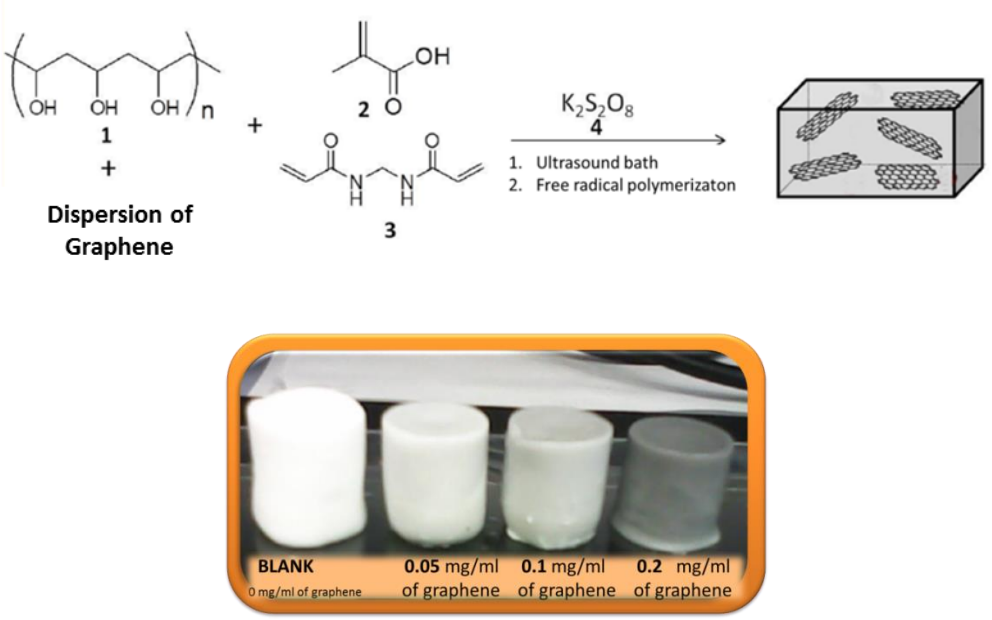

Figure 3. Synthetic scheme and digital picture of the four final graphene-based semi-IPNs at the swelling degree equilibrium.

4.3.2. Swelling degree and scanning electron microscopy (SEM)

As already introduced in Chapter 2, the swelling ratio is an important parameter since it describes the amount of water that is contained within the hydrogel. It is a function of the network structure, hydrophilicity, and degree of ionisation of the functional groups. This parameter is measured by using the following equation:

$$\text{Swelling Degree} = \frac{W_t - W_0}{W_0}$$

where W_t is the weight of the gels at time "t", and W_0 is the weight of the dried gels.

Figure 4 shows the swelling results during the ten initial minutes and at swelling equilibrium, which is the maximum swelling degree reached by the hydrogels:

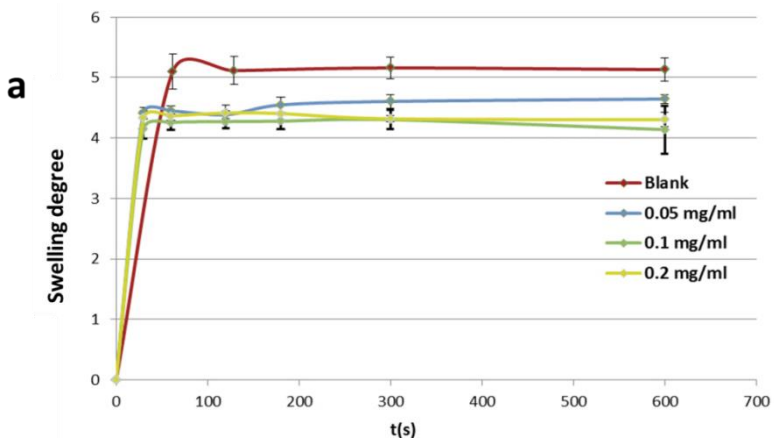

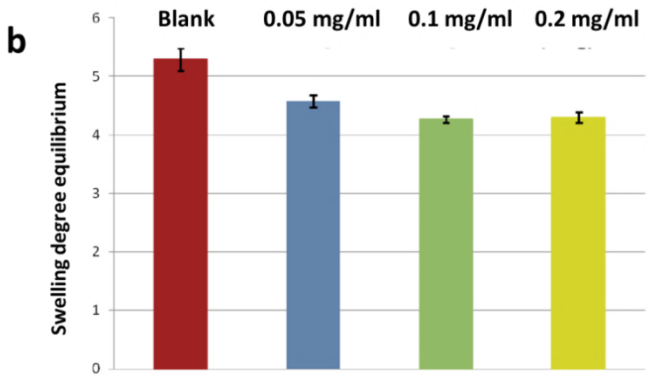

Figure 4. Swelling degree studies of the four materials a) at several time intervals and b) at swelling equilibrium.

All the hydrogels reached the final swelling degree in few minutes, but it is noteworthy that the higher the graphene concentration, the smaller the swelling degree at equilibrium.

This fact is in agreement with what we could see in the digital picture of the hydrogels (Figure 3), where the higher the graphene concentration, the smaller the size of the material at the swelling degree equilibrium. It is also corroborated by the structure studies, which were carried out by Scanning Electron Microscopy (SEM) using a PHILIPS XL30 device. Figure 5 shows SEM pictures of the four materials:

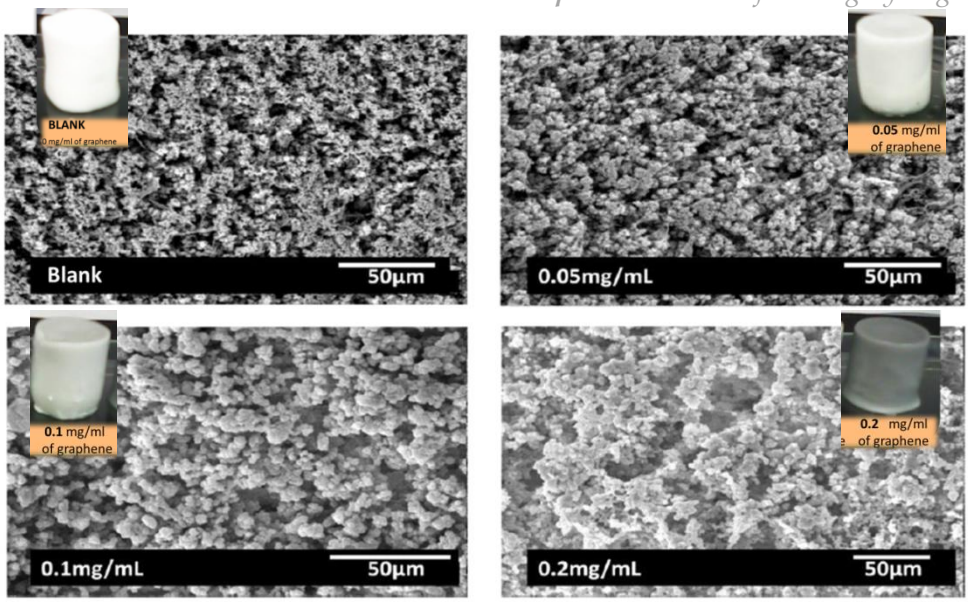

Figure 5. SEM pictures of the four IPNs prepared with different graphene concentration.

The main information that we can obtain from the SEM images is that these materials have not got the typical hydrogel pores. Instead, they have a curious structure based on cavities where the water flows easily. In fact, the water imbibed is released instantly with only slight pressure on the hydrogel surface, and it is absorbed again within a few minutes.

We can also observe that the structure becomes denser if the graphene concentration is increased. This fact is, again, in agreement with all the previous results.

4.3.3. Electromechanical behaviour

Electroresponsive hydrogels typically deswell and/or bend under the influence of an electric field, generally depending on the position of the gel with respect to the electrodes.[40] There are three competing forces acting on the gel polymer network: the polymer elasticity, the polymer-polymer affinity, and the ion pressures. These forces, collectively called osmotic pressure, determine the equilibrium state of the gel.[41]

Normally, electroresponsive hydrogels are prepared from polyelectrolytes, polymers that contain a relatively high concentration of ionisable groups along the backbone chain. These materials are attractive as they are able to implement an isothermal energy conversion from chemical free energy directly into mechanical work, actuated by an external electric stimulus. Therefore, mechanical energy is triggered by an electric signal. This fact results in one of their important functions as biosensors/actuators, in which the electrical-stimulus responsive hydrogels with fixed-charge groups can bend reversibly when an electric field is applied on the material; this feature makes them useful in drug delivery applications, among others.[42]

Tanaka and co-workers[43] suggested that the electric field produces a force on both the mobile counterions and the immobile charged groups of the gel´s polymeric network. For instance, in partially hydrolysed polyacrylamide hydrogels fixed to one of the electrodes, the mobile H^+ ions migrate towards the cathode while the negatively charged immobile acrylate groups in the polymer network are attracted towards the anode. The anionic charged polymeric network is pulled towards the anode. The pull creates a uniaxial stress along the gel axis; the stress being greatest at the anode and smallest at the cathode (Figure 6). This stress gradient is thought to contribute to the anisotropic gel deformation.

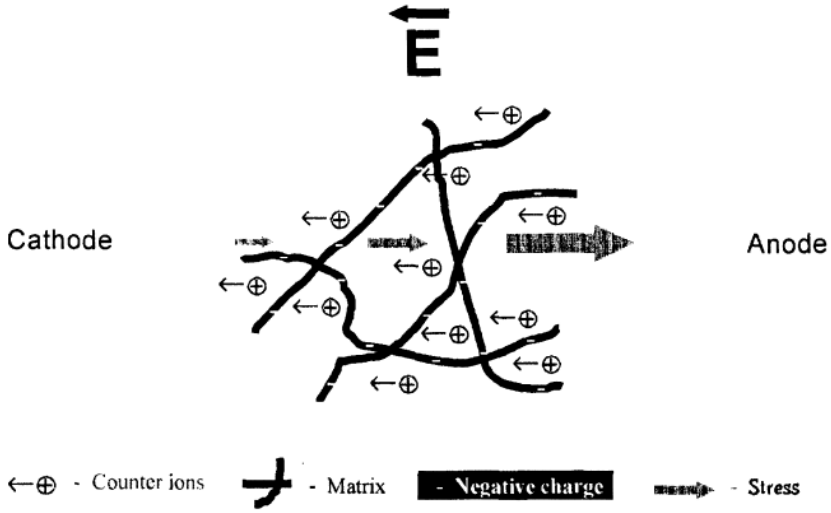

Figure 6. The effect of an electric field on a polyelectrolyte gel.[44]

The magnitude of the gel response and the degree of reversibility decreases with time and with increasing number of ON/OFF cycles as the gel fatigues.

In order to test the bending behaviour of our samples, a home-made device was used (Figure 7) which consists of a pair of carbon electrodes, separated 1 cm each other and directly joined to a power supply, a solution of NaCl in a determined concentration, and a protractor in order to measure the bending angle. Upon application of a direct current (DC) electric field (20 V in all the cases), the degree of bending was measured, quantifying the angle of deviation from the vertical position.

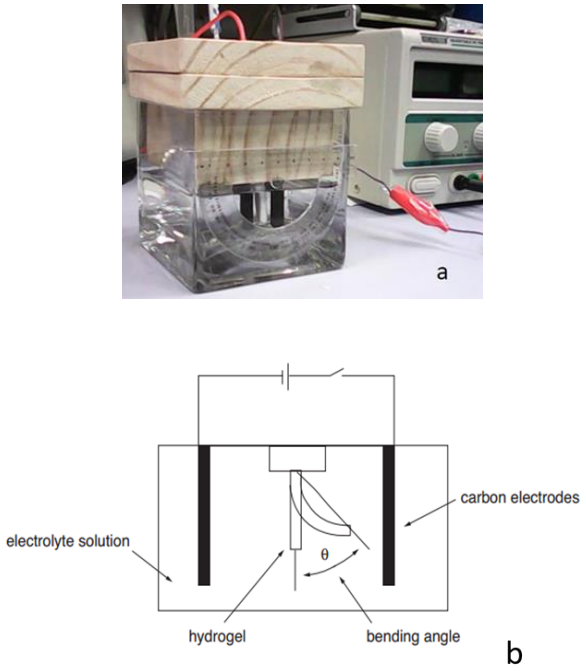

Figure 7. a) Digital image and b) schematic diagram of the device for testing the bending behaviour of the hydrogels.

The best results were obtained using a 0.05 M NaCl solution, and only 2 minutes are needed to reach the maximum bending (Figure 8):

Figure 8. Digital pictures of the bending behaviour by the Blank a) after 1 minute of electric field application, b) without any electric field application, thus the sample is on a vertical position, c) after 1 minute of electric field application changing the current direction.

It is possible to observe how the gel bends towards the cathode or the anode depending on the current direction. The power supply was ON and OFF in order to achieve the vertical position of the sample by itself before changing the current direction. The cycles of bending showed by the Blank and the hydrogel which contains 0.2 mg/ml of graphene are represented in Figure 9. The differences are not very appreciable between both samples. This result has a very positive meaning because graphene does not restrict the electromechanical properties of the materials in the concentration which was used for these studies.

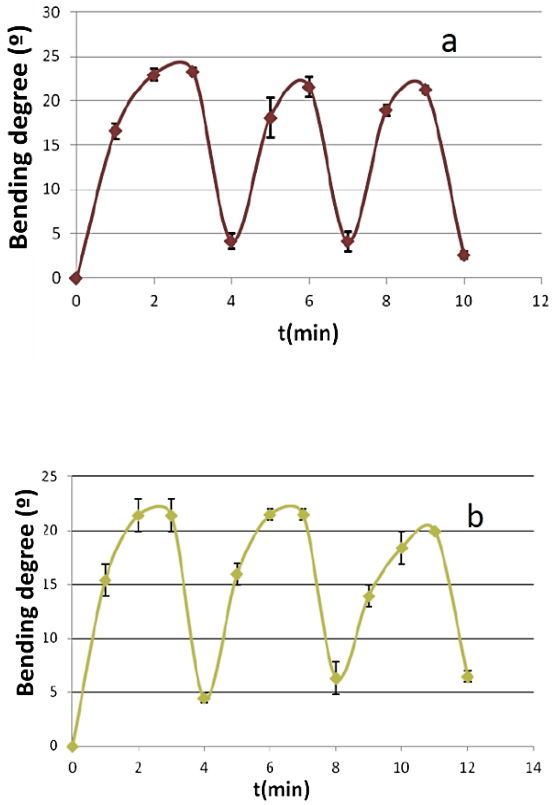

Figure 9. Cycles of bending showed by a) the Blank and b) the hydrogel that contains 0.2 mg/ml of graphene.

4.3.4. Self-healing ability

Herein, an autonomous and irreversible self-healing ability is presented due to the reaction of residual functional groups which interdiffuse to the joining zone, achieving the total union of the two pieces. Unlike reversible self-healing ability, irreversible auto-repairing processes cannot heal a once ruptured area a second time.

We prepared two pieces of hydrogel; one of them containing fluorescein as dye in order to distinguish the interface between the two pieces easily. The hydrogels were put in contact and after 72 hours a complete adhesion was observed (Figure 10).

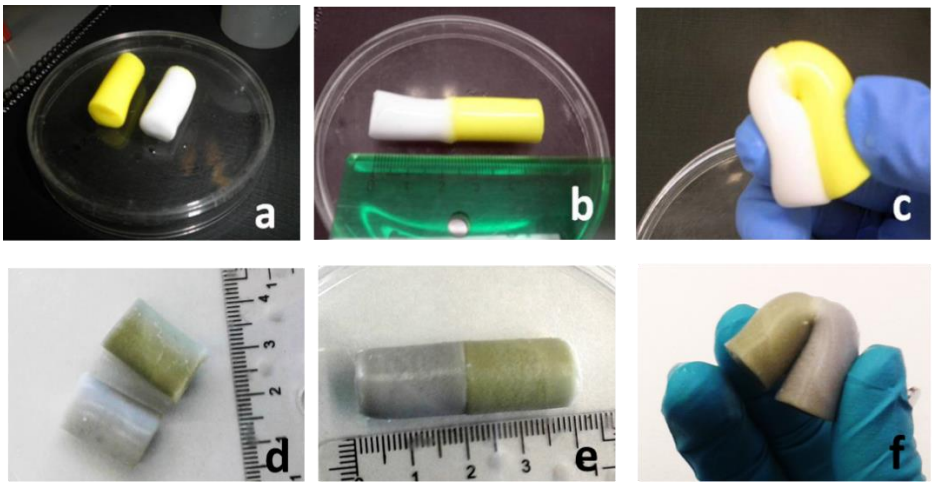

Figure 10. a) Two separated pieces of Blank (dyed and not dyed), b) after 72 hours joined, c) and being stressed after 72 hours joined. d) Two separated pieces of the hydrogel that contains 0.1 mg/ml of graphene (as a representative example) (dyed and not dyed), e) after 72 hours joined, f) and being stressed after 72 hours joined.

As it can be observed, all the materials, including the graphene-based composites, exhibited a good self-healing ability, so it has to be highlighted that the nanomaterial does not limit the self-healing capacity of the hydrogels. This fact is important from the

point of view of the increased number of possible applications of this kind of composite materials.

The following SEM picture shows the zone of contact after joining (Figure 11). It is possible to observe the self-healing zone where new polymer cavities have been created by crosslinking reactions:

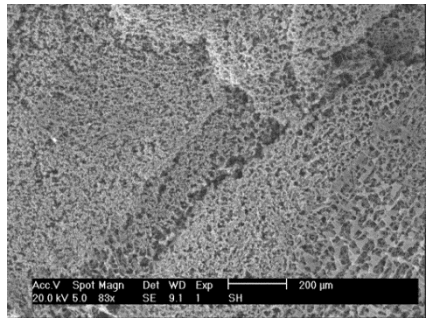

Figure 11. SEM picture of the repaired zone of Blank as a representative sample. Scale bar:200 µm.

It is well known that hydrogels based on PVA can be prepared by freeze-thaw cycles, as they are physically cross-linked by the presence of crystalline regions.[45] Therefore, the self-healing ability of our systems was also proved regarding the possible crystallisation of the PVA chains. Two pieces were put in contact, and freeze thaw cycles were done afterwards. However, no better self-healing capacity was achieved.

Moreover, PVA gels can self-repair by hydrogen bond interactions among the PVA chains if an appropriate balance exists between free hydroxyl groups on chains and chain mobility in the hydrogel.[6] However, self-healing ability has not been demonstrated due to hydrogen bond interactions in our case, and a higher content of PVA would probably be necessary for our materials in order to self-heal in that way.

4.4. Poly([2-(Acryloyloxy)ethyl] trimethyl-ammonium chloride) / poly(methacrylic acid) hydrogels

Besides forming interpenetrating polymer networks based on MAAc and PVA, the self-healing ability of a second type of hydrogels was studied. In this case, the materials were prepared from MAAc in combination with a different monomer: [2-(acryloyloxy)ethyl]trimethylammonium chloride (AETA), which is mainly used as an intermediate in industrial settings. However, AETA has not been widely used in hydrogel formation until now and very few examples exist[46,47,48] although it is a cheap, biodegradable and non-toxic molecule.

This second type of self-healing hydrogels is based on oppositely charged polyelectrolytes. Thus, AETA is used as the cationic monomer and the methacrylic acid is used as the negative one. By this way, self-healing capacity is reached due to the existence of ionic interactions in the material.[49,8,50]

Different hydrogels were prepared depending on the synthetic process: (i) copolymerisation of both monomers, forming a unique double charged network and (ii) formation of semi-IPNs in which free p(MAAc) chains are embedded into the cationic network of AETA. In that sense, self-healing ability in the semi-IPNs would be easier than in the copolymers, because the free chains would be able to diffuse through the interface guided by the ionic interactions to restore the damaged area.

Moreover, graphene was used as filler again in order to study if the nanomaterial modifies the healing capacity of the final materials.

4.4.1. Synthesis of the copolymers

The first kind of double charged hydrogels was prepared by a copolymerisation process. Figure 12 shows a general scheme of the synthesis pathway. By following this methodology, both charged monomers (MAAc and AETA) react at the same time with the *N,N´*-methylenebisacrylamide (MBA), which acts as cross-linker forming a unique double charged network. Potassium peroxydisulfate (KPS) was used as an initiator. Moreover, a dispersion of graphene (0.2 mg/ml) was used as solvent instead of water to form the copolymer in the presence of the nanomaterial.

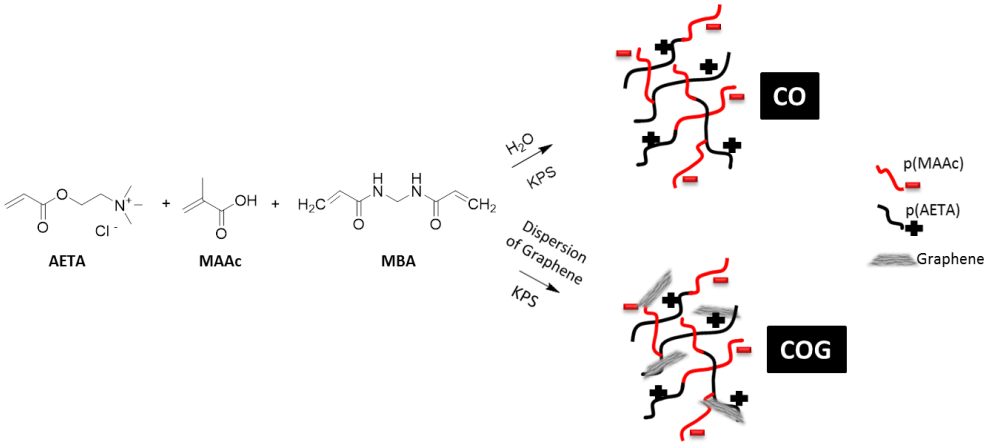

Figure 12. Synthetic scheme of the copolymer hydrogels: without graphene (**CO**) and with graphene (0.2 mg/ml) (**COG**).

The obtained homogeneous hydrogels present a transparent and orange colour aspect (Figure 13).

Figure 13. Digital picture of both copolymers hydrogels: without graphene (**CO**) and with graphene (0.2 mg/ml) (**COG**).

4.4.2. Synthesis of the semi-IPNs

Interpenetrating polymer networks were also prepared to compare the self-healing ability between the copolymers and these different types of hydrogels because, as it is known, the free chains in semi-IPNs can diffuse through the interfase easily.

Two different strategies were proposed in order to obtain the desired semi-IPNs:

Strategy 1 consists of two reaction steps (Figure 14): step 1 is the radical polymerisation process of the MAAc to form the p(MAAc) chains; step 2 is the formation of the cationic network of p(AETA) by using the cationic monomer, the linker and the radical initiator in the presence of the p(MAAc) chains. By this way, the chains of p(MAAc) would be theoretically free and embedded into the cationic network. A dispersion of graphene (0.2 mg/ml) was also used as solvent instead of water to form the hydrogel in the presence of the nanomaterial.

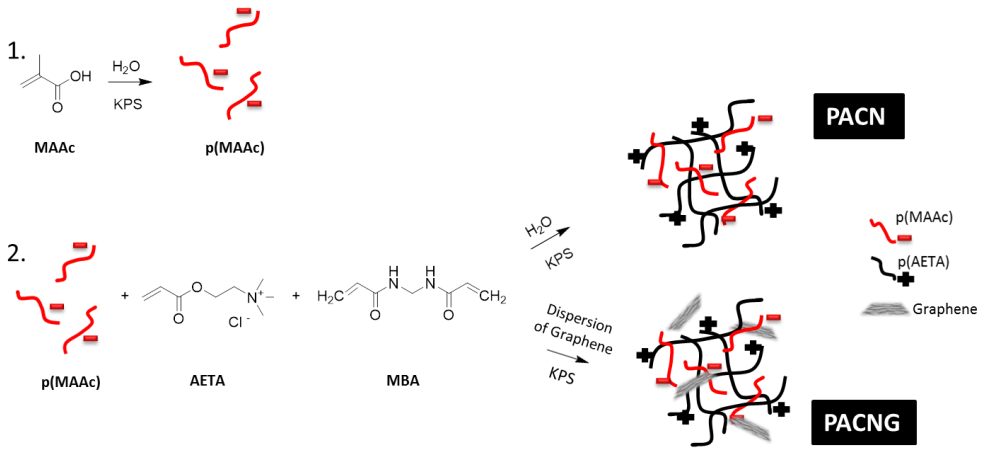

Figure 14. Synthetic scheme of the semi-IPNs synthesised by following the Strategy 1: without graphene (**PACN**) and with graphene (0.2 mg/ml) (**PACNG**).

Homogeneous semi-IPNs were obtained by following the first strategy. They present an orange tonality apart from a transparent appearance, as in the case of the copolymers (Figure 15).

Figure 15. Digital picture of the semi-IPNs synthesised by following the Strategy 1: without graphene (**PACN**) and with graphene (0.2 mg/ml) (**PACNG**).

Strategy 2 consists of two reaction steps too (Figure 16), but this time just in reverse order than Strategy 1. In this case, step 1 is the formation of the cationic network of p(AETA) (**CN**) by using the cationic monomer, the linker and the radical initiator. The self-healing ability of **CN** was studied in order to compare that capacity regarding the no existence of free p(MAAc) chains in this material. A dispersion of graphene of 0.2 mg/ml was also used as solvent (**CNG**). In fact, step 2 in Strategy 2 is

the radical polymerisation of the MAAc into the cationic network to form the free p(MAAc) chains inside of it.

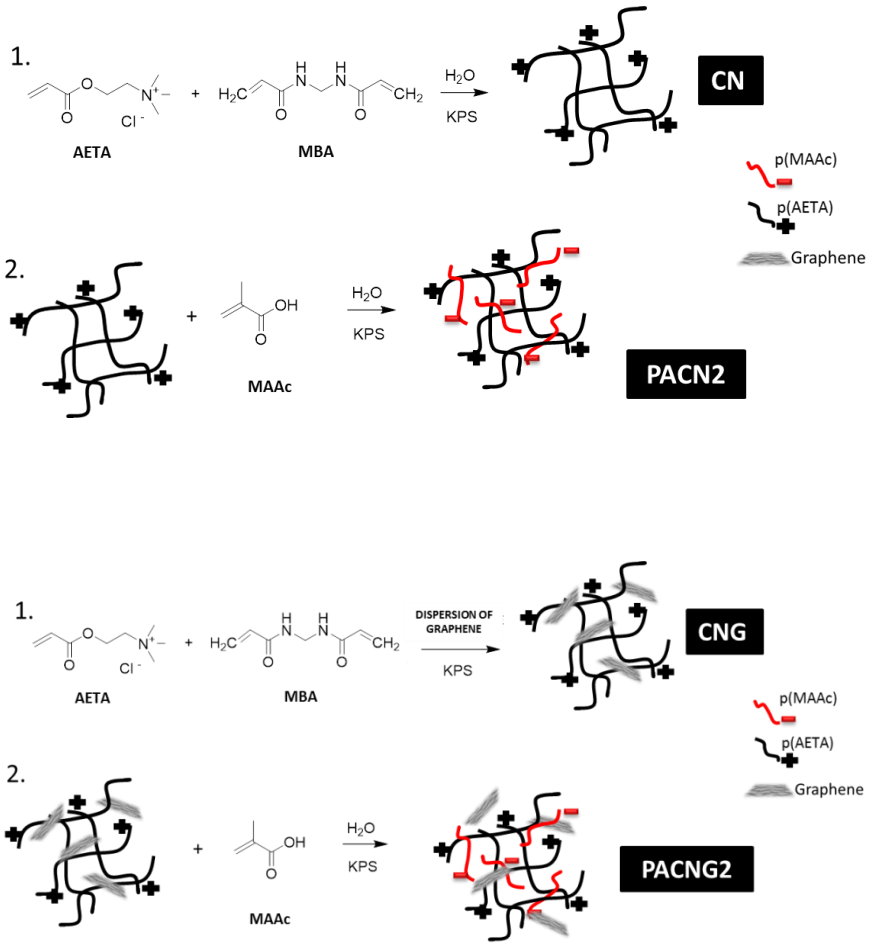

Figure 16. Synthetic schemes of the semi-IPNs synthesised by following the Strategy 2: without graphene (**PACN2**) and with graphene (0.2 mg/ml) (**PACNG2**). **CN** is the cationic network prepared just from AETA, MBA and KPS and **CNG** is the same network formed using graphene dispersion as solvent.

Homogeneous semi-IPNs were obtained again by following the second strategy, with orange tonality and a transparent appearance too (Figure 17).

Figure 17. Digital picture of the semi-IPNs synthesised by following the Strategy 2: without graphene (**PACN2**) and with graphene (0.2 mg/ml) (**PACNG2**).

4.4.3. Results and discussion

4.4.3.1. CO, COG, PACN and PACNG

First studies were carried out comparing the properties of copolymers and semi-IPNs prepared following the strategy 1. Moreover, **CN** was used as "blank" to compare the healing efficiency of the rest of materials as it is not a semi-IPN (because it has not got free polymer chains inside) and it is only positively charged.

Figure 18 shows a scheme of the tensile experiments carried out to measure the self-healing capacity of the materials.

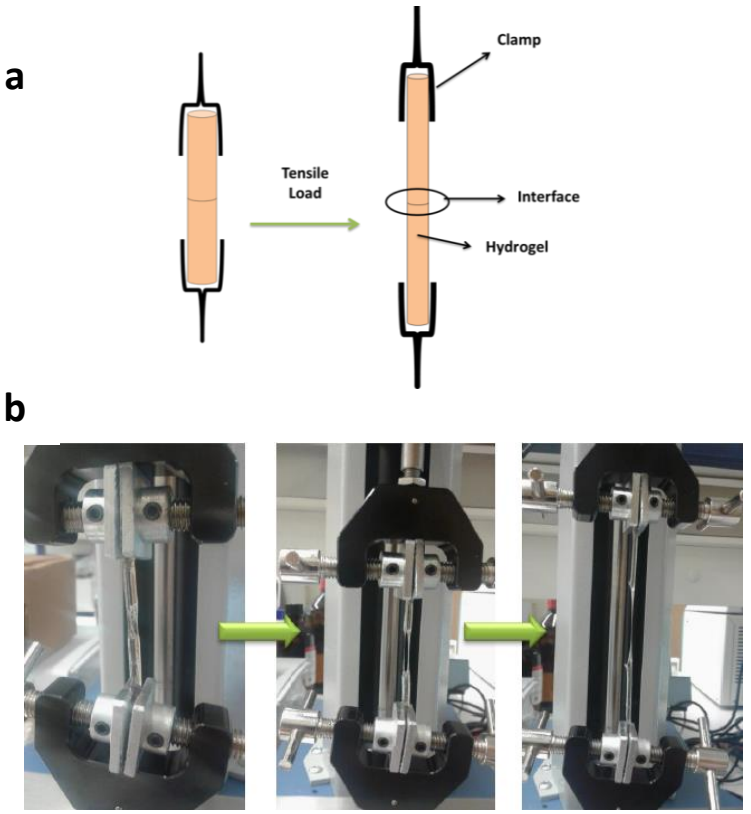

Figure 18. a) Schematic diagram and b) digital picture of the tensile experiments carried out to measure the healing efficiency.

By this way, the healing efficiency (η) was calculated using the following equation:

$$\eta = \frac{K_{IC}^{Healed}}{K_{IC}^{Virgin}} \times 100$$

where K_{IC}^{Healed} is the fracture toughness of the healed specimen and K_{IC}^{Virgin} is the fracture toughness of the virgin hydrogel.[1]

These studies were performed on samples that had been put in contact for 1 hour or 3 days after having been cut with a blade. The healing efficiencies obtained by **CO**, **COG**, **PACN** and **PACNG** are shown in figure 19:

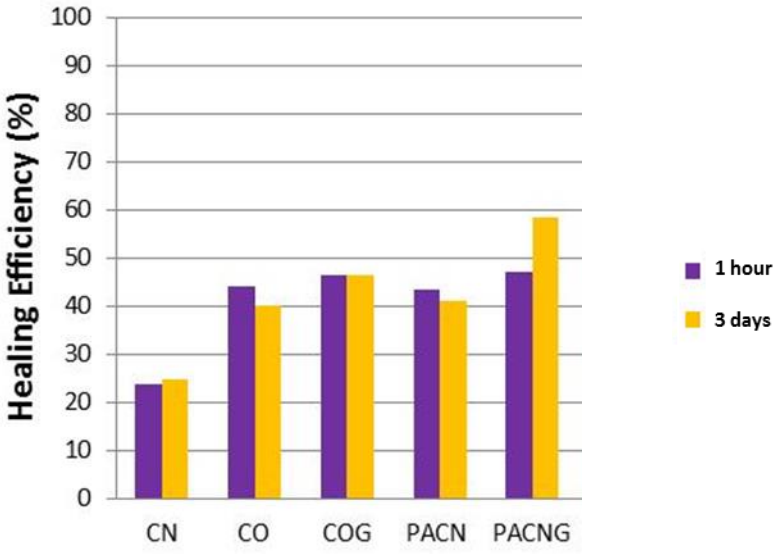

Figure 19. Healing efficiency values from all the samples.

As it can be observed, **CO**, **COG**, **PACN** and **PACNG** present higher healing efficiencies than **CN**, as it was expected, and the healing degree obtained in only 1 hour is the same as the healing degree reached in 3 days.

It has to be highlighted that the nanomaterial does not limit the self-healing capacity of the hydrogels. This fact is important from the point of view of the increased number of possible applications of these composite materials.

However, an increase in the healing efficiency of the semi-IPNs with respect to the copolymers is not observed.

In order to have an idea of the molecular weight of the p(MAAc) chains embedded in the hydrogel, the mass spectrum of the polymer obtained from step 1 in strategy 1 (p(MAAc)), was analysed. We could observe a very low molecular weight, around 600 m/z.

These facts make us think that, instead of a semi-IPN, a different copolymer could be formed following the strategy 1. Taking into account that step 2 follows to step 1 without stopping the radical polymerisation, the formed p(MAAc) chains could have free reactant radicals, acting in this way as longer monomers, resulting in a new network, similar to CO, but with bigger pores.

This idea was corroborated by the swelling studies. Figure 20 shows higher swelling degrees for **PACN** and **PACNG** with respect to **CO** and **COG**, as a consequence of the possible bigger pores in the first two materials.

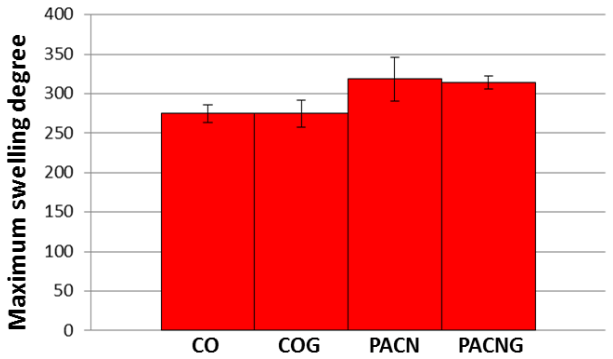

Figure 20. Swelling degree studies of **CO**, **COG**, **PACN** and **PACNG**.

Due to all this evidences, we could say that the self-healing in these four materials is related to the diffusion of the pendant chains of the network, through the interfase, due to the ionic interactions between the oppositely charged moieties, fact that repairs the damaged zone.

The self-healing capacity was also corroborated by SEM pictures. It was possible to observe how the interfase remains visible in the case of **CN**, but not in the rest of the materials, where the interface is disappearing, almost completely in some cases, due to healing process. Figure 21 shows the interfase region of the samples **CN** and **PACN** as an example:

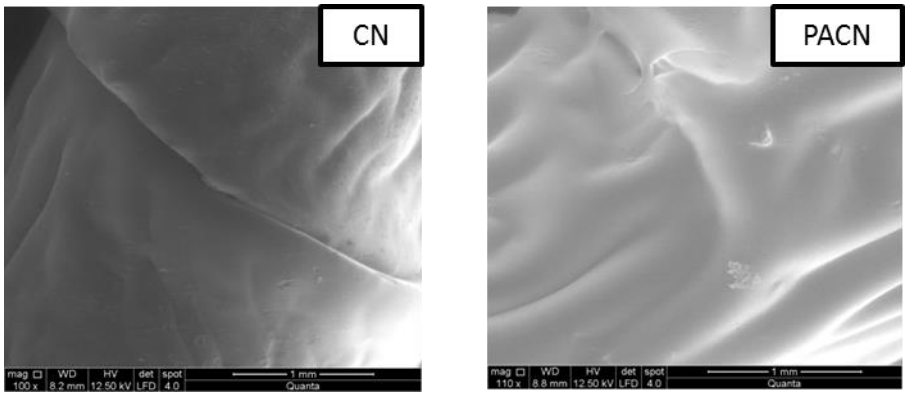

Figure 21. SEM pictures of the still damaged region of **CN** and the partially healed zone in **PACN**. Scale bars:1 mm.

Trying to improve this self-healing capacity, the formation of semi-IPNs by the second strategy (strategy 2) was carried out.

4.4.3.2. PACN2 and PACNG2

Second studies were carried out with semi-IPNs prepared following the strategy 2. In order to compare the healing efficiencies, the tensile conditions were the same than the ones used for the previous materials.

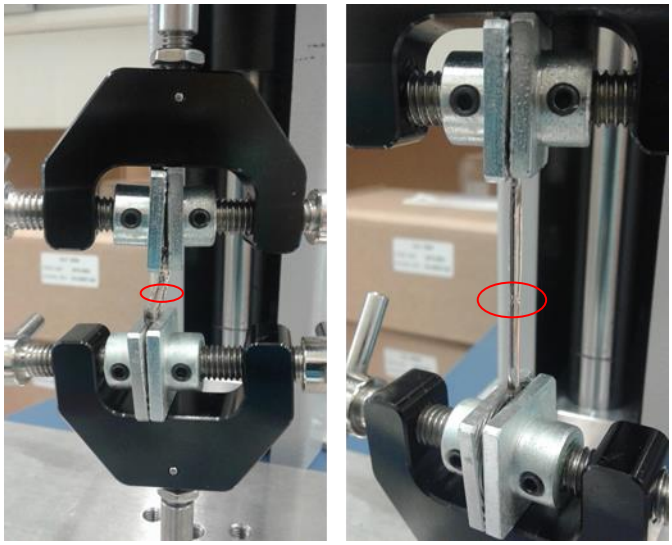

Figure 22. Digital picture of the tensile experiments carried out to measure the healing efficiency of **PACN2**. Red circles show the interface zones.

These studies were performed on samples that had been put in contact for only 1 day after having been cut. The healing efficiencies obtained for **PACN2** and **PACNG2** are shown in figure 23:

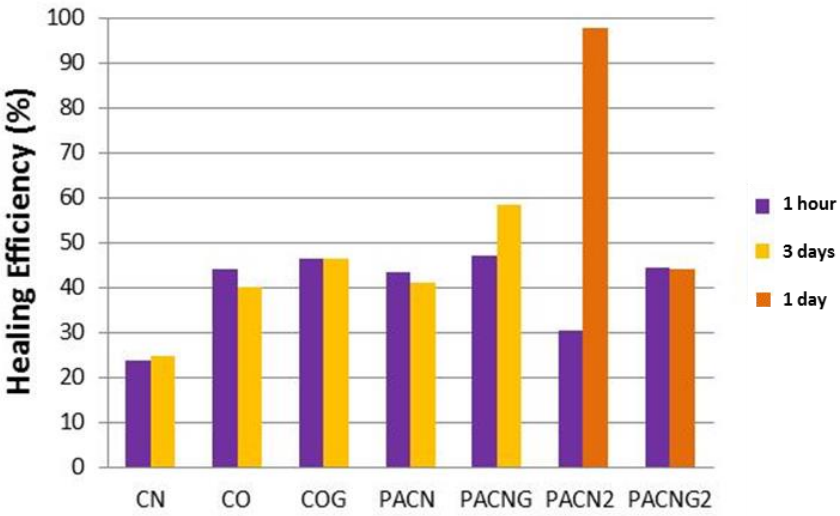

Figure 23. Healing efficiency values obtained from all the samples.

As expected, the healing efficiency of **PACN2** is considerately higher than the healing efficiency of **CN**, and also higher than the previous materials. In this case, free polymer chains of methacrylic acid are able to move easily across the interface. Because of that, self-healing capacity increases with time, reaching almost a 100% value of healing efficiency in only 1 day.

However, the same material prepared in the presence of graphene (**PACNG2**) did not show higher healing efficiencies. Although the value obtained after 1h of contact was comparable to the healing efficiencies of the rest of materials, a higher healing value was not obtained after 1 day of contact. Taking into account the high healing efficiency obtained for **PACN2** after 1 day; in the case of **PACNG2** the graphene sheets could be hindering the free chain diffusion. More experiments are being performed in order to better study this behaviour.

Finally, the electrical properties of these new materials were analysed. Electrical conductivity (σ, in S/cm), or its inverse, resistivity (ρ, in Ω·cm) are an intrinsic property of materials which depend on their natural ability to allow transit of charge carriers within their structure.[51] Turning an insulating or poorly conductive material into conducting or semiconducting can be easily reached, for instance, by adding conductive fillers. Therefore, in order to see if graphene improves this feature, the electrical properties of these materials were measured. Moreover, **CN** was used as "control" sample. Figure 24 shows the results:

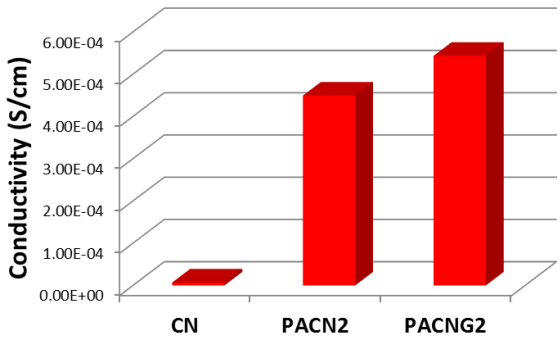

Figure 24. Conductivity values of **CN**, **PACN2** and **PACNG2**.

As expected, the incorporation of the nanomaterial into the polymer network, results in an enhancement of the conductivity of the final composite. Although the increment between the conductivity values of **PACN2** and **PACNG2** is not too high, it is at least remarkable. Moreover, there is a clear improvement in the conductivity of the semi-IPNs regarding the value obtained for **CN**. The reason could be the presence of the free polymer chains of p(MAAc), as it occurs in some works described in literature.[52]

4.5. Experimental procedures

4.5.1. Poly(methacrylic acid) / poly(vinyl alcohol) hydrogels

4.5.1.1. Synthesis of the semi-IPNs

The graphene used has been prepared following a procedure developed in our group,[33] using commercial melamine and graphite from Bay Carbon, Inc. (SP-1 graphite powder, www.baycarbon.com). The milling treatment was carried out in a Retsch PM100 Planetary Mill.

The preparation of the semi-IPNs was carried out by radical polymerisation of the methacrylic acid (MAAc) and the cross-linker *N,N´*-methylenebisacrylamide (MBA), in the presence of poly(vinyl alcohol) (PVA), using potassium peroxydisulfate (KPS) as initiator. Aqueous graphene dispersion was used as a solvent in different concentrations. The mixture, which has a final volume of 5ml, is sonicated for 5 minutes until homogenisation and put in an oven at 80 ^{o}C for 4 hours.

Table 1 shows the compositions of the semi-IPNs:

SAMPLE	SOLVENT: GRAPHENE CONCENTRATION IN WATER (mg/ml)	PVA:MAAc (%w/w)*	MBA: MAAc (mol/mol)	KPS: MAAc (mol/mol)
Blank	0	30:70	1:100	1:1000
0.05	0.05			
0.1	0.1			
0.2	0.2			

Table 1. Reagents ratios as well as graphene concentration used in every sample. *Weight percentage ratio between PVA and MAAc.

4.5.1.2. Swelling studies

Swelling studies were carried out for the hydrogels with increasing graphene concentration by immersing the lyophilised gels in 10 ml of ultrapure Milli-Q water at room temperature. All the samples have an approximate volume of 1 cm^3. The weights of the swollen hydrogels were recorded at regular time intervals until they reached a constant weight. Excess water on the surface of the gels was removed with filter paper. The swelling degree was then evaluated by using the following equation:

$$\textbf{Swelling Degree} = \frac{W_t - W_0}{W_0}$$

where W_t is the weight of the gels at time t, and W_0 is the weight of the dried gels.

4.5.1.3. SEM studies

Scanning Electron Microscopy (SEM) of the swollen hydrogels structure was performed using a PHILIPS XL30 system. The dried gels were immersed in ultrapure Milli-Q water at room temperature until the samples reach the maximum swelling

degree. Then, the completely swollen hydrogels are lyophilised by using a freeze-drier. The samples were then placed under vacuum and coated with a 10 nm layer of gold, and the surface of each gel was analysed by SEM.

4.5.1.4. Electroactivity studies

Cylindrical samples of 1.5 cm of length and 0.4 cm of diameter were prepared to carry out the electroactivity experiments. The hydrogels were dried and then swollen in a NaCl 0.05 M solution. Every sample was then fixed between a pair of carbon electrodes which were separated by 1 cm. All these elements were submerged in a NaCl 0.05 M solution as shown previously in Figure 7.

Once the electrodes were directly connected to a power supply HQ POWERTM PS23023, the current was applied. A voltage of 20 V was used in all the cases.

4.5.1.5. Self-healing ability

Two prepared hydrogel pieces were put in contact for 72 hours at room temperature. One of them was synthesised in the presence of fluorescein (0.4 mg/ml) in order to distinguish the interface between the two pieces easily after contact.

After that time, self-healing ability was evidenced by tensile tests by hand. A digital camera was used to corroborate the reparation.

4.5.2. Poly([2-(Acryloyloxy)ethyl]trimethylammonium chloride) / poly(methacrylic acid) hydrogels

4.5.2.1. Synthesis of the copolymers

The graphene used has been prepared following the same procedure than for the previous gels.

The preparation of the copolymers was carried out by radical polymerisation of the methacrylic acid (0.57 ml, 6.62 mmol), the [2-(acryloyloxy)ethyl]trimethylammonium chloride (5.66 ml, 26.4 mmol) and the cross-linker *N,N´*-methylenebisacrylamide (0.01 g, 0.06 mmol). The potassium peroxydisulfate (0.017 g, 0.06 mmol) was used as an initiator. 5 ml of Milli-Q water was used as a solvent to synthesise **CO**, and 5 ml of aqueous graphene dispersion (0.2 mg/ml) was used as a solvent to synthesise **COG**. The mixtures were sonicated until homogenisation and after put in the oven at 80 ^{o}C for 9 hours.

4.5.2.2. Synthesis of the semi-IPNs

- **Strategy 1**

Strategy 1 was carried out in two different steps:

Step 1: 0.57 ml of methacrylic acid (6.62 mmol) and 1 mg of potassium peroxydisulfate ($3.5 \cdot 10^{-3}$ mmol) were added to 5 ml of Milli-Q water to form **PACN**. In the case of the **PACNG** formation, 5 ml of aqueous graphene dispersion (0.2 mg/ml) instead of water was used as solvent. The mixtures were sonicated for 2 minutes until homogenisation and the polymerisation was carried out at 80 ^{o}C for 90 minutes.

Step 2: 5.66 ml of the [2-(acryloyloxy)ethyl]trimethylammonium chloride (26.4 mmol) and 0.01 g of *N,N´*-methylenebisacrylamide (0.06 mmol) were added to each of the mixtures obtained from step 1 and potassium peroxydisulfate (0.017 g, 0.06 mmol) was added as initiator. The mixtures were sonicated for 5 minutes until homogenisation and put in the oven at 80 ^{o}C for 9 hours.

- **Strategy 2**

The preparation of the semi-IPNs by strategy 2 consisted of two different steps:

Step 1: 5.66 ml of [2-(acryloyloxy)ethyl]trimethylammonium chloride (26.4 mmol) and 0.01 g of *N,N´*-methylenebisacrylamide (0.06 mmol) were added to 5 ml of Milli-Q water or 5 ml of a dispersion of graphene (0.2 mg/ml) and potassium peroxydisulfate (0.017 g, 0.06 mmol) was added as initiator. The mixtures were sonicated for 5 minutes until homogenisation and put after in the oven at 80 ^{o}C for 9 hours. **CN** and **CNG** are the resulted networks obtained from this step.

The resulting gels were immersed in water for at least 5 days, and the water was changed every day in order to remove any unreacted monomer and initiator molecules.

Step 2: the samples obtained from Step 1 were dried and then immersed in a solution that contained 0.57 ml of the methacrylic acid (6.62 mmol) and 1 mg of potassium peroxydisulfate ($3.5 \cdot 10^{-3}$ mmol) in 5 ml of Milli-Q water. Once the hydrogels absorbed the solution, they were put in an oven at 80 ^{o}C for 90 minutes. Free poly(methacrylic acid) chains are formed by this way inside the cationic networks, achieving the semi-IPNs **PACN2** and **PACNG2**.

4.5.2.3. Swelling studies

Swelling studies were carried out for the hydrogels by immersing the lyophilised gels in 10 ml of ultrapure Milli-Q water at room temperature. All the samples have a cylindrical shape of approximately 0.5 cm of length and 0.5 cm of diameter. The weights of the swollen hydrogels were recorded at regular time intervals until they reached a constant weight. Excess water on the surface of the gels was removed with a paper filter. The swelling degree was then evaluated by using the following equation:

$$\textbf{Swelling Degree} = \frac{W_t - W_0}{W_0}$$

where W_t is the weight of the gels at time "t", and W_0 is the weight of the dried gels.

4.5.2.4. SEM studies

Scanning Electron Microscopy (SEM) of the interfaces in the prepared semi-IPNs was performed using a FEI QUANTA 250 system. The just prepared gels were put in contact for 1 hour after have been cut. The hydrogels are then lyophilised by using a freeze-drier and the surfaces of the damaged/repaired areas were analysed by SEM.

4.5.2.5. Self-healing ability

Cylindrical samples of every gel were prepared for the tensile experiments. The samples had a length of approximately 2 cm and a diameter around 0.5 cm. Each experiment was repeated at least twice, and lengths and diameters were measured each time to normalise the final healing efficiency values. The samples were completely cracked at the middle by using a blade, and then the two separated pieces were put in contact again for different periods of time at room temperature. A Mecmesin MultiTest 2.5-i machine was used to measure the healing efficiency of each material by following the next equation:

$$\eta = \frac{K_{IC}^{Healed}}{K_{IC}^{Virgin}} \times 100$$

where K_{IC}^{Healed} is the fracture toughness of the healed specimen and K_{IC}^{Virgin} is the fracture toughness of the virgin hydrogel. The samples were stressed under a load of 0.5 N at 15 mm/min until a displacement of 30 mm.

4.5.2.6. Electrical properties

Direct current electrical resistance (R) measurements were performed with an Agilent multimeter, in a two-point probe configuration, to cylindrical specimens of 5 mm diameter and 10 mm length (moulded in plastic syringes). At least three

measurements were performed for each sample, by contacting crocodile-type electrodes to the hydrogel ends, which were previously covered by a thin layer of Ag painting. Electrical conductivity (σ) was calculated as the inverse of resistivity (ρ), obtained in turn from its relationship with R:

$$R = \rho \frac{l}{s}$$

where l and s are the specimen's length and section area respectively.

4.6. Conclusions

Autonomous self-healing capacity has been achieved in different novel composite hydrogels. The materials were synthesised from different monomers and by several strategies depending on the desired structure. Moreover, graphene was used as filler in some cases.

Healing efficiency was corroborated not only by SEM analysis of the damaged/healed region, but also by tensile experiments.

All the materials have excellent self-healing ability, reaching almost the 100% of healing efficiency in the case of **PACN2**, in which real free chains are able to diffuse through the interface, guided by the existent ionic interactions. Moreover, graphene only declines the healing efficiency in the case of **PACNG2**, but not in the rest of the materials, which is important from the point of view of the possible applications of these kinds of materials, taking into account that the presence of graphene improves the conductivity of the final composite.

Electroresponsive hydrogels have been prepared in which mechanical energy is triggered by an electric signal. Hydrogels can bend reversibly when an electric field is applied on the material; this feature makes them useful as biosensors/actuators, among others applications.

However, this work is currently in progress, and new graphene-based materials are being studied, not only regarding the self-healing ability, but also the mechanical or electrical properties of the final composites.

4.7. References

(1) Murphy, E. B.; Wudl, F. The World of Smart Healable Materials. *Prog. Polym. Sci.* **2010**, *35*, 223–251.

(2) Diesendruck, C. E.; Sottos, N. R.; Moore, J. S.; White, S. R. Biomimetic Self-Healing. *Angew. Chemie Int. Ed.* **2015**, *54*, 2–22.

(3) Xu, K.; An, H.; Lu, C.; Tan, Y.; Li, P.; Wang, P. Facile Fabrication Method of Hydrophobic-Associating Cross-Linking Hydrogel with Outstanding Mechanical Performance and Self-Healing Property in the Absence of Surfactants. *Polymer* **2013**, *54*, 5665–5672.

(4) Herbst, F.; Döhler, D.; Michael, P.; Binder, W. H. Self-Healing Polymers via Supramolecular Forces. *Macromol. Rapid Commun.* **2013**, *34*, 203–220.

(5) McKee, J. R.; Appel, E.; Seitsonen, J.; Kontturi, E.; Scherman, O.; Ikkala, O. Healable, Stable and Stiff Hydrogels: Combining Conflicting Properties Using Dynamic and Selective Three-Component Recognition with Reinforcing Cellulose Nanorods. *Adv. Funct. Mater.* **2014**, *24*, 2706–2713.

(6) Zhang, H.; Xia, H.; Zhao, Y. Poly(vinyl Alcohol) Hydrogel Can Autonomously Self-Heal. *ACS Macro Lett.* **2012**, *1*, 1–4.

(7) Cong, H.-P.; Wang, P.; Yu, S.-H. Stretchable and Self-Healing Graphene Oxide–Polymer Composite Hydrogels: A Dual-Network Design. *Chem. Mater.* **2013**, *25*, 3357–3362.

(8) Bai, T.; Liu, S.; Sun, F.; Sinclair, A.; Zhang, L.; Shao, Q.; Jiang, S. Zwitterionic Fusion in Hydrogels and Spontaneous and Time-Independent Self-Healing under Physiological Conditions. *Biomaterials* **2014**, *35*, 3926–3933.

(9) Wei, H.; Du, S.; Liu, Y.; Zhao, H.; Chen, C.; Li, Z.; Lin, J.; Zhang, Y.; Zhang, J.; Wan, X. Tunable, Luminescent, and Self-Healing Hybrid Hydrogels of Polyoxometalates and Triblock Copolymers Based on Electrostatic Assembly. *Chem. Commun.* **2014**, *50*, 1447–1450.

(10) Burattini, S.; Colquhoun, H. M.; Fox, J. D.; Friedmann, D.; Greenland, B. W.; Harris, P. J. F.; Hayes, W.; Mackay, M. E.; Rowan, S. J. A Self-Repairing, Supramolecular Polymer System: Healability as a Consequence of Donor-Acceptor π-π Stacking Interactions. *Chem. Commun.* **2009**, *44*, 6717–6719.

(11) Gemert, G. M. L. Van; Peeters, J. W.; Söntjens, S. H. M.; Janssen, H. M.; Bosman, A. W. Self-Healing Supramolecular Polymers In Action. *Macromol. Chem. Phys.* **2012**, *213*, 234–242.

(12) Li, W.; Liu, M.; Chen, H.; Xu, J.; Gao, Y.; Li, H. Phenylboronate-Diol Crosslinked polymer/SWCNT Hybrid Gels with Reversible Sol-Gel Transition. *Polym. Adv. Technol.* **2014**, *25*, 233–239.

(13) Yang, Y.; Urban, M. W. Self-Healing Polymeric Materials. *Chem. Soc. Rev.* **2013**, *42*, 7446–7467.

(14) Wei, Z.; Yang, J. H.; Zhou, J.; Xu, F.; Zrínyi, M.; Dussault, P. H.; Osada, Y.; Chen, Y. M. Self-Healing Gels Based on Constitutional Dynamic Chemistry and Their Potential Applications. *Chem. Soc. Rev.* **2014**, *43*, 8114–8131.

(15) Wool, R. P. and O´Connor, K. M. A Theory of Crack Healing in Polymers. *J. Appl. Phys.* **1981**, *52*, 5953–5963.

(16) Kim, Y.; Wool, R. A Theory of Healing at a Polymer-Polymer Interface. *Macromolecules* **1983**, *16*, 1115–1120.

(17) Nji, J.; Li, G. A Biomimic Shape Memory Polymer Based Self-Healing Particulate

Composite. *Polymer* **2010**, *51*, 6021–6029.

(18) Rodriguez, E. D.; Luo, X.; Mather, P. T. Linear/network Poly(??-Caprolactone) Blends Exhibiting Shape Memory Assisted Self-Healing (SMASH). *ACS Appl. Mater. Interfaces* **2011**, *3*, 152–161.

(19) Urban, M. W. *Handbook of Stimuli-Responsive Materials*; Urban, M. W., Ed.; Verlag & Co. KGaA: Weinheim, 2011.

(20) Meng, H.; Li, G. A Review of Stimuli-Responsive Shape Memory Polymer Composites. *Polymer* **2013**, *54*, 2199–2221.

(21) Swait, T. J.; Rauf, A.; Grainger, R.; Bailey, P. B. S.; Lafferty, A. D.; Fleet, E. J.; Hayes, S. A. Smart Composite Materials for Self-Sensing and Self-Healing. *Plast. Rubber Compos.* **2012**, *41*, 215–225.

(22) Esser-Kahn, A. P.; Odom, S. a.; Sottos, N. R.; White, S. R.; Moore, J. S. Triggered Release from Polymer Capsules. *Macromolecules* **2011**, *44*, 5539–5553.

(23) Blaiszik, B. J.; Sottos, N. R.; White, S. R. Nanocapsules for Self-Healing Materials. *Compos. Sci. Technol.* **2008**, *68*, 978–986.

(24) Tuncaboylu, D. C.; Sari, M.; Oppermann, W.; Okay, O. Tough and Self-Healing Hydrogels Formed via Hydrophobic Interactions. *Macromolecules* **2011**, *44*, 4997–5005.

(25) Tuncaboylu, D. C.; Sahin, M.; Argun, A.; Oppermann, W.; Okay, O. Dynamics and Large Strain Behavior of Self-Healing Hydrogels with and without Surfactants. *Macromolecules* **2012**, *45*, 1991–2000.

(26) Roy, S.; Baral, A.; Banerjee, A. An Amino-Acid-Based Self-Healing Hydrogel: Modulation of the Self-Healing Properties by Incorporating Carbon-Based

Nanomaterials. *Chem. Eur. J.* **2013**, *19*, 14950–14957.

(27) Dragan, E. S. Design and Applications of Interpenetrating Polymer Network Hydrogels. A Review. *Chem. Eng. J.* **2014**, *243*, 572–590.

(28) Liu, J.; Song, G.; He, C.; Wang, H. Self-Healing in Tough Graphene Oxide Composite Hydrogels. *Macromol. Rapid Commun.* **2013**, *34*, 1002–1007.

(29) Zhang, E.; Wang, T.; Zhao, L.; Sun, W.; Liu, X.; Tong, Z. Fast Self-Healing of Graphene Oxide-Hectorite Clay-Poly (N , N - Dimethylacrylamide) Hybrid Hydrogels Realized by Near-Infrared Irradiation. *ACS Appl. Mater. Interfaces* **2014**, *6*, 22855–22861.

(30) Penq, R.; Yu, Y.; Chen, S.; Yang, Y.; Tanq, Y. Conductive Nanocomposite Hydrogels with Self-Healing Property. *RSC Adv.* **2014**, *4*, 35149–35155.

(31) Das, S.; Irin, F.; Ma, L.; Bhattacharia, S. K.; Hedden, R. C.; Green, M. J. Rheology and Morphology of Pristine Graphene / Polyacrylamide Gels. *ACS Appl. Mater. Interfaces* **2013**, *5*, 8633–8640.

(32) Hou, C.; Duan, Y.; Zhang, Q.; Wang, H.; Li, Y. Bio-Applicable and Electroactive near-Infrared Laser-Triggered Self-Healing Hydrogels Based on Graphene Networks. *J. Mater. Chem.* **2012**, *22*, 14991–14996.

(33) León, V.; Quintana, M.; Herrero, M. A.; Fierro, J. L. G.; de la Hoz, A.; Prato, M.; Vázquez, E. Few-Layer Graphenes from Ball-Milling of Graphite with Melamine. *Chem. Commun.* **2011**, *47*, 10936–10938.

(34) Shivashankar, M.; Mandal, B. K. A Review on Interpenetrating Polymer Network. *Int. J. Pharm. Sci.* **2012**, *4*, 1–7.

(35) Ostroha, J.; Pong, M.; Lowman, A.; Dan, N. Controlling the Collapse/swelling

Transition in Charged Hydrogels. *Biomaterials* **2004**, *25*, 4345–4353.

(36) Jianqi, F.; Lixia, G. PVA/PAA Thermo-Crosslinking Hydrogel Fiber: Preparation and pH-Sensitive Properties in Electrolyte Solution. *Eur. Polym. J.* **2002**, *38*, 1653–1658.

(37) Servant, A.; Leon, V.; Jasim, D.; Methven, L.; Limousin, P.; Vazquez Fernandez-Pacheco, E.; Prato, M.; Kostarelos, K. Graphene-Based Electroresponsive Scaffolds as Polymeric Implants for on-Demand Drug Delivery. *Adv. Healthc. Mater.* **2014**, *3*, 1334–1343.

(38) Jiang, S.; Liu, S.; Feng, W. PVA Hydrogel Properties for Biomedical Application. *J. Mech. Behav. Biomed. Mater.* **2011**, *4*, 1228–1233.

(39) Hong, H.; Liao, H.; Chen, S.; Zhang, H. Facile Method to Prepare Self-Healable PVA Hydrogels with High Water Stability. *Mater. Lett.* **2014**, *122*, 227–229.

(40) Kim, S. O. Y.; Shin, H. S. O. O.; Lee, Y. M. O. O.; Jeong, C. N. A. M. Properties of Electroresponsive Poly (Vinyl Alcohol)/ Poly (Acrylic Acid) IPN Hydrogels Under an Electric Stimulus. *J. Appl. Polym. Sci.* **1999**, *73*, 1675–1683.

(41) Kurauchi, T.; Shiga, T.; Hirose, Y.; Okada, A. *POLYMER GELS Fundamentals and Biomedical Applications*; DeRossi, D.; Kajiwara, K.; Osada, Y.; Yamauchi, A. 1991; p. 237.

(42) Murdan, S. Electro-Responsive Drug Delivery from Hydrogels. *J. Control. Release* **2003**, *92*, 1–17.

(43) Tanaka, T.; Nishio, I.; Sun, S.T.; Ueno-Nishio, S. Collapse of Gels in a Electric Field. *Science* **1982**, *218*, 467–769.

(44) Tomer, R.; Dimitrijevic, D.; Florence, A.T. Electrically Controlled Release of Macromolecules from T-Ross-Linked Hyaluronic Acid Hydrogels. *J. Control. Release*

1995, *33*, 405–413.

(45) Hassan, C. M.; Peppas, N. A. Structure and Morphology of Freeze / Thawed PVA Hydrogels. *Macromolecules* **2000**, *33*, 2472–2479.

(46) Khutoryanskiy, V. V; Nurkeeva, Z. S.; Mun, G. a; Sergaziyev, A. D.; Ryskalieva, Z.; Rosiak, J. M. Polyelectrolyte Complexes of Soluble Poly-2- [(Methacryloyloxy) Ethyl] Trimethylammonium Chloride and Its Hydrogels with Poly (Acrylic Acid). *Eur. Polym. J.* **2003**, *39*, 761–766.

(47) He, M.; Chu, C. C. Dual Stimuli Responsive Glycidyl Methacrylate Chitosan-Quaternary Ammonium Hybrid Hydrogel and Its Bovine Serum Albumin Release. *J. Appl. Polym. Sci.* **2013**, *130*, 3736–3745.

(48) Shukla, N. B.; Madras, G. Adsorption of Anionic Dyes on a Reversibly Swelling Cationic Superabsorbent Polymer. *J. Appl. Polym. Sci.* **2013**, *127*, 2251–2258.

(49) Kostina, N. Y.; Sharifi, S.; De Los Santos Pereira, a; Michálek, J.; Grijpma, D. W.; Rodriguez-Emmenegger, C. Novel Antifouling Self-Healing Poly(carboxybetaine Methacrylamide-Co-HEMA) Nanocomposite Hydrogels with Superior Mechanical Properties. *J. Mater. Chem. B* **2013**, *1*, 5644–5650.

(50) Luo, F.; Sun, T. L.; Nakajima, T.; Kurokawa, T.; Zhao, Y.; Sato, K.; Ihsan, A. Bin; Li, X.; Guo, H.; Gong, J. P. Oppositely Charged Polyelectrolytes Form Tough, Self-Healing, and Rebuildable Hydrogels. *Adv. Mater.* **2015**, *27*, 2722–2727.

(51) González-Domínguez, J.M.; Díez-Pascual, A.M.; Ansón-Casaos, A.; Gómez-Fatou, M.A.; Martínez, M. Functionalization Strategies for Single-Walled Carbon Nanotubes Integration into Epoxy Matrices. In *Polymer Nanotube Nanocomposites*; Mittal, V. 2014; pp. 45–116.

(52) Kumar, S.; Gangopadhyay, R. Conducting Polymer Gel : Formation of a Novel

Semi-IPN from Polyaniline and Crosslinked Poly(2-Acrylamido-2-Methyl Propanesulphonicacid). *Polymer* **2005**, *46*, 2993–3000.

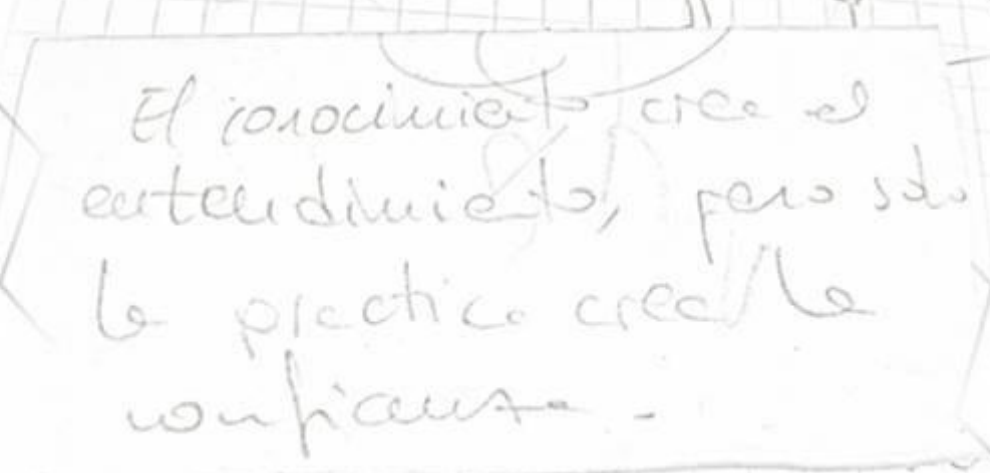
El conocimiento crea el
entendimiento, pero solo
la practica crea la
confianza.